https://ntrs.nasa.gov/search.jsp?R=19820024446 2020-03-21T06:19:37+00:00Z

NASA
TP
2054
c.1

TECH LIBRARY KAFB, NM
0068163

NASA
Technical
Paper
2054

September 1982

Experimental Investigation of Two Nonaxisymmetric Wedge Nozzles at Free-Stream Mach Numbers up to 1.20

Mary L. Mason and
William K. Abeyounis

LOAN COPY: RETURN TO
AFWL TECHNICAL LIBRARY
KIRTLAND AFB, N.M.

NASA

ERRATA

NASA Technical Paper 2054

EXPERIMENTAL INVESTIGATION OF TWO NONAXISYMMETRIC WEDGE NOZZLES AT FREE-STREAM MACH NUMBERS UP TO 1.20

Mary L. Mason and William K. Abeyounis
September 1982

Replace page 53 of this report with the attached corrected page 53. A term in one of the equations was found to be in error.

ISSUE DATE: APRIL 1983

4/26/83

TECH LIBRARY KAFB, NM

0068163

NASA
Technical
Paper
2054

1982

Experimental Investigation of Two Nonaxisymmetric Wedge Nozzles at Free-Stream Mach Numbers up to 1.20

Mary L. Mason and
William K. Abeyounis
Langley Research Center
Hampton, Virginia

National Aeronautics
and Space Administration

Scientific and Technical
Information Branch

SUMMARY

An experiment has been conducted in the Langley 16-Foot Transonic Tunnel to determine the static and wind-on performance of two nonaxisymmetric wedge nozzles. This experiment continued efforts to compile a detailed and comprehensive data base on nonaxisymmetric nozzles. The nozzle geometries represented two different nozzle throat areas and expansion ratios. Tests were conducted at wind-off conditions and at free-stream Mach numbers of 0.60, 0.80, 0.90, 0.94, and 1.20. The range of nozzle pressure ratios varied with nozzle geometry and Mach number. Data are presented as discharge coefficients, internal thrust ratios, thrust-minus-nozzle drag ratios, ideal thrust coefficients, and internal and external static-pressure distributions. The static-pressure data were analyzed to determine characteristics of the nozzle internal and external flow fields.

INTRODUCTION

Current jet fighter aircraft are designed for high maneuverability over a wide range of Mach numbers and power settings. A propulsion exhaust-nozzle system with variable geometry enhances the aircraft performance at different engine throttle settings. Recent investigations of the effects of nozzle design on advanced jet aircraft performance have shown that nonaxisymmetric nozzles can not only meet performance requirements but also allow several valuable propulsion-system design options (refs. 1 to 4). The nonaxisymmetric nozzle geometry integrates well into multiengine airframe designs and results in low installed drag. The utilization of nonaxisymmetric nozzles also facilitates thrust vectoring and thrust reversing capabilities which improve the overall aircraft maneuverability and handling characteristics and reduce take-off and landing distances (ref. 5).

An extensive data base is needed to fully assess the isolated and integrated performance of nonaxisymmetric nozzle designs. A detailed, comprehensive data base gives insight into the appropriate use of different nonaxisymmetric nozzle geometries. A data base also provides data for test cases which are essential in the development and evaluation of computational methods for predicting isolated and installed nozzle flow fields. Internal static-pressure data from several nonaxisymmetric nozzle configurations (refs. 6 and 7) have been used to evaluate the accuracy of two-dimensional and three-dimensional computational models in predicting nozzle internal flow (refs. 8 to 10).

To expand the current nonaxisymmetric nozzle data base, an investigation has been conducted to measure pressures and forces on a wedge nozzle, one of several different generic types of nonaxisymmetric nozzles. Two wedge nozzle configurations representing two different throat areas and expansion ratios were chosen for the investigation. These two configurations were based on nozzle geometries which were tested at static conditions in an earlier experimental investigation (ref. 11). The nozzles were redesigned for wind-on testing and were also modified to include extensive pressure-orifice instrumentation. The two wedge nozzles were tested in the Langley 16-Foot Transonic Tunnel over a range of free-stream Mach numbers and nozzle pressure ratios. Static and wind-on data are presented as discharge coefficients, internal thrust ratios, thrust-minus-nozzle drag ratios, ideal thrust coefficients, and internal and external pressure distributions.

SYMBOLS

All forces and angles are referred to the model center line (body axis). Wind axes are equivalent to body axes since the angle of attack was 0° for this investigation.

A_e	nozzle exit area, cm^2
A_e/A_t	nozzle expansion ratio
A_m	maximum cross-sectional area of model, cm^2
A_{seal}	cross-sectional area enclosed by seal strip at station 67.31, cm^2
A_t	nozzle throat area, cm^2
$a(x')$	function used in defining horizontal component of superellipse geometry in figures 2 and 3
a_n	constants used in evaluating $a(x')$ in figure 2
$b(x')$	function used in defining vertical component of superellipse geometry in figures 2 and 3
b_n	constants used in evaluating $b(x')$ in figure 2
$C_{F,i}$	ideal isentropic gross thrust coefficient, $F_i/p_\infty A_m$ for static conditions and $F_i/q_\infty A_m$ for wind-on conditions
C_p	pressure coefficient, $(p - p_\infty)/q_\infty$
D_f	external skin-friction drag measured from metric break (station 67.31) to start of nozzle (station 139.83), positive downstream, N
D_n	nozzle drag, Pressure drag + Friction drag, N
d	maximum height of model, cm
F	measured thrust along body axis, N
$F_{A,mom}$	momentum tare axial force due to bellows, N
F_{bal}	axial force measured by main balance, N
F_i	ideal isentropic gross thrust, $w_p\sqrt{RT_{t,j}{}^{2\gamma/(\gamma-1)}\left[1-\left(\frac{p_\infty}{p_{t,j}}\right)^{(\gamma-1)/\gamma}\right]}$, N
h	half-height of nozzle at start of nozzle boattail (station 141.73), cm
h_e	internal height of nozzle exit, cm
h_t	height of nozzle throat, cm

l	nozzle length from start of boattail (station 141.73) to end of wedge, cm
l_e	length from start of boattail (station 141.73) to nozzle exit, cm
l_w	length of wedge, cm
M_∞	free-stream Mach number
N_{Re}	Reynolds number per meter
p	local static pressure, Pa
$\bar{p}_{es}$	average static pressure at external seal at the metric break (station 67.31), Pa
$\bar{p}_i$	average internal static pressure, Pa
p_t	tunnel total pressure, Pa
$p_{t,j}$	jet total pressure, Pa
p_∞	free-stream static pressure, Pa
q_∞	free-stream dynamic pressure, Pa
R	gas constant (for $\gamma = 1.3997$), 287.3 J/kg-K
$r'(x')$	radius used in defining superellipse geometry in figures 2 and 3, cm
r_s	radius used to define sidewall geometry in figure 5, cm
$r_{w,1}, r_{w,2}$	radii used to define wedge geometry in figure 5, cm
r_1, r_2, r_3	radii used to define internal and external flap geometry in figure 5, cm
T_t	tunnel total temperature, K
$T_{t,j}$	jet total temperature, K
w_i	ideal mass-flow rate, $\left[\left(\frac{2}{\gamma + 1}\right)^{\gamma/(2\gamma-2)} \sqrt{\frac{9.80665\gamma}{R}}\right] \frac{p_{t,j}A_t}{\sqrt{T_{t,j}}}$, kg/sec
w_p	measured mass-flow rate, kg/sec
w_p/w_i	discharge coefficient
x	axial distance measured from start of boattail (station 141.73), positive downstream, cm
x'	axial distance measured from start of model nose, positive downstream, cm
x_e	axial coordinate of nozzle exit, cm

$x_{f,t}$	axial flap coordinate at nozzle throat (see fig. 5), cm
x_n	axial coordinates used to define flap geometry in figure 5, cm
$x_{r,2}, x_{r,3}$	axial coordinates used to define flap radius locations in figure 5, cm
$x_{s,1}$	axial coordinate used to define sidewall geometry in figure 5, cm
$x_{w,r}$	axial coordinate used to define wedge radius in figure 5, cm
$x_{w,t}$	axial wedge coordinate at nozzle throat (see fig. 5), cm
$x_{w,0}, x_{w,1}, x_{w,2}, x_{w,3}$	axial coordinates used to define wedge geometry in figure 5, cm
y	vertical distance from model center line, positive up, used in coordinate system of figures 5 and 6, cm
$y'(x')$	vertical distance from model center line, positive up, used in coordinate system of figures 2 and 3, cm
y_b	vertical coordinate of external flap edge at nozzle exit (see fig. 5), cm
y_e	vertical coordinate of internal flap edge at nozzle exit (see fig. 5), cm
$y_{f,t}$	vertical flap coordinate at nozzle throat (see fig. 5), cm
y_n	vertical coordinates used to define flap geometry in figure 5, cm
$y_{r,1}, y_{r,2}, y_{r,3}$	vertical coordinates used to define flap radius locations in figure 5, cm
y_s	vertical coordinate of sidewall external edge at end of nozzle (see fig. 5), cm
$y_{w,e}$	vertical wedge coordinate at nozzle exit (see fig. 5), cm
$y_{w,r}$	vertical coordinate used to define wedge radius in figure 5, cm
$y_{w,t}$	vertical wedge coordinate at nozzle throat (see fig. 5), cm
$y_{w,1}, y_{w,2}$	vertical coordinates used to define wedge geometry in figure 5, cm
z	lateral distance from model center line, positive to right looking upstream, used in coordinate system of figures 5 and 6, cm
$z'(x')$	lateral distance from model center line, positive to right looking upstream, used in coordinate system of figures 2 and 3, cm
$z_{s,b}$	lateral coordinate of external sidewall edge at nozzle exit (see fig. 5), cm
$z_{s,r}$	lateral coordinate used to define a radius to the sidewall in figure 5, cm

$z_{s,0}, z_{s,1}, z_{s,2}$	lateral coordinates used to define sidewall geometry in figure 5, cm
α	nozzle internal flap angle, deg
β	nozzle boattail angle measured in x-y plane in figure 5, deg
β_s	nozzle boattail angle measured in x-z plane in figure 5, deg
$\Delta\alpha$	rotation angle to increase nozzle expansion ratio (see fig. 5), deg
γ	ratio of specific heats, 1.3997 for air
$\eta(x')$	exponent of superellipse equation used in figures 2 and 3
θ	angle used to compute values of $y'(x')$ and $z'(x')$ from superellipse geometry given in figures 2 and 3, deg

APPARATUS AND METHODS

Wind Tunnel

The experimental investigation was conducted in the Langley 16-Foot Transonic Tunnel (ref. 12). This facility is a single-return, continuous-flow, atmospheric wind tunnel. The tunnel test section is octagonal with eight longitudinal slots. The wall divergence in the test section is adjusted as a function of the airstream dew point and Mach number; thus, any longitudinal static-pressure gradients in the test section are negligible. The test-section Mach number is continuously variable to a maximum of 1.30. The average Reynolds number per meter ranges from about 4.5×10^6 at a free-stream Mach number of 0.20 to about 13.0×10^6 at a free-stream Mach number of 1.30.

Model and Support System

General arrangement.- The single-engine air-powered nacelle model of reference 13 was used during this experiment. A detailed sketch of the single-engine nacelle propulsion simulation system, with a nonaxisymmetric wedge nozzle installed, is presented in figure 1. As illustrated in the figure, the model was composed of five major sections: a nose-forebody, a low-pressure plenum, an instrumentation section, a transition section, and a wedge nozzle. The length and model station location of each model segment is given in the following table:

Model segment	Length, cm	Model station, cm
Nose-forebody	67.31	0.00 to 67.31
Low-pressure plenum	36.70	67.31 to 104.01
Instrumentation	18.93	104.01 to 122.94
Transition	16.89	122.94 to 139.83
Nozzle	27.32	139.83 to 167.15

The nose-forebody section was nonmetric, that is, was not attached to the strain-gage balance which was used to measure forces and moments on the model. All sections of the model downstream of the nose-forebody were attached to the balance and were therefore metric. A low-friction Du Pont Teflon seal was inserted in a slot at the metric break between the nose-forebody and the low-pressure plenum. The Teflon seal eliminates cross flow through the nonmetric-metric interface and stabilizes the variation in cavity pressure without transmitting axial force across the interface.

Model support system.- The single-engine nacelle model was supported in the tunnel by a sting-strut support system. Part of the support system is shown in figure 1. The nose-forebody of the model was attached to the top of the strut. The center line of the model was aligned with the test-section center line, and the center line of the sting was 55.88 cm below the test-section center line. The cross section of the sting was 5.08 by 10.16 cm; the top and bottom of the sting were capped by half-cylinders of 2.54-cm radius. The strut blade was 5 percent thick with a 50.8-cm chord in the streamwise direction and with the leading and trailing edges swept 45°. The model blockage was 0.14 percent of the test-section cross section; the maximum-blockage cross section of the model and support system was 0.19 percent.

Internal air supply.- The exhaust jet flow was simulated by airflow from a high-pressure air system external to the model. A continuous flow of clean, dry, high-pressure air at a stagnation temperature of about 300 K entered the high-pressure plenum in the nose-forebody through six supply lines in the support strut. The supply lines and flow directions are shown in figure 1. From the high-pressure plenum, the pressurized air was discharged perpendicular to the model axis into the low-pressure plenum through eight sonic nozzles. The sonic nozzles were equally spaced around the high-pressure plenum supply pipe. The decelerated airflow in the low-pressure plenum was diffused over the balance housing and straightened by a 79-percent open-area baffle plate. The airflow passed into the instrumentation section of the model, where stagnation temperature and pressure were measured, and then entered the transition section of the model. In the transition section, the internal cross-sectional geometry changed from circular to rectangular to provide compatible internal geometry at the nonaxisymmetric nozzle connect station. A sketch of the cross-sectional geometry at the beginning and end of the transition section is shown in figure 1. Details of the internal transition geometry are discussed later. From the transition section, the airflow was exhausted through the nonaxisymmetric nozzle.

Force-balance air system.- As the airflow passed from the high-pressure plenum to the low-pressure plenum through the eight sonic nozzles, it was discharged radially to the model axis. Since the sonic nozzles were equally spaced in a radial direction, an opposing nozzle force was positioned to cancel each force due to jet impingement. This arrangement minimizes any forces resulting from the transfer of axial momentum as the air passes from the nonmetric to the metric part of the model. Two flexible metal bellows were used to seal the low-pressure plenum and compensate for any axial forces resulting from model pressurization.

Nose-forebody external geometry.- The nose-forebody section of the model allowed a smooth external transition from a circular cross section at the conical nose to a rectangular cross section with large rounded corners at the beginning of the low-pressure plenum. The maximum external cross-sectional area of 265.61 cm^2 occurred at the metric break. The cross-sectional area and the external geometry remained constant from the metric break to the nozzle connect station.

The external geometry of the nose-forebody section is presented in figure 2. In figure 2(a), a computer-generated sketch illustrates the basic nose-forebody geometry. The external geometry is given as a superellipse equation defined at particular horizontal stations along the model. Appropriate definitions of the components of the superellipse equation are given as functions of the horizontal variable x'. A table of the function values at particular values of x' is also included. Figure 2(b) defines the general cross-sectional geometry of the nose-forebody section and gives the relationships for calculating the cross-sectional horizontal component $z'(x')$ and the vertical component $y'(x')$.

Transition geometry.- The model low-pressure plenum internal geometry and the end of the constant-geometry instrumentation section had a circular cross section. The nonaxisymmetric wedge nozzles used in this investigation had a rectangular internal cross-sectional geometry at the nozzle connect station. A transition section was required to provide the changes in internal geometry which were necessary for matching the wedge nozzles with the propulsion simulation system. The transition section of the model provided modifications to the internal geometry which were similar to the modifications in external geometry provided by the nose-forebody section. The internal geometry of the transition section changed smoothly from a circular cross section at the beginning of transition to a rectangular cross section at the end of transition. The internal cross-sectional area remained constant throughout the transition section.

The internal geometry of the transition section is presented in figure 3. A superellipse equation is used to define the cross-sectional geometry up to model station 134.29. From station 134.29 to the end of the transition section, the internal cross section is rectangular, and the equations for calculating $y'(x')$ and $z'(x')$ are given. In addition to these equations, the functions which define the internal geometry for the full length of the transition section are tabulated in figure 3.

Nozzle geometry.- Two nonaxisymmetric wedge nozzle configurations representing two different power settings were tested during this investigation. The nozzle designs were based on earlier wedge nozzles described in references 11 and 13. The baseline configuration had an expansion ratio of 1.06 and is referred to as the low-expansion-ratio nozzle. The other configuration had an expansion ratio of 1.20 and is referred to as the high-expansion-ratio nozzle. A photograph of each nozzle is shown in figure 4.

Each nozzle was made up of five components: two sidewalls, an upper and a lower flap, and a wedge centerbody. Both nozzles used the same wedge and the same sidewalls. The flaps were different, resulting in the different expansion ratios for each nozzle. Sketches and geometry details of each nozzle component are given in figure 5. In this report, the downstream end of the nozzle upper and lower flaps is referred to as the nozzle exit. (See fig. 1.) The exit for the low-expansion-ratio nozzle occurs at $x_e = 15.7820$ cm; the exit for the high-expansion-ratio nozzle occurs at $x_e = 16.0247$ cm.

The geometry for the high-expansion-ratio nozzle was constructed from the geometry for the low-expansion-ratio nozzle by rotating the flaps away from the nozzle internal center line in the x-y plane. (See fig. 5(b).) The center of rotation was at point $(x_{r,2},y_{r,2})$. Rotating the flaps in this way increased the throat area, the exit area, and the expansion ratio. Since the nozzle sidewall geometry was held constant during this test, a triangular-shaped gap was opened between the outside edge of the trailing edge of the flap to the point (x_3,y_3), which is upstream of the nozzle throat. The resulting nozzle geometry is similar to the cutaway or vented sidewall concept discussed in reference 14. The effects of venting the nozzle upstream of the throat are discussed later in this report.

Instrumentation

Basic model instrumentation is shown in the sketch of figure 1. A five-component strain-gage balance was used to measure the forces and moments on the model downstream of the metric break (station 67.31). A rake of 12 total-pressure probes was used to measure the jet total pressure at a fixed location in the instrumentation section of the model. An iron-constantan thermocouple was used to measure the jet total temperature in the instrumentation section.

Each nozzle configuration was instrumented with 14 rows of static-pressure orifices which are shown in figure 6. Rows 1 to 3 were located on the internal side of the top flap; rows 4 and 5 were located on the outside of the top flap; rows 6 to 8 were located on the outside of the right sidewall; row 9 was on the inside of the left sidewall; rows 10 to 14 were along the top of the wedge. Tables which define the exact coordinates of each orifice are also given in figure 6.

Tests

The experimental investigation was conducted in the Langley 16-Foot Transonic Tunnel at wind-off conditions and at free-stream Mach numbers from 0.60 to 1.20. The model angle of attack was held constant at 0° throughout the investigation. The nozzle pressure ratio was varied from jet-off to a maximum which depended on Mach number, configuration, and model-facility airflow limits. The basic data were taken by holding the Mach number fixed and varying the nozzle pressure ratio. The Reynolds number per meter, the average tunnel total temperature, the average tunnel total pressure, and the average jet total temperature at each Mach number are given in the following table:

M_∞	T_t, K	p_t, kPa	$T_{t,j}$, K	N_{Re}
0.60	316.97	101.28	297.44	10.60×10^6
.80	325.44	101.22	296.96	12.19
.90	328.80	101.22	299.34	12.67
.94	328.51	101.22	300.34	12.89
1.20	339.03	101.04	300.20	12.92

Boundary-layer transition on the model was fixed by using a grit transition-strip procedure (ref. 15). A 0.254-cm-wide strip of No. 100 grit was attached around the nose of the model at 2.54 cm from the nose tip. The same grit size and location were used for both nozzle configurations.

Data Reduction

All wind-tunnel parameters and model data were recorded simultaneously on magnetic tape. Averaged values of the data measurements were used to compute basic nozzle performance parameters and nondimensionalized pressure coefficients or ratios.

The basic measurement used in evaluating isolated nozzle performance is thrust minus nozzle drag measured along the body axis of the model. This parameter was derived from the balance axial-force measurements using the following relationship:

$$F - D_n = F_{bal} + (\bar{p}_{es} - p_\infty)(A_m - A_{seal}) + (\bar{p}_i - p_\infty)A_{seal} + D_f - F_{A,mom}$$

The term F_{bal} includes all internal and external forces on the balance. The second term $(\bar{p}_{es} - p_\infty)(A_m - A_{seal})$ represents pressure force due to the forward seal at the metric break (station 67.31). The third term $(\bar{p}_i - p_\infty)A_{seal}$ represents interior pressure forces. The term D_f is the calculated external skin friction on the constant cross-section part of the model from the metric break to the start of the nozzle (station 139.83). The term $F_{A,mom}$ is a momentum tare correction and is a function of the average bellows internal pressure with the model jet operating. Although the bellows were designed to minimize momentum and pressurization tares, small bellows tares still exist when the jet is operating. These tares result from small differences in the upstream and downstream bellows spring constants when the bellows are pressurized and also from small pressure differences between the ends of the bellows when internal flow velocities are high.

Procedures for calibrating and correcting these bellows tares are discussed in detail in references 11 and 16. To simulate realistic test conditions, a series of axisymmetric calibration nozzles with known performance were tested over the expected test range of normal-force and pitching-moment loadings. The calibration tests were performed wind-off, with and without external loadings on the model, and with and without jet exhaust flow. The resulting corrections were then applied to the balance data by a procedure similar to the main balance data-reduction algorithm of reference 16.

RESULTS AND DISCUSSION

Basic Data

Basic data for evaluating the isolated performance of the two wedge nozzles are presented in figures 7 to 10. The ideal thrust coefficient $C_{F,i}$ presented in figure 10 can be combined with the normalized thrust data in figures 7 and 9 to obtain the measured thrust and thrust-minus-drag levels.

The static-force data in figure 7 show trends similar to those of static-force data presented in reference 11 for two wedge nozzles with expansion ratios identical to those of the current test. The wind-on thrust-minus-nozzle drag ratios in figure 9 show trends and levels similar to earlier thrust-minus-nozzle drag data presented in reference 11 for wedge nozzle configurations. In general, thrust-minus-nozzle drag ratio decreases as the free-stream Mach number increases. The decrease in $(F - D_n)/F_i$ with increasing Mach number results from an increase in nozzle drag on the external surface with increasing Mach number. In addition, at a constant nozzle pressure ratio, the nozzle drag term D_n of $(F - D_n)/F_i$ becomes a higher percentage of ideal thrust as Mach number increases, resulting in a decrease in the thrust-minus-nozzle drag ratio.

The data in figure 7 indicate that the thrust-ratio data of the high-expansion-ratio nozzle fall below the thrust-ratio data of the low-expansion-ratio nozzle over the range of nozzle pressure ratios tested at static conditions ($M_\infty = 0$). Similar results are shown by data in references 11, 13, and 14 for several nonaxisymmetric nozzle configurations at static conditions. This decrease in thrust ratio with increased expansion ratio indicates that a performance loss may result from the changes in nozzle geometry. In this investigation, additional performance losses for the high-expansion-ratio configuration may be due to the vent or gap between the nozzle flap and sidewall which extends upstream of the nozzle throat.

The static-discharge-coefficient (w_p/w_i) data presented in figure 7 show levels which are similar to discharge-coefficient levels for several wedge-type nozzles in reference 14. In general, the value of discharge coefficient is greater than one at unchoked flow conditions ($p_{t,j}/p_\infty < 1.89$) and less than one at choked flow conditions ($p_{t,j}/p_\infty > 1.89$). However, in figure 8 the wind-on discharge-coefficient levels for the low-expansion-ratio nozzle are higher than discharge-coefficient levels presented in reference 13 for a similar wedge nozzle. At wind-on conditions, both configurations in this investigation had values of discharge coefficient which were greater than one at choked flow conditions. Reference 14 discusses the phenomenon of high-discharge-coefficient data ($w_p/w_i > 1.0$) at choked flow conditions for wedge nozzle configurations. It is extremely difficult to determine the actual throat area of nonaxisymmetric wedge-type nozzles. The numerator of discharge coefficient, the w_p-term, is computed strictly from data measurements; its value reflects the actual flow-field conditions and nozzle throat area. The denominator of discharge coefficient, the w_i-term, is computed using a fixed value of throat area, the nozzle throat area as designed and, therefore, may include some error that varies with flow conditions. This error in throat area can result in values of discharge coefficient greater than 1, as reference 14 shows for several wedge nozzle configurations. Thus, the high magnitude of the wedge nozzle discharge coefficients presented in figures 7 and 8 apparently results from unrecorded variations in nozzle throat area corresponding to changes in the internal flow field with varying nozzle pressure ratio and free-stream Mach number.

Static-Pressure Data

Extensive static-pressure measurements were made on both nozzle configurations. Selected cases of pressure distributions are presented in figures 11 to 28. Complete listings of all static-pressure data are given in tables 1 to 14 for the low-expansion-ratio nozzle and in tables 15 to 28 for the high-expansion-ratio nozzle. All data are presented as functions of x/d, where x is the distance from the start of the nozzle boattail (station 141.73) and d is the maximum nozzle height. (See fig. 5(a).) Internal static-pressure data are presented as values of $p/p_{t,j}$, the measured local static pressure nondimensionalized by the measured jet total pressure. Static pressures measured along the wedge surface are also presented as the ratios $p/p_{t,j}$. External static-pressure data are presented as values of pressure coefficient C_p.

Comparisons of static-pressure distributions are made at different spanwise locations to determine two-dimensional or three-dimensional characteristics in the nozzle flow field. In figure 11, pressures from the five rows of static-pressure orifices on the surface of the wedge are plotted against x/d for the low-expansion-ratio nozzle. Three values of nozzle pressure ratio $p_{t,j}/p_\infty$ are presented for a Mach number of 0.60 and for a Mach number of 1.20. In each case of figure 11(a), at $M_\infty = 0.60$, the static pressures upstream of the nozzle exit, defined as the end of the nozzle flap in figure 1, show little variation with spanwise location. This lack of variation indicates that the internal flow field near the wedge surface is two-dimensional. At $p_{t,j}/p_\infty = 2.0$ and $M_\infty = 0.60$, there is a sharp increase in static pressure at the nozzle exit. Downstream of the exit, the static pressure becomes nearly constant. The sharp increase in wedge static pressure near the exit is probably due to a strong shock wave occurring on the surface of the wedge in the nozzle exhaust flow. The near-constant static pressures downstream of the pressure increase indicate that the exhaust flow on the wedge is separated downstream of the shock wave. Similar flow-field characteristics were also observed for wind-off wedge static-pressure distributions presented in reference 6 for a wedge-type nozzle with a low expansion ratio ($A_e/A_t = 1.05$). At the higher values of nozzle pressure ratio presented in figure 11(a), the shock wave moves downstream and becomes weaker in strength. The static-pressure distributions in the separated flow region downstream of the shock show more spanwise variation for these two nozzle pressure ratios.

The three cases of static-pressure distributions at $M_\infty = 1.20$ in figure 11(b) show basically the same flow-field characteristics as observed at $M_\infty = 0.60$. Upstream of the nozzle exit, the static pressures show no variation with spanwise location and, in fact, show no effect of increasing the free-stream Mach number. (Compare fig. 11(a) with fig. 11(b).) An increase in the wedge static pressures occurs downstream of the nozzle exit ($x/d = 1.00$), which may indicate that a shock occurs on the wedge surface. The point of increase in static pressure, that is, the shock location, moves downstream as the nozzle pressure ratio increases. Jet exhaust flow separation from the wedge surface occurs downstream of the shock. The wedge static-pressure distributions show some spanwise variation in the separated flow region. The change in free-stream Mach number from 0.60 to 1.20 mainly affects the location of the shock wave and subsequent flow separation.

In summary, the static-pressure distributions of figure 11 show that the flow along the surface of the wedge of the low-expansion-ratio nozzle is two-dimensional upstream of the nozzle exit. A shock occurs on the wedge surface downstream of the nozzle exit, followed by flow separation from the surface of the wedge. The location of the shock and subsequent flow separation depends primarily on the nozzle pressure ratio and, to a lesser extent, on the free-stream Mach number. Similar characteristics of static-pressure distributions along a wedge surface are presented in reference 6 at wind-off conditions, with values of nozzle pressure ratio up to 6.00. The data of reference 6 also include oil-flow photographs of the wedge surface downstream of the nozzle exit. These photographs clearly show the downstream movement of the jet exhaust shock on the wedge and subsequent flow separation with increasing nozzle pressure ratio.

Figure 12 presents wedge static-pressure distributions for the high-expansion-ratio nozzle. Three cases of nozzle pressure ratio are presented for $M_\infty = 0.60$ in figure 12(a) and for $M_\infty = 1.20$ in figure 12(b). The same trends observed for the low-expansion-ratio nozzle also occur in these pressure distributions. A shock occurs downstream of the nozzle exit ($x/d = 1.02$) followed by flow separation from the wedge surface. The static pressures downstream of the shock show variation with spanwise location. However, for this nozzle, spanwise variation in the static-pressure data occurs as far upstream of the nozzle exit as $x/d = 0.90$. These three-dimensional effects upstream of the nozzle exit may result from the higher expansion ratio ($A_e/A_t = 1.20$) of this configuration. The vent in the sidewall, which extends upstream of the nozzle throat, may also contribute three-dimensional effects to the nozzle internal flow.

Static-pressure distributions along the internal surface of the top flap are presented in figure 13 for the low-expansion-ratio nozzle and in figure 14 for the high-expansion-ratio nozzle. Two values of nozzle pressure ratio are shown at $M_\infty = 0.60$ and at $M_\infty = 1.20$. The lack of spanwise variation in the pressure distributions shown in figure 13 indicates that the internal flow is two-dimensional for the low-expansion-ratio nozzle. However, the internal pressures for the high-expansion-ratio nozzle (fig. 14) show spanwise variation, particularly at the flap edge near the sidewall. The variation is more pronounced for $p_{t,j}/p_{\infty} = 5.06$ at $M_{\infty} = 0.60$ and for $p_{t,j}/p_{\infty} = 7.99$ at $M_{\infty} = 1.20$. Free-stream Mach number has only a small effect on the spanwise variation. The throat of the high-expansion-ratio nozzle is, by design, located at $x/d = 0.82$, whereas the three-dimensional effect can be seen as far forward as $x/d = 0.76$. This spanwise variation in static pressure near the edge of the flap is probably caused by the gap or vent between the flap and sidewall for the high-expansion-ratio nozzle. This vent probably caused the similar three-dimensional characteristics upstream of the nozzle exit ($x/d = 1.02$), which were observed in the static-pressure distributions along the surface of the wedge for this configuration. Internal static-pressure distributions on the nozzle flap presented in reference 14 for similar nozzle configurations without vented sidewalls showed no three-dimensional effects. Thus, the three-dimensional characteristics of the internal flow of the high-expansion-ratio nozzle of this investigation may be attributed to the vent between the flap and sidewall. The three-dimensional effects upstream of the throat of the high-expansion-ratio nozzle probably correspond to the extension of the gap or vent to a point upstream of the nozzle throat.

External static pressures along the top of the flap and along the outside of the right sidewall are presented for the low-expansion-ratio nozzle in figure 15. The same results for the high-expansion-ratio nozzle are given in figure 16. Row 8, the outside corner row, is included with both the top flap data (rows 4 and 5) and with the sidewall data (rows 6 and 7).

The static pressures along rows 4 and 5 on the top flap for both nozzle configurations show only small spanwise variation in static pressure at $M_{\infty} = 0.60$. At supersonic conditions, $M_{\infty} = 1.20$, the high-expansion-ratio nozzle continues this trend, whereas the low-expansion-ratio nozzle shows spanwise variation in static pressures on the aft portion of the nozzle ($x/d \geqslant 0.80$). When compared with the top flap data, the static-pressure data of row 8 show close spanwise agreement upstream of $x/d = 0.10$ for both nozzle configurations at all test conditions. However, as the value of x/d increases, there is considerable variation between the corner-row static pressures and the top-flap static pressures.

In figure 15, the sidewall external static-pressure distributions along rows 6 and 7 for the low-expansion-ratio nozzle show spanwise variation downstream of $x/d = 0.50$ at all test conditions. The sidewall static pressures for the high-expansion-ratio nozzle show only small spanwise variation at $M_{\infty} = 0.60$ but show the same type of variation observed for the low-expansion-ratio nozzle at $M_{\infty} = 1.20$. Comparisons of the corner-row static-pressure distributions with those of rows 6 and 7 show the same trends observed in the comparisons of the corner row with the flap rows. The static pressures of rows 6, 7, and 8 generally agree upstream of $x/d = 0.10$ but show considerable spanwise variation downstream of this point.

In general, the top-flap and sidewall static-pressure data indicate that the external flow starts out nearly two-dimensional near the nozzle boattail since the static-pressure data show good spanwise agreement upstream of $x/d = 0.10$. As the value of x/d increases, however, regions of three-dimensional flow occur in the external flow field. The three-dimensional effects probably initiate from the outside corner region.

Since the spanwise variation in the static-pressure data has been discussed for figures 11 to 16, the subsequent data plots will deal only with center-line pressure profiles. The effect of nozzle pressure ratio on the wedge center-line static-pressure distribution is presented in figure 17 for the low-expansion-ratio nozzle and in figure 18 for the high-expansion-ratio nozzle. In general, for all five values of free-stream Mach number, the nozzle pressure ratio affects the location of the exhaust-flow shock and attendant flow separation on the wedge surface. As nozzle pressure ratio increases, the exhaust-flow shock location and separation region move downstream from the nozzle exit ($x/d = 1.0$ for the low-expansion-ratio nozzle and $x/d = 1.02$ for the high-expansion-ratio nozzle). A similar effect of nozzle pressure ratio on a wedge center-line static-pressure distribution can be observed in the static-pressure data plots and oil-flow photographs of reference 6.

The effect of free-stream Mach number on the wedge center-line static pressures is presented in figures 19 and 20 for two values of nozzle pressure ratio, 2.00 and 6.00. Figure 19 shows the Mach number effects on the low-expansion-ratio nozzle, and figure 20 shows the effects on the high-expansion-ratio nozzle. Free-stream Mach number variation affects the static-pressure distributions only in the separated flow regions on the wedge which occur downstream of the exhaust-flow shock wave. The effect of Mach number is more evident at the lower nozzle pressure ratio ($p_{t,j}/p_{\infty} = 2.00$) shown in figures 19 and 20 since flow separation is more extensive at this nozzle pressure ratio. At a nozzle pressure ratio equal to 2.00, the nozzle is operating overexpanded. The jet exhaust flow shocks down and separates from the surface of the wedge at or near the nozzle exit. At the higher pressure ratio shown in figures 19 and 20, the flow remains attached along most of the wedge surface and there is little variation with Mach number.

Figure 21 presents the effects of free-stream Mach number on the internal flap center-line static pressures for the low-expansion-ratio nozzle. The corresponding data for the high-expansion-ratio nozzle are presented in figure 22. Two nozzle pressure ratios, 2.00 and 6.00, are presented in each figure. The internal flow along the flap center line is two-dimensional, and the pressure distributions indicate that there is no effect of Mach number on the nozzle center-line internal flow.

Figures 23 to 28 examine the effects of nozzle pressure ratio and free-stream Mach number on the external flow along the flap center line and along the sidewall center line. Figures 23 and 24 show the effects of nozzle pressure ratio on external static-pressure distributions at five free-stream Mach numbers for the low-expansion-ratio nozzle. Figures 25 and 26 show similar comparisons for the high-expansion-ratio nozzle. For both nozzle configurations, the flap static pressures generally decrease with initial increases in nozzle pressure ratio; further increases in nozzle pressure ratio generally increase the flap static pressures. Although the pressure distributions along the sidewall and upstream of the nozzle exit were not as sensitive to varying nozzle pressure ratio, they generally show the same trends as the flap data. Downstream of the nozzle exit, the sidewall static pressures generally tend to decrease as the nozzle pressure ratio increases, particularly at subsonic Mach numbers. The high-expansion-ratio nozzle exhibits more variation in sidewall static-pressure distributions with nozzle pressure ratio than does the low-expansion-ratio nozzle. This larger variation in the static pressures with nozzle pressure ratio is probably due to the vented sidewall geometry and to the higher expansion ratio and resulting larger flap angle α. (See fig. 5(b).)

The effect of varying the free-stream Mach number on the center-line flap and sidewall static-pressure distributions at a nozzle pressure ratio of 4.00 is presented in figure 27 for the low-expansion-ratio nozzle. Similar data are presented in figure 28 for the high-expansion-ratio nozzle. Both configurations show the same general results. Along the nozzle flap and - to a lesser extent - along the nozzle sidewall, the location of maximum flow expansion, indicated by the minimum pressure coefficient, tends to move downstream with increasing free-stream Mach number. The extent of pressure recovery on the downstream part of each surface also tends to decrease with increasing free-stream Mach number.

CONCLUDING REMARKS

An experiment has been conducted in the Langley 16-Foot Transonic Tunnel to determine the static and wind-on performance of two nonaxisymmetric wedge nozzles. This experiment continued efforts to compile a detailed and comprehensive data base on nonaxisymmetric nozzles. The nozzle geometries represented two different nozzle throat areas and expansion ratios. Tests were conducted at wind-off conditions and at free-stream Mach numbers of 0.60, 0.80, 0.90, 0.94, and 1.20. The range of nozzle pressure ratios varied with nozzle geometry and Mach number. Data are presented as discharge coefficients, internal thrust ratios, thrust-minus-nozzle drag ratios, ideal thrust coefficients, and internal and external static-pressure distributions.

The static-pressure data were analyzed to determine characteristics of the nozzle internal and external flow fields. The internal flow upstream of the nozzle exit is predominantly two-dimensional for the low-expansion-ratio nozzle. The internal flow field of the high-expansion-ratio nozzle exhibits three-dimensional effects due to the sidewall geometry, which had a gap or vent that extended upstream of the nozzle throat. The external flow field is predominantly two-dimensional for both wedge nozzles, except near the outside corners where the flow shows three-dimensional characteristics. In the jet region on the wedge, the flow for both nozzles is characterized by a shock wave occurring at or downstream of the nozzle exit and generally followed by flow separation from the surface of the wedge.

Langley Research Center
National Aeronautics and Space Administration
Hampton, VA 23665
August 2, 1982

REFERENCES

1. Capone, Francis J.: Summary of Propulsive-Lift Research in the Langley 16-Ft. Transonic Tunnel. J. Aircr., vol. 13, no. 10, Oct. 1976, pp. 803-808.

2. Hiley, P. E.; Wallace, H. W.; and Booz, D. E.: Nonaxisymmetric Nozzles Installed in Advanced Fighter Aircraft. J. Aircr., vol. 13, no. 12, Dec. 1976, pp. 1000-1006.

3. Berrier, Bobby L.; Palcza, J. Lawrence; and Richey, G. Keith: Nonaxisymmetric Nozzle Technology Program - An Overview. AIAA Paper 77-1225, Aug. 1977.

4. Capone, Francis J.: The Nonaxisymmetric Nozzle - It Is for Real. AIAA Paper 79-1810, Aug. 1979.

5. Capone, Francis J.; and Maiden, Donald L.: Performance of Twin Two-Dimensional Wedge Nozzles Including Thrust Vectoring and Reversing Effects at Speeds up to Mach 2.20. NASA TN D-8449, 1977.

6. Carson, George T., Jr.; and Mason, Mary L.: Experimental and Analytical Investigation of a Nonaxisymmetric Wedge Nozzle at Static Conditions. NASA TP-1188, 1978.

7. Mason, Mary L.; Putnam, Lawrence E.; and Re, Richard J.: The Effect of Throat Contouring on Two-Dimensional Converging-Diverging Nozzles at Static Conditions. NASA TP-1704, 1980.

8. Swanson, R. C.: Navier-Stokes Solutions for Nonaxisymmetric Nozzle Flows. AIAA-81-1217, June 1981.

9. Cline, Michael C.; and Wilmoth, Richard G.: Computation of High Reynolds Number Internal/External Flows. AIAA-81-1194, June 1981.

10. Thomas, P. D.: Numerical Method for Predicting Flow Characteristics and Performance of Nonaxisymmetric Nozzles. Part 2 - Applications. NASA CR-3264, 1980.

11. Capone, Francis J.: Static Performance of Five Twin-Engine Nonaxisymmetric Nozzles With Vectoring and Reversing Capability. NASA TP-1224, 1978.

12. Corson, Blake W., Jr.; Runckel, Jack F.; and Igoe, William B.: Calibration of the Langley 16-Foot Transonic Tunnel With Test Section Air Removal. NASA TR R-423, 1974.

13. Maiden, Donald L.: Performance of an Isolated Two-Dimensional Variable-Geometry Wedge Nozzle With Translating Shroud and Collapsing Wedge at Speeds up to Mach 2.01. NASA TN D-7906, 1975.

14. Berrier, Bobby L.; and Re, Richard J.: Effect of Several Geometric Parameters on the Static Internal Performance of Three Nonaxisymmetric Nozzle Concepts. NASA TP-1468, 1979.

15. Braslow, Albert L.; Hicks, Raymond M.; and Harris, Roy V., Jr.: Use of Grit-Type Boundary-Layer-Transition Trips on Wind-Tunnel Models. NASA TN D-3579, 1966.

16. Capone, Francis J.: Aeropropulsive Characteristics of Twin Nonaxisymmetric Vectoring Nozzles Installed With Forward-Swept and Aft-Swept Wings. NASA TP-1778, 1981.

TABLE 1.- STATIC PRESSURES FOR LOW-EXPANSION-RATIO NOZZLE, ROW 1

M_∞	$\frac{p_{t,j}}{p_\infty}$	$p/p_{t,j}$ for x/d of -								
		0.300	0.450	0.550	0.650	0.750	0.800	0.875	0.927	0.975
0.000	1.51	.972	.970	.965	.943	.856	.799	.673	.563	.606
.000	1.99	.972	.971	.965	.943	.856	.800	.673	.553	.465
.000	3.00	.972	.971	.964	.942	.855	.798	.672	.552	.468
.000	4.01	.973	.971	.964	.943	.854	.798	.671	.551	.470
.000	4.99	.975	.973	.966	.945	.855	.799	.671	.550	.471
.000	6.00	.978	.975	.968	.948	.856	.800	.671	.550	.473
.000	6.63	.982	.979	.972	.951	.858	.802	.672	.551	.475
.602	1.49	.970	.967	.963	.944	.862	.808	.702	.641	.664
.600	1.99	.969	.967	.963	.941	.856	.798	.674	.554	.464
.601	3.00	.970	.969	.963	.941	.855	.798	.673	.553	.466
.601	3.99	.971	.970	.963	.941	.854	.798	.672	.552	.468
.602	5.99	.975	.972	.965	.944	.854	.798	.671	.550	.471
.601	8.00	.979	.976	.969	.948	.856	.800	.671	.550	.474
.802	1.52	.968	.968	.965	.947	.867	.813	.713	.655	.675
.800	1.98	.972	.969	.964	.943	.857	.799	.675	.555	.465
.800	2.99	.972	.970	.964	.942	.856	.799	.675	.555	.466
.801	3.99	.971	.970	.963	.942	.855	.798	.673	.553	.467
.800	5.99	.972	.971	.964	.943	.854	.798	.671	.551	.470
.800	8.02	.976	.973	.966	.946	.855	.799	.671	.550	.472
.800	9.84	.980	.977	.970	.950	.857	.801	.672	.551	.474
.901	1.50	.970	.966	.962	.947	.864	.808	.700	.630	.653
.901	1.97	.968	.966	.962	.943	.856	.797	.673	.552	.466
.901	2.99	.970	.969	.963	.942	.856	.799	.674	.553	.465
.901	4.02	.971	.970	.963	.942	.856	.799	.673	.553	.467
.901	5.99	.973	.971	.964	.943	.855	.798	.672	.551	.469
.899	8.01	.975	.973	.966	.945	.855	.798	.671	.550	.471
.899	9.99	.978	.975	.968	.948	.856	.800	.671	.550	.473
.940	1.49	.964	.965	.958	.947	.861	.803	.690	.606	.623
.940	2.00	.970	.967	.961	.944	.857	.796	.673	.553	.465
.940	2.98	.971	.970	.963	.943	.857	.798	.674	.554	.466
.938	4.01	.971	.971	.963	.942	.856	.798	.673	.553	.466
.941	6.00	.972	.971	.963	.943	.854	.798	.672	.551	.469
.941	8.02	.975	.972	.965	.945	.855	.798	.671	.550	.471
.940	9.95	.978	.975	.968	.947	.856	.799	.671	.550	.473
1.202	1.50	.972	.967	.958	.951	.863	.800	.688	.587	.578
1.200	2.00	.968	.966	.959	.947	.859	.795	.674	.553	.463
1.201	2.99	.971	.969	.961	.945	.858	.797	.674	.553	.465
1.200	4.01	.970	.970	.962	.943	.857	.797	.673	.553	.465
1.201	5.99	.972	.971	.963	.943	.856	.798	.673	.552	.467
1.202	7.99	.972	.972	.963	.943	.855	.798	.672	.551	.469
1.200	9.99	.975	.973	.965	.945	.855	.798	.672	.550	.471

TABLE 2.- STATIC PRESSURES FOR LOW-EXPANSION-

RATIO NOZZLE, ROW 2

M_∞	$\frac{p_{t,j}}{p_\infty}$	$p/p_{t,j}$ for x/d of -	
		0.750	0.927
0.000	1.51	.851	.572
.000	1.99	.850	.559
.000	3.00	.848	.558
.000	4.01	.848	.557
.000	4.99	.849	.556
.000	6.00	.852	.556
.000	6.63	.855	.557
.602	1.49	.859	.644
.600	1.99	.850	.560
.601	3.00	.848	.558
.601	3.99	.848	.557
.602	5.99	.849	.556
.601	8.00	.853	.556
.802	1.52	.862	.657
.800	1.98	.851	.559
.800	2.99	.849	.559
.801	3.99	.848	.558
.800	5.99	.848	.556
.800	8.02	.850	.556
.800	9.84	.854	.557
.901	1.50	.859	.634
.901	1.97	.850	.558
.901	2.99	.848	.559
.901	4.02	.847	.558
.901	5.99	.847	.557
.899	8.01	.849	.556
.899	9.99	.852	.556
.940	1.49	.857	.609
.940	2.00	.850	.559
.940	2.98	.848	.559
.938	4.01	.847	.558
.941	6.00	.847	.557
.941	8.02	.849	.556
.940	9.95	.851	.556
1.202	1.50	.856	.591
1.200	2.00	.850	.558
1.201	2.99	.849	.559
1.200	4.01	.847	.559
1.201	5.99	.847	.558
1.202	7.99	.847	.556
1.200	9.99	.848	.556

TABLE 3.- STATIC PRESSURES FOR LOW-EXPANSION-RATIO NOZZLE, ROW 3

M_∞	$\frac{p_{t,j}}{p_\infty}$	$p/p_{t,j}$ for x/d of -		
		0.750	0.927	1.002
0.000	1.51	.857	.573	.659
.000	1.99	.857	.552	.497
.000	3.00	.329	.550	.329
.000	4.01	.246	.549	.246
.000	4.99	.198	.548	.198
.000	6.00	.165	.548	.165
.000	6.63	.149	.549	.149
.602	1.49	.864	.643	.678
.600	1.99	.857	.554	.498
.601	3.00	.334	.551	.334
.601	3.99	.255	.550	.255
.602	5.99	.172	.548	.172
.601	8.00	.128	.548	.128
.802	1.52	.868	.656	.677
.800	1.98	.859	.555	.507
.800	2.99	.342	.553	.342
.801	3.99	.262	.551	.262
.800	5.99	.176	.549	.176
.800	8.02	.130	.548	.130
.800	9.84	.106	.548	.106
.901	1.50	.864	.637	.669
.901	1.97	.857	.555	.498
.901	2.99	.335	.553	.335
.901	4.02	.255	.551	.255
.901	5.99	.174	.549	.174
.899	8.01	.131	.548	.131
.899	9.99	.105	.548	.105
.940	1.49	.862	.612	.650
.940	2.00	.858	.556	.475
.940	2.98	.321	.554	.321
.938	4.01	.243	.552	.243
.941	6.00	.165	.549	.165
.941	8.02	.127	.549	.127
.940	9.95	.103	.548	.103
1.202	1.50	.861	.591	.469
1.200	2.00	.270	.559	.270
1.201	2.99	.263	.555	.263
1.200	4.01	.228	.554	.228
1.201	5.99	.151	.551	.151
1.202	7.99	.115	.550	.115
1.200	9.99	.093	.549	.093

TABLE 4.- PRESSURE COEFFICIENTS FOR LOW-EXPANSION-RATIO NOZZLE, ROW 4

M_∞	$\frac{p_{t,j}}{p_\infty}$	C_p for x/d of -									
		-0.100	0.000	0.100	0.150	0.200	0.250	0.300	0.400	0.450	0.500
0.000	1.51	.003	.002	.002	.002	.001	.002	.002	.002	.002	.002
.000	1.99	.001	.000	.000	.000	.000	-.000	.000	.000	.001	.001
.000	3.00	.001	.000	-.000	-.000	.000	-.000	-.000	.000	.000	-.000
.000	4.01	.001	-.000	-.001	-.000	-.001	-.001	-.000	-.000	-.001	-.000
.000	4.99	.001	-.000	-.000	-.001	-.001	-.000	-.000	-.001	-.001	-.000
.000	6.00	.000	-.000	-.000	-.001	-.001	-.001	-.001	-.001	-.000	-.000
.000	6.63	.000	-.000	-.001	-.001	-.001	-.001	-.001	-.001	-.001	-.001
.602	1.49	-.188	-.288	-.434	-.451	-.447	-.437	-.406	-.347	-.248	-.186
.600	1.99	-.196	-.278	-.430	-.454	-.453	-.440	-.407	-.355	-.264	-.209
.601	3.00	-.187	-.279	-.427	-.439	-.457	-.443	-.422	-.354	-.257	-.199
.601	3.99	-.187	-.283	-.437	-.452	-.451	-.435	-.400	-.342	-.241	-.189
.602	5.99	-.182	-.272	-.418	-.436	-.432	-.413	-.385	-.319	-.213	-.156
.601	8.00	-.183	-.266	-.411	-.425	-.431	-.415	-.370	-.296	-.180	-.121
.802	1.52	-.198	-.284	-.518	-.570	-.586	-.579	-.487	-.398	-.306	-.227
.800	1.98	-.198	-.297	-.523	-.578	-.597	-.577	-.497	-.416	-.313	-.237
.800	2.99	-.202	-.299	-.532	-.591	-.611	-.586	-.498	-.408	-.307	-.230
.801	3.99	-.197	-.287	-.503	-.556	-.573	-.565	-.480	-.393	-.278	-.198
.800	5.99	-.192	-.277	-.481	-.534	-.548	-.521	-.439	-.342	-.234	-.158
.800	8.02	-.183	-.274	-.442	-.498	-.508	-.479	-.402	-.300	-.183	-.107
.800	9.84	-.182	-.261	-.437	-.484	-.496	-.444	-.354	-.260	-.132	-.066
.901	1.50	-.157	-.196	-.367	-.464	-.535	-.608	-.351	-.273	-.228	-.193
.901	1.97	-.153	-.195	-.341	-.427	-.506	-.586	-.365	-.300	-.248	-.213
.901	2.99	-.156	-.208	-.332	-.414	-.500	-.598	-.417	-.328	-.266	-.229
.901	4.02	-.156	-.198	-.328	-.412	-.496	-.624	-.401	-.328	-.264	-.228
.901	5.99	-.157	-.220	-.393	-.475	-.542	-.619	-.341	-.253	-.204	-.173
.899	8.01	-.151	-.200	-.340	-.421	-.510	-.536	-.271	-.203	-.159	-.126
.899	9.99	-.149	-.200	-.339	-.421	-.526	-.522	-.230	-.158	-.126	-.104
.940	1.49	-.130	-.157	-.246	-.329	-.412	-.506	-.372	-.308	-.255	-.220
.940	2.00	-.121	-.151	-.240	-.321	-.405	-.486	-.411	-.314	-.252	-.216
.940	2.98	-.129	-.161	-.259	-.340	-.418	-.530	-.543	-.424	-.341	-.283
.938	4.01	-.126	-.161	-.253	-.337	-.418	-.512	-.530	-.431	-.342	-.282
.941	6.00	-.126	-.157	-.258	-.338	-.412	-.504	-.521	-.387	-.308	-.262
.941	8.02	-.119	-.156	-.254	-.335	-.417	-.516	-.400	-.303	-.240	-.207
.940	9.95	-.123	-.155	-.261	-.343	-.420	-.496	-.311	-.221	-.190	-.165
1.202	1.50	-.045	-.056	-.182	-.220	-.249	-.363	-.418	-.469	-.509	-.525
1.200	2.00	-.047	-.056	-.182	-.222	-.256	-.360	-.421	-.463	-.488	-.502
1.201	2.99	-.044	-.059	-.182	-.217	-.245	-.360	-.419	-.443	-.482	-.505
1.200	4.01	-.039	-.056	-.174	-.216	-.240	-.358	-.417	-.442	-.484	-.506
1.201	5.99	-.037	-.053	-.149	-.198	-.239	-.350	-.415	-.435	-.460	-.400
1.202	7.99	-.038	-.048	-.129	-.177	-.219	-.337	-.418	-.436	-.365	-.310
1.200	9.99	-.037	-.047	-.119	-.165	-.210	-.318	-.416	-.405	-.327	-.276

TABLE 4.- Concluded

M_∞	$\frac{p_{t,j}}{p_\infty}$	C_p for x/d of -				
		0.550	0.600	0.800	0.900	1.002
0.000	1.51	.002	.002	.002	.001	-.006
0.000	1.99	.000	.000	.000	-.000	-.010
0.000	3.00	-.000	-.000	-.000	-.001	-.011
0.000	4.01	-.001	-.001	-.001	-.001	-.010
0.000	4.99	-.000	-.000	-.001	-.001	-.010
0.000	6.00	-.001	-.001	-.001	-.003	-.010
0.000	6.63	-.001	-.001	-.001	-.001	-.010
.602	1.49	-.122	-.067	.072	.104	.101
.600	1.99	-.150	-.103	.033	.053	.057
.601	3.00	-.145	-.105	.028	.055	.063
.601	3.99	-.131	-.088	.052	.082	.107
.602	5.99	-.096	-.042	.103	.133	.158
.601	8.00	-.067	-.014	.129	.154	.176
.802	1.52	-.160	-.107	.018	.060	.114
.800	1.98	-.164	-.106	.035	.057	.094
.800	2.99	-.158	-.103	.017	.054	.090
.801	3.99	-.130	-.080	.053	.076	.115
.800	5.99	-.091	-.041	.087	.109	.141
.800	8.02	-.045	-.003	.081	.105	.150
.800	9.84	-.016	.014	.092	.107	.159
.901	1.50	-.175	-.157	-.113	-.084	.025
.901	1.97	-.190	-.179	-.127	-.101	.015
.901	2.99	-.207	-.192	-.127	-.084	.011
.901	4.02	-.203	-.182	-.121	-.088	.012
.901	5.99	-.149	-.135	-.076	-.047	.028
.899	8.01	-.108	-.096	-.049	-.022	.043
.899	9.99	-.083	-.067	-.033	-.005	.062
.940	1.49	-.202	-.197	-.167	-.155	-.046
.940	2.00	-.202	-.195	-.190	-.181	-.061
.940	2.98	-.247	-.223	-.187	-.167	-.061
.938	4.01	-.247	-.229	-.187	-.168	-.061
.941	6.00	-.232	-.206	-.167	-.139	-.064
.941	8.02	-.191	-.184	-.153	-.120	-.054
.940	9.95	-.153	-.144	-.129	-.100	-.032
1.202	1.50	-.530	-.463	-.238	-.171	-.121
1.200	2.00	-.515	-.521	-.297	-.242	-.144
1.201	2.99	-.514	-.520	-.222	-.182	-.110
1.200	4.01	-.514	-.448	-.216	-.190	-.112
1.201	5.99	-.346	-.306	-.217	-.187	-.103
1.202	7.99	-.270	-.242	-.192	-.166	-.086
1.200	9.99	-.238	-.214	-.174	-.154	-.069

TABLE 5.- PRESSURE COEFFICIENTS FOR LOW-EXPANSION-RATIO NOZZLE, ROW 5

M_∞	$\frac{p_{t,j}}{p_\infty}$	C_p for x/d of -		
		0.000	0.150	0.800
0.000	1.51	.001	.002	.000
.000	1.99	.000	.000	-.002
.000	3.00	-.000	-.000	-.001
.000	4.01	.000	-.001	-.002
.000	4.99	-.000	-.000	-.002
.000	6.00	-.000	-.001	-.002
.000	6.63	-.000	-.001	-.001
.602	1.49	-.293	-.468	.012
.600	1.99	-.249	-.415	-.008
.601	3.00	-.249	-.420	.005
.601	3.99	-.249	-.417	.028
.602	5.99	-.245	-.404	.057
.601	8.00	-.230	-.383	.077
.802	1.52	-.261	-.531	-.187
.800	1.98	-.270	-.552	-.158
.800	2.99	-.272	-.552	-.136
.801	3.99	-.266	-.541	-.106
.800	5.99	-.242	-.521	-.075
.800	8.02	-.245	-.500	-.006
.800	9.84	-.238	-.468	-.010
.901	1.50	-.212	-.513	-.285
.901	1.97	-.212	-.517	-.255
.901	2.99	-.207	-.504	-.253
.901	4.02	-.177	-.519	-.233
.901	5.99	-.192	-.498	-.202
.899	8.01	-.183	-.486	-.180
.899	9.99	-.190	-.454	-.162
.940	1.49	-.186	-.361	-.359
.940	2.00	-.215	-.410	-.325
.940	2.98	-.181	-.437	-.345
.938	4.01	-.189	-.438	-.339
.941	6.00	-.180	-.416	-.328
.941	8.02	-.168	-.407	-.305
.940	9.95	-.179	-.416	-.303
1.202	1.50	-.047	-.230	-.226
1.200	2.00	-.046	-.227	-.215
1.201	2.99	-.047	-.228	-.190
1.200	4.01	-.051	-.228	-.066
1.201	5.99	-.050	-.224	-.068
1.202	7.99	-.051	-.219	-.083
1.200	9.99	-.058	-.176	-.088

TABLE 6.- PRESSURE COEFFICIENTS FOR LOW-EXPANSION-RATIO NOZZLE, ROW 6

M_∞	$\frac{p_{t,j}}{p_\infty}$	C_p for x/d of -							
		-0.100	0.000	0.100	0.300	0.500	1.002	1.224	1.400
0.000	1.51	.002	.001	.002	.001	.003	-.000	.003	.002
.000	1.99	.001	.000	.000	.000	.000	-.001	.001	-.000
.000	3.00	.000	.001	-.000	-.000	.001	-.001	.001	.000
.000	4.01	.001	.000	-.000	-.000	.000	-.002	.000	-.001
.000	4.99	.000	.001	.000	-.000	.000	-.002	-.001	-.002
.000	6.00	.000	.000	-.000	-.001	.000	-.002	-.002	-.002
.000	6.63	.000	-.000	-.000	-.000	-.000	-.002	-.002	-.003
.602	1.49	-.139	-.160	-.227	-.156	-.095	.026	.098	.118
.600	1.99	-.134	-.158	-.223	-.153	-.099	-.001	.090	.125
.601	3.00	-.135	-.185	-.238	-.156	-.099	-.007	.069	.120
.601	3.99	-.135	-.187	-.242	-.155	-.095	-.007	.037	.108
.602	5.99	-.129	-.179	-.231	-.158	-.100	-.035	-.056	-.077
.601	8.00	-.122	-.176	-.234	-.144	-.093	-.073	-.101	-.190
.802	1.52	-.148	-.224	-.301	-.194	-.123	-.071	.114	.168
.800	1.98	-.156	-.231	-.308	-.203	-.123	-.039	.116	.159
.800	2.99	-.144	-.225	-.301	-.201	-.133	-.051	.103	.154
.801	3.99	-.154	-.225	-.303	-.200	-.122	-.018	.063	.145
.800	5.99	-.137	-.215	-.294	-.186	-.109	-.032	-.018	-.029
.800	8.02	-.133	-.200	-.280	-.177	-.096	-.023	-.047	-.136
.800	9.84	-.134	-.208	-.282	-.160	-.082	-.034	-.081	-.215
.901	1.50	-.130	-.186	-.348	-.330	-.151	-.046	.100	.156
.901	1.97	-.128	-.185	-.349	-.333	-.154	-.095	.096	.166
.901	2.99	-.124	-.214	-.357	-.352	-.171	-.088	.097	.166
.901	4.02	-.130	-.223	-.362	-.355	-.177	-.085	.069	.175
.901	5.99	-.119	-.218	-.359	-.309	-.139	-.038	.016	.044
.899	8.01	-.124	-.223	-.369	-.272	-.119	-.076	-.035	-.081
.899	9.99	-.128	-.220	-.368	-.242	-.101	-.058	-.054	-.181
.940	1.49	-.095	-.186	-.317	-.362	-.309	-.168	.073	.138
.940	2.00	-.101	-.176	-.305	-.362	-.345	-.179	.050	.142
.940	2.98	-.124	-.193	-.322	-.367	-.369	-.168	.084	.168
.938	4.01	-.110	-.159	-.313	-.364	-.353	-.145	.070	.178
.941	6.00	-.115	-.181	-.319	-.359	-.340	-.176	.010	.065
.941	8.02	-.120	-.150	-.320	-.358	-.308	-.154	-.011	.002
.940	9.95	-.097	-.155	-.328	-.355	-.244	-.104	-.044	-.138
1.202	1.50	-.039	-.047	-.138	-.180	-.169	-.201	-.220	.002
1.200	2.00	-.044	-.054	-.142	-.185	-.170	-.207	-.336	-.033
1.201	2.99	-.042	-.052	-.136	-.183	-.173	-.201	-.275	-.120
1.200	4.01	-.041	-.048	-.141	-.182	-.174	-.195	-.178	-.183
1.201	5.99	-.049	-.050	-.138	-.181	-.174	-.173	-.127	-.172
1.202	7.99	-.040	-.052	-.141	-.183	-.171	-.141	-.110	-.167
1.200	9.99	-.045	-.054	-.144	-.179	-.171	-.089	-.097	-.163

TABLE 7.- PRESSURE COEFFICIENTS FOR LOW-EXPANSION-RATIO NOZZLE, ROW 7

M_∞	$\frac{p_{t,j}}{p_\infty}$	C_p for x/d of -		
		0.150	0.500	0.800
0.000	1.51	.002	.002	.002
.000	1.99	.001	.001	.000
.000	3.00	.000	.000	-.000
.000	4.01	.000	.000	.000
.000	4.99	.000	-.000	-.000
.000	6.00	-.000	.000	-.000
.000	6.63	-.000	.000	-.001
.602	1.49	-.226	-.120	-.035
.600	1.99	-.224	-.121	-.038
.601	3.00	-.226	-.130	-.052
.601	3.99	-.225	-.123	-.048
.602	5.99	-.215	-.116	-.040
.601	8.00	-.214	-.096	-.015
.802	1.52	-.279	-.147	-.026
.800	1.98	-.297	-.150	-.026
.800	2.99	-.287	-.150	-.036
.801	3.99	-.275	-.137	-.027
.800	5.99	-.280	-.129	-.019
.800	8.02	-.275	-.106	.004
.800	9.84	-.251	-.092	.005
.901	1.50	-.403	-.157	-.049
.901	1.97	-.404	-.184	-.065
.901	2.99	-.402	-.193	-.064
.901	4.02	-.396	-.174	-.053
.901	5.99	-.402	-.153	-.039
.899	8.01	-.386	-.126	-.029
.899	9.99	-.384	-.104	-.025
.940	1.49	-.362	-.322	-.081
.940	2.00	-.369	-.347	-.093
.940	2.98	-.360	-.380	-.126
.938	4.01	-.371	-.364	-.099
.941	6.00	-.365	-.355	-.107
.941	8.02	-.366	-.330	-.130
.940	9.95	-.361	-.213	-.077
1.202	1.50	-.179	-.193	-.274
1.200	2.00	-.176	-.194	-.278
1.201	2.99	-.173	-.193	-.275
1.200	4.01	-.175	-.197	-.274
1.201	5.99	-.178	-.192	-.272
1.202	7.99	-.183	-.195	-.238
1.200	9.99	-.179	-.194	-.219

TABLE 8.- PRESSURE COEFFICIENTS FOR LOW-EXPANSION-RATIO NOZZLE, ROW 8

M_∞	$\frac{p_{t,j}}{p_\infty}$	C_p for x/d of -								
		0.000	0.100	0.200	0.300	0.400	0.500	0.600	0.800	1.200
0.000	1.51	-.000	-.000	-.000	.002	.001	.001	.001	.001	.000
.000	1.99	-.000	-.000	-.000	.001	.000	.000	.000	-.000	-.001
.000	3.00	-.001	-.001	-.001	.000	-.000	-.000	-.000	-.001	-.002
.000	4.01	-.001	-.001	-.001	-.000	-.001	-.001	-.001	-.001	-.003
.000	4.99	-.001	-.001	-.001	-.000	-.000	-.001	-.001	-.001	-.003
.000	6.00	-.001	-.001	-.001	.000	-.001	-.001	-.001	-.001	-.002
.000	6.63	-.001	-.001	-.001	-.001	-.001	-.001	-.001	-.001	-.003
.602	1.49	-.174	-.227	-.268	-.314	-.431	-.512	-.337	-.106	.021
.600	1.99	-.176	-.230	-.272	-.317	-.438	-.526	-.344	-.126	-.006
.601	3.00	-.177	-.231	-.273	-.325	-.452	-.532	-.333	-.121	-.005
.601	3.99	-.176	-.229	-.271	-.313	-.449	-.519	-.326	-.101	.026
.602	5.99	-.171	-.223	-.262	-.300	-.412	-.481	-.292	-.048	.058
.601	8.00	-.167	-.218	-.255	-.292	-.397	-.437	-.255	-.013	.066
.802	1.52	-.212	-.293	-.354	-.382	-.532	-.539	-.311	-.084	.040
.800	1.98	-.213	-.294	-.356	-.383	-.522	-.537	-.322	-.106	.024
.800	2.99	-.214	-.294	-.356	-.381	-.516	-.538	-.321	-.095	.024
.801	3.99	-.211	-.291	-.351	-.382	-.509	-.523	-.313	-.081	.046
.800	5.99	-.204	-.281	-.335	-.351	-.486	-.474	-.252	-.029	.079
.800	8.02	-.198	-.271	-.322	-.339	-.435	-.426	-.202	.011	.067
.800	9.84	-.192	-.261	-.307	-.317	-.412	-.364	-.151	.050	.055
.901	1.50	-.192	-.302	-.428	-.514	-.481	-.258	-.185	-.097	-.002
.901	1.97	-.193	-.303	-.429	-.516	-.554	-.278	-.207	-.118	-.028
.901	2.99	-.193	-.303	-.429	-.519	-.588	-.287	-.209	-.113	-.025
.901	4.02	-.193	-.303	-.429	-.520	-.563	-.287	-.208	-.104	-.000
.901	5.99	-.192	-.301	-.426	-.498	-.453	-.251	-.171	-.079	.020
.899	8.01	-.191	-.301	-.424	-.483	-.364	-.218	-.135	-.045	.031
.899	9.99	-.189	-.298	-.419	-.452	-.307	-.180	-.092	-.006	.037
.940	1.49	-.159	-.262	-.384	-.461	-.531	-.210	-.167	-.125	-.055
.940	2.00	-.159	-.262	-.384	-.467	-.630	-.291	-.221	-.166	-.107
.940	2.98	-.159	-.261	-.384	-.443	-.596	-.291	-.198	-.143	-.081
.938	4.01	-.160	-.263	-.386	-.468	-.664	-.331	-.221	-.158	-.083
.941	6.00	-.156	-.259	-.381	-.471	-.642	-.294	-.202	-.142	-.066
.941	8.02	-.156	-.259	-.381	-.466	-.566	-.246	-.163	-.100	-.024
.940	9.95	-.156	-.260	-.382	-.469	-.548	-.182	-.144	-.084	-.007
1.202	1.50	-.038	-.090	-.165	-.233	-.387	-.610	-.604	-.538	-.393
1.200	2.00	-.038	-.091	-.167	-.231	-.387	-.606	-.608	-.538	-.475
1.201	2.99	-.039	-.091	-.166	-.232	-.383	-.604	-.608	-.540	-.386
1.200	4.01	-.039	-.091	-.167	-.230	-.386	-.605	-.606	-.529	-.244
1.201	5.99	-.038	-.090	-.166	-.233	-.384	-.596	-.604	-.351	-.153
1.202	7.99	-.038	-.090	-.165	-.231	-.385	-.593	-.564	-.239	-.131
1.200	9.99	-.039	-.091	-.167	-.235	-.385	-.591	-.471	-.170	-.121

TABLE 9.- STATIC PRESSURES FOR LOW-EXPANSION-RATIO NOZZLE, ROW 9

M_∞	$\frac{p_{t,j}}{p_\infty}$	$p/p_{t,j}$ for x/d of -				
		0.750	0.920	1.002	1.200	1.400
0.000	1.51	.853	.544	.637	.665	.665
.000	1.99	.856	.529	.405	.505	.504
.000	3.00	.310	.340	.400	.310	.340
.000	4.01	.398	.235	.249	.235	.249
.000	4.99	.396	.179	.191	.179	.191
.000	6.00	.395	.134	.152	.134	.152
.000	6.63	.395	.108	.134	.108	.134
.602	1.49	.858	.624	.671	.688	.697
.600	1.99	.852	.531	.408	.517	.524
.601	3.00	.315	.343	.401	.315	.343
.601	3.99	.400	.219	.251	.219	.251
.602	5.99	.397	.133	.161	.133	.161
.601	8.00	.395	.102	.097	.102	.097
.802	1.52	.860	.638	.679	.700	.712
.800	1.98	.852	.535	.456	.534	.546
.800	2.99	.335	.344	.402	.335	.344
.801	3.99	.222	.264	.401	.222	.264
.800	5.99	.398	.135	.163	.135	.163
.800	8.02	.396	.100	.092	.100	.092
.800	9.84	.395	.101	.083	.101	.083
.901	1.50	.855	.617	.668	.719	.731
.901	1.97	.850	.530	.459	.549	.561
.901	2.99	.347	.347	.402	.347	.347
.901	4.02	.223	.271	.402	.223	.271
.901	5.99	.399	.134	.150	.134	.150
.899	8.01	.397	.099	.093	.099	.093
.899	9.99	.395	.098	.081	.098	.081
.940	1.49	.852	.588	.643	.712	.726
.940	2.00	.851	.531	.413	.539	.552
.940	2.98	.398	.321	.340	.321	.340
.938	4.01	.398	.231	.271	.231	.271
.941	6.00	.395	.132	.154	.132	.154
.941	8.02	.395	.099	.093	.099	.093
.940	9.95	.395	.098	.082	.098	.082
1.202	1.50	.852	.561	.528	.648	.686
1.200	2.00	.394	.528	.394	.486	.510
1.201	2.99	.398	.246	.298	.246	.298
1.200	4.01	.399	.176	.182	.176	.182
1.201	5.99	.399	.103	.100	.103	.100
1.202	7.99	.397	.094	.083	.094	.083
1.200	9.99	.396	.093	.080	.093	.080

TABLE 10.- STATIC PRESSURES FOR LOW-EXPANSION-RATIO NOZZLE, ROW 10

M_∞	$\frac{p_{t,j}}{p_\infty}$	$p/p_{t,j}$ for x/d of -									
		0.573	0.591	0.650	0.700	0.750	0.800	0.850	0.912	0.950	1.002
0.000	1.51	.999	.968	.933	.890	.830	.746	.628	.461	.570	.641
.000	1.99	.391	.968	.934	.891	.831	.747	.627	.460	.426	.391
.000	3.00	.390	.341	.245	.268	.281	.313	.367	.459	.427	.390
.000	4.01	.389	.339	.247	.158	.129	.144	.153	.301	.426	.389
.000	4.99	.388	.339	.247	.160	.111	.080	.089	.175	.425	.388
.000	6.00	.388	.339	.249	.163	.113	.081	.067	.130	.424	.388
.000	6.63	.388	.340	.250	.164	.114	.082	.062	.125	.425	.388
.602	1.49	.997	.971	.934	.895	.838	.757	.653	.570	.635	.680
.600	1.99	.396	.968	.933	.891	.830	.745	.628	.460	.430	.396
.601	3.00	.392	.342	.251	.287	.307	.355	.342	.460	.430	.392
.601	3.99	.391	.340	.245	.157	.149	.162	.172	.303	.429	.391
.602	5.99	.389	.339	.247	.161	.112	.081	.095	.142	.426	.389
.601	8.00	.388	.339	.249	.164	.115	.082	.062	.111	.425	.388
.802	1.52	.999	.973	.935	.899	.842	.762	.663	.590	.641	.688
.800	1.98	1.000	.971	.933	.893	.832	.746	.629	.462	.431	.471
.800	2.99	.393	.342	.264	.307	.336	.332	.628	.461	.432	.393
.801	3.99	.392	.340	.246	.157	.158	.173	.188	.314	.430	.392
.800	5.99	.389	.338	.245	.160	.111	.080	.124	.148	.427	.389
.800	8.02	.388	.338	.247	.162	.114	.082	.061	.112	.425	.388
.800	9.84	.388	.339	.250	.166	.115	.083	.063	.070	.425	.388
.901	1.50	.998	.972	.933	.890	.839	.756	.653	.562	.608	.671
.901	1.97	.998	.969	.931	.887	.831	.744	.626	.461	.430	.450
.901	2.99	.392	.342	.249	.272	.326	.337	.627	.461	.431	.392
.901	4.02	.392	.340	.244	.156	.132	.153	.237	.313	.431	.392
.901	5.99	.390	.339	.246	.160	.112	.081	.157	.156	.428	.390
.899	8.01	.388	.338	.247	.162	.113	.082	.062	.111	.426	.388
.899	9.99	.387	.338	.248	.163	.115	.083	.063	.071	.425	.387
.940	1.49	.995	.970	.931	.883	.834	.750	.643	.534	.569	.651
.940	2.00	.998	.969	.932	.885	.831	.744	.627	.462	.430	.404
.940	2.98	.393	.343	.248	.249	.288	.344	.627	.462	.432	.393
.938	4.01	.393	.341	.244	.156	.118	.215	.250	.277	.431	.393
.941	6.00	.390	.339	.245	.160	.111	.083	.162	.159	.428	.390
.941	8.02	.388	.338	.246	.162	.113	.082	.062	.108	.426	.388
.940	9.95	.388	.339	.248	.163	.114	.083	.063	.075	.425	.388
1.202	1.50	.996	.976	.937	.878	.840	.751	.641	.512	.518	.599
1.200	2.00	.396	.971	.933	.880	.832	.744	.627	.464	.429	.396
1.201	2.99	.392	.340	.247	.204	.259	.293	.308	.326	.430	.392
1.200	4.01	.391	.340	.243	.158	.111	.099	.140	.207	.430	.391
1.201	5.99	.391	.339	.243	.160	.112	.080	.105	.138	.430	.391
1.202	7.99	.389	.338	.243	.160	.112	.081	.061	.089	.428	.389
1.200	9.99	.388	.339	.245	.161	.113	.082	.062	.069	.427	.388

TABLE 10.- Concluded

M_∞	$\frac{p_{t,j}}{p_\infty}$	$p/p_{t,j}$ for x/d of -							
		1.050	1.100	1.155	1.200	1.250	1.300	1.400	1.500
0.000	1.51	.657	.665	.667	.667	.665	.666	.667	.679
.000	1.99	.545	.511	.509	.505	.503	.504	.503	.513
.000	3.00	.341	.245	.268	.281	.313	.435	.367	.267
.000	4.01	.339	.247	.158	.129	.144	.153	.301	.362
.000	4.99	.339	.247	.160	.111	.080	.089	.175	.201
.000	6.00	.339	.249	.163	.113	.081	.067	.130	.131
.000	6.63	.340	.250	.164	.114	.082	.062	.125	.124
.602	1.49	.693	.698	.701	.702	.701	.703	.693	.721
.600	1.99	.556	.532	.531	.527	.526	.528	.519	.546
.601	3.00	.342	.251	.287	.307	.355	.437	.342	.291
.601	3.99	.340	.245	.157	.149	.162	.172	.303	.384
.602	5.99	.339	.247	.161	.112	.081	.095	.142	.139
.601	8.00	.339	.249	.164	.115	.082	.062	.111	.105
.802	1.52	.701	.708	.710	.712	.714	.716	.694	.736
.800	1.98	.568	.555	.556	.554	.552	.553	.536	.575
.800	2.99	.342	.264	.307	.336	.442	.444	.332	.328
.801	3.99	.340	.246	.157	.158	.173	.188	.314	.380
.800	5.99	.338	.245	.160	.111	.080	.124	.148	.148
.800	8.02	.338	.247	.162	.114	.082	.061	.112	.107
.800	9.84	.339	.250	.166	.115	.083	.063	.070	.081
.901	1.50	.686	.698	.715	.724	.730	.738	.707	.762
.901	1.97	.553	.539	.547	.554	.563	.569	.549	.594
.901	2.99	.342	.249	.272	.326	.477	.443	.337	.416
.901	4.02	.340	.244	.156	.132	.153	.237	.313	.310
.901	5.99	.339	.246	.160	.112	.081	.157	.156	.162
.899	8.01	.338	.247	.162	.113	.082	.062	.111	.109
.899	9.99	.338	.248	.163	.115	.083	.063	.071	.084
.940	1.49	.661	.686	.706	.715	.724	.736	.704	.770
.940	2.00	.525	.502	.514	.525	.534	.546	.539	.587
.940	2.98	.343	.248	.249	.288	.444	.457	.344	.424
.938	4.01	.341	.244	.156	.118	.215	.250	.277	.323
.941	6.00	.339	.245	.160	.111	.083	.162	.159	.164
.941	8.02	.338	.246	.162	.113	.082	.062	.108	.107
.940	9.95	.339	.248	.163	.114	.083	.063	.075	.089
1.202	1.50	.640	.651	.673	.683	.699	.704	.682	.728
1.200	2.00	.421	.514	.518	.495	.513	.527	.524	.595
1.201	2.99	.340	.247	.204	.259	.293	.308	.326	.475
1.200	4.01	.340	.243	.158	.111	.099	.140	.207	.315
1.201	5.99	.339	.243	.160	.112	.080	.105	.138	.132
1.202	7.99	.338	.243	.160	.112	.081	.061	.089	.091
1.200	9.99	.339	.245	.161	.113	.082	.062	.069	.033

TABLE 11.- STATIC PRESSURES FOR LOW-EXPANSION-RATIO NOZZLE, ROW 11

M_∞	$\frac{p_{t,j}}{p_\infty}$	$p/p_{t,j}$ for x/d of -					
		0.912	1.002	1.050	1.100	1.155	1.200
0.000	1.51	.468	.642	.658	.664	.666	.666
.000	1.99	.397	.397	.549	.511	.507	.504
.000	3.00	.397	.342	.242	.273	.284	.284
.000	4.01	.395	.343	.248	.155	.129	.129
.000	4.99	.394	.343	.247	.157	.112	.112
.000	6.00	.394	.344	.246	.160	.114	.114
.000	6.63	.395	.344	.249	.161	.115	.115
.602	1.49	.573	.682	.695	.698	.699	.701
.600	1.99	.462	.407	.563	.532	.528	.527
.601	3.00	.398	.343	.246	.285	.308	.308
.601	3.99	.397	.344	.247	.153	.150	.150
.602	5.99	.395	.344	.245	.158	.112	.112
.601	8.00	.394	.344	.248	.161	.115	.115
.802	1.52	.591	.692	.704	.708	.711	.712
.800	1.98	.463	.465	.574	.554	.550	.551
.800	2.99	.344	.263	.306	.341	.306	.341
.801	3.99	.398	.344	.248	.154	.164	.164
.800	5.99	.395	.344	.244	.158	.112	.112
.800	8.02	.395	.344	.246	.159	.114	.114
.800	9.84	.395	.345	.249	.161	.116	.116
.901	1.50	.564	.676	.689	.703	.714	.724
.901	1.97	.462	.453	.561	.541	.549	.558
.901	2.99	.399	.343	.249	.283	.334	.334
.901	4.02	.398	.343	.246	.155	.133	.133
.901	5.99	.396	.344	.243	.157	.111	.111
.899	8.01	.395	.344	.246	.159	.114	.114
.899	9.99	.395	.344	.248	.161	.115	.115
.940	1.49	.536	.654	.663	.685	.695	.710
.940	2.00	.465	.412	.531	.505	.511	.524
.940	2.98	.399	.343	.249	.244	.279	.279
.938	4.01	.398	.344	.245	.154	.116	.116
.941	6.00	.396	.344	.244	.158	.111	.111
.941	8.02	.395	.344	.244	.159	.113	.113
.940	9.95	.394	.344	.246	.160	.115	.115
1.202	1.50	.512	.600	.642	.660	.663	.676
1.200	2.00	.463	.402	.417	.517	.505	.500
1.201	2.99	.398	.340	.254	.225	.273	.273
1.200	4.01	.399	.342	.246	.156	.110	.110
1.201	5.99	.397	.343	.239	.157	.111	.111
1.202	7.99	.395	.343	.239	.157	.112	.112
1.200	9.99	.395	.343	.243	.160	.114	.114

TABLE 12.- STATIC PRESSURES FOR LOW-EXPANSION-RATIO NOZZLE, ROW 12

M_∞	$\frac{p_{t,j}}{p_\infty}$	$p/p_{t,j}$ for x/d of -											
		0.591	0.650	0.750	0.850	0.950	1.002	1.050	1.100	1.155	1.200	1.300	1.500
0.000	1.51	.976	.937	.830	.625	.570	.644	.659	.665	.666	.667	.666	.677
.000	1.99	.977	.938	.833	.626	.431	.400	.548	.513	.509	.505	.506	.510
.000	3.00	.400	.346	.246	.271	.278	.400	.346	.246	.271	.278	.447	.278
.000	4.01	.398	.345	.247	.154	.129	.151	.345	.247	.154	.129	.151	.371
.000	4.99	.397	.345	.248	.155	.109	.082	.345	.248	.155	.109	.082	.200
.000	6.00	.396	.345	.250	.157	.111	.061	.345	.250	.157	.111	.061	.122
.000	6.63	.397	.345	.251	.158	.112	.062	.345	.251	.158	.112	.062	.109
.602	1.49	.974	.938	.838	.650	.632	.683	.694	.698	.699	.700	.701	.718
.600	1.99	.975	.937	.832	.626	.432	.408	.560	.533	.528	.527	.526	.542
.601	3.00	.346	.252	.282	.300	.431	.402	.346	.252	.282	.300	.442	.289
.601	3.99	.400	.346	.244	.153	.151	.169	.346	.244	.153	.151	.169	.379
.602	5.99	.398	.345	.246	.155	.109	.150	.345	.246	.155	.109	.150	.154
.601	8.00	.396	.345	.250	.158	.113	.062	.345	.250	.158	.113	.062	.094
.802	1.52	.974	.939	.842	.661	.640	.692	.703	.707	.710	.711	.713	.734
.800	1.98	.975	.938	.833	.628	.433	.486	.572	.554	.553	.549	.549	.570
.800	2.99	.348	.278	.303	.335	.433	.403	.348	.278	.303	.335	.448	.329
.801	3.99	.347	.245	.155	.166	.185	.401	.347	.245	.155	.166	.185	.369
.800	5.99	.399	.346	.245	.156	.109	.155	.346	.245	.156	.109	.155	.162
.800	8.02	.397	.345	.248	.157	.111	.062	.345	.248	.157	.111	.062	.094
.800	9.84	.397	.345	.251	.158	.113	.063	.345	.251	.158	.113	.063	.073
.901	1.50	.973	.936	.838	.651	.610	.678	.693	.706	.714	.721	.735	.760
.901	1.97	.974	.936	.832	.626	.430	.462	.562	.543	.548	.559	.569	.592
.901	2.99	.347	.248	.287	.332	.431	.401	.347	.248	.287	.332	.442	.456
.901	4.02	.347	.242	.155	.137	.201	.401	.347	.242	.155	.137	.201	.318
.901	5.99	.399	.346	.244	.155	.109	.126	.346	.244	.155	.109	.126	.150
.899	8.01	.398	.345	.247	.156	.111	.062	.345	.247	.156	.111	.062	.096
.899	9.99	.396	.345	.250	.158	.112	.062	.345	.250	.158	.112	.062	.077
.940	1.49	.972	.933	.835	.643	.570	.655	.669	.679	.699	.712	.733	.767
.940	2.00	.975	.935	.832	.626	.429	.409	.533	.514	.523	.536	.557	.589
.940	2.98	.347	.243	.238	.272	.431	.402	.347	.243	.238	.272	.463	.445
.938	4.01	.347	.240	.154	.115	.238	.401	.347	.240	.154	.115	.238	.307
.941	6.00	.399	.346	.244	.156	.109	.143	.346	.244	.156	.109	.143	.152
.941	8.02	.397	.345	.246	.156	.111	.062	.345	.246	.156	.111	.062	.090
.940	9.95	.397	.345	.249	.157	.113	.068	.345	.249	.157	.113	.068	.080
1.202	1.50	.975	.935	.835	.639	.513	.591	.643	.644	.656	.665	.694	.740
1.200	2.00	.398	.935	.832	.625	.427	.398	.411	.487	.509	.483	.510	.586
1.201	2.99	.399	.346	.243	.264	.262	.261	.346	.243	.264	.262	.261	.427
1.200	4.01	.400	.346	.238	.157	.109	.153	.346	.238	.157	.109	.153	.280
1.201	5.99	.399	.346	.240	.156	.108	.061	.346	.240	.156	.108	.061	.119
1.202	7.99	.398	.345	.242	.155	.110	.062	.345	.242	.155	.110	.062	.080
1.200	9.99	.398	.345	.246	.156	.111	.062	.345	.246	.156	.111	.062	.029

TABLE 13.- STATIC PRESSURES FOR LOW-EXPANSION-RATIO NOZZLE, ROW 13

M_∞	$\frac{p_{t,j}}{p_\infty}$	$p/p_{t,j}$ for x/d of -					
		0.912	1.002	1.050	1.100	1.155	1.200
0.000	1.51	.460	.644	.659	.666	.667	.666
.000	1.99	.451	.402	.549	.512	.509	.503
.000	3.00	.348	.242	.270	.285	.270	.285
.000	4.01	.398	.348	.249	.151	.131	.131
.000	4.99	.396	.348	.248	.154	.108	.108
.000	6.00	.395	.348	.248	.156	.109	.109
.000	6.63	.396	.349	.249	.157	.110	.110
.602	1.49	.566	.681	.693	.694	.695	.694
.600	1.99	.452	.419	.560	.528	.524	.520
.601	3.00	.349	.253	.278	.293	.278	.293
.601	3.99	.349	.247	.150	.156	.150	.156
.602	5.99	.397	.348	.245	.154	.108	.108
.601	8.00	.396	.349	.247	.156	.110	.110
.802	1.52	.584	.691	.701	.703	.705	.704
.800	1.98	.453	.469	.570	.548	.544	.542
.800	2.99	.351	.292	.301	.316	.301	.316
.801	3.99	.350	.246	.153	.169	.153	.169
.800	5.99	.398	.348	.244	.153	.108	.108
.800	8.02	.396	.348	.246	.156	.110	.110
.800	9.84	.396	.349	.248	.157	.111	.111
.901	1.50	.558	.681	.697	.704	.713	.719
.901	1.97	.451	.463	.566	.544	.550	.553
.901	2.99	.349	.263	.286	.321	.286	.321
.901	4.02	.348	.245	.151	.155	.151	.155
.901	5.99	.399	.348	.243	.153	.107	.107
.899	8.01	.397	.348	.246	.155	.109	.109
.899	9.99	.396	.348	.247	.156	.111	.111
.940	1.49	.525	.660	.674	.689	.703	.713
.940	2.00	.450	.417	.544	.521	.525	.533
.940	2.98	.350	.245	.256	.284	.256	.284
.938	4.01	.348	.244	.151	.126	.151	.126
.941	6.00	.399	.348	.243	.154	.108	.108
.941	8.02	.396	.348	.245	.155	.109	.109
.940	9.95	.396	.348	.245	.155	.110	.110
1.202	1.50	.483	.572	.631	.630	.635	.659
1.200	2.00	.398	.379	.379	.464	.473	.479
1.201	2.99	.399	.348	.249	.253	.237	.237
1.200	4.01	.349	.243	.153	.144	.153	.144
1.201	5.99	.398	.347	.239	.154	.107	.107
1.202	7.99	.397	.347	.241	.155	.109	.109
1.200	9.99	.395	.348	.242	.155	.110	.110

TABLE 14.- STATIC PRESSURES FOR LOW-EXPANSION-RATIO NOZZLE, ROW 14

M_∞	$\frac{p_{t,j}}{p_\infty}$	$p/p_{t,j}$ for x/d of -									
		0.573	0.591	0.650	0.750	0.850	0.912	0.950	1.002	1.050	1.100
0.000	1.51	.997	.975	.934	.828	.633	.483	.573	.638	.660	.666
.000	1.99	.997	.976	.934	.830	.631	.467	.428	.407	.528	.513
.000	3.00	.398	.350	.248	.265	.293	.387	.426	.398	.350	.248
.000	4.01	.395	.349	.242	.151	.135	.263	.424	.395	.349	.242
.000	4.99	.393	.349	.242	.153	.105	.159	.423	.393	.349	.242
.000	6.00	.392	.347	.244	.154	.107	.081	.423	.392	.347	.244
.000	6.63	.392	.347	.245	.154	.108	.070	.423	.392	.347	.245
.602	1.49	.998	.974	.939	.833	.658	.577	.630	.674	.687	.691
.600	1.99	.997	.974	.935	.827	.633	.466	.428	.435	.537	.526
.601	3.00	.399	.349	.270	.270	.288	.466	.427	.399	.349	.270
.601	3.99	.397	.349	.241	.150	.147	.220	.426	.397	.349	.241
.602	5.99	.394	.348	.242	.151	.113	.157	.424	.394	.348	.242
.601	8.00	.392	.347	.245	.153	.114	.063	.422	.392	.347	.245
.802	1.52	.999	.975	.940	.836	.669	.592	.641	.683	.694	.698
.800	1.98	.998	.976	.937	.828	.635	.466	.431	.504	.553	.544
.800	2.99	.399	.348	.304	.289	.315	.467	.429	.399	.348	.304
.801	3.99	.398	.349	.239	.158	.162	.219	.428	.398	.349	.239
.800	5.99	.394	.348	.238	.151	.114	.161	.425	.394	.348	.238
.800	8.02	.392	.347	.242	.151	.117	.061	.424	.392	.347	.242
.800	9.84	.391	.346	.246	.155	.118	.065	.423	.391	.346	.246
.901	1.50	.998	.975	.939	.832	.660	.570	.622	.675	.691	.703
.901	1.97	.997	.975	.936	.826	.632	.465	.428	.490	.547	.542
.901	2.99	.397	.343	.285	.279	.322	.467	.427	.397	.343	.285
.901	4.02	.396	.344	.235	.153	.153	.241	.427	.396	.344	.235
.901	5.99	.393	.342	.235	.149	.114	.073	.425	.393	.342	.235
.899	8.01	.390	.345	.241	.149	.114	.062	.423	.390	.345	.241
.899	9.99	.390	.345	.242	.153	.118	.061	.423	.390	.345	.242
.940	1.49	.996	.975	.936	.828	.649	.534	.578	.653	.671	.688
.940	2.00	.997	.977	.935	.826	.634	.464	.418	.412	.522	.522
.940	2.98	.399	.343	.243	.254	.293	.466	.421	.399	.343	.243
.938	4.01	.395	.342	.238	.155	.142	.251	.421	.395	.342	.238
.941	6.00	.394	.341	.239	.152	.115	.099	.426	.394	.341	.239
.941	8.02	.393	.342	.239	.157	.117	.061	.421	.393	.342	.239
.940	9.95	.389	.341	.239	.153	.120	.062	.421	.389	.341	.239
1.202	1.50	.998	.976	.936	.828	.648	.501	.498	.553	.611	.625
1.200	2.00	.395	.362	.935	.826	.636	.460	.422	.395	.362	.458
1.201	2.99	.396	.344	.238	.247	.229	.244	.423	.396	.344	.238
1.200	4.01	.396	.344	.238	.154	.147	.126	.423	.396	.344	.238
1.201	5.99	.395	.344	.238	.154	.119	.064	.422	.395	.344	.238
1.202	7.99	.392	.343	.242	.154	.120	.063	.423	.392	.343	.242
1.200	9.99	.391	.341	.243	.154	.120	.063	.417	.391	.341	.243

TABLE 14.- Concluded

M_∞	$\frac{p_{t,j}}{p_\infty}$	$p/p_{t,j}$ for x/d of -			
		1.155	1.200	1.300	1.500
0.000	1.51	.667	.666	.666	.670
.000	1.99	.507	.506	.504	.506
.000	3.00	.265	.293	.387	.315
.000	4.01	.151	.135	.263	.264
.000	4.99	.153	.105	.159	.205
.000	6.00	.154	.107	.081	.177
.000	6.63	.154	.108	.070	.160
.602	1.49	.691	.691	.696	.708
.600	1.99	.517	.516	.518	.534
.601	3.00	.270	.288	.404	.336
.601	3.99	.150	.147	.220	.289
.602	5.99	.151	.113	.157	.169
.601	8.00	.153	.114	.063	.107
.802	1.52	.699	.701	.707	.721
.800	1.98	.538	.539	.541	.558
.800	2.99	.289	.315	.417	.380
.801	3.99	.158	.162	.219	.291
.800	5.99	.151	.114	.161	.170
.800	8.02	.151	.117	.061	.101
.800	9.84	.155	.118	.065	.082
.901	1.50	.707	.712	.725	.746
.901	1.97	.543	.547	.557	.575
.901	2.99	.279	.322	.427	.420
.901	4.02	.153	.153	.241	.272
.901	5.99	.149	.114	.073	.131
.899	8.01	.149	.114	.062	.100
.899	9.99	.153	.118	.061	.075
.940	1.49	.696	.707	.724	.747
.940	2.00	.530	.534	.545	.566
.940	2.98	.254	.293	.423	.413
.938	4.01	.155	.142	.251	.272
.941	6.00	.152	.115	.099	.153
.941	8.02	.157	.117	.061	.095
.940	9.95	.153	.120	.062	.077
1.202	1.50	.642	.647	.690	.709
1.200	2.00	.456	.484	.495	.562
1.201	2.99	.247	.229	.244	.341
1.200	4.01	.154	.147	.126	.223
1.201	5.99	.154	.119	.064	.098
1.202	7.99	.154	.120	.063	.074
1.200	9.99	.154	.120	.063	.061

TABLE 15.- STATIC PRESSURES FOR HIGH-EXPANSION-RATIO NOZZLE, ROW 1

M_∞	$\frac{p_{t,j}}{p_\infty}$	$p/p_{t,j}$ for x/d of -								
		0.000	0.300	0.560	0.661	0.763	0.814	0.889	0.942	0.990
0.000	1.50	.904	.888	.856	.815	.638	.572	.478	.495	.635
.000	2.01	.394	.334	.854	.810	.633	.566	.469	.394	.334
.000	3.02	.393	.333	.853	.808	.632	.563	.466	.393	.333
.000	4.02	.393	.332	.857	.821	.640	.570	.467	.393	.332
.000	4.12	.393	.331	.853	.813	.644	.568	.465	.393	.331
.601	1.50	.901	.892	.854	.819	.645	.572	.476	.455	.643
.603	2.01	.394	.332	.853	.816	.640	.568	.469	.394	.332
.603	3.01	.394	.333	.853	.815	.638	.565	.467	.394	.333
.601	4.00	.393	.332	.853	.816	.637	.565	.467	.393	.332
.602	5.06	.393	.332	.853	.816	.636	.564	.466	.393	.332
.801	1.49	.902	.893	.854	.817	.647	.571	.477	.560	.659
.802	2.02	.394	.333	.852	.812	.641	.567	.469	.394	.333
.801	3.00	.394	.334	.852	.811	.639	.565	.468	.394	.334
.801	4.01	.393	.332	.852	.810	.637	.564	.467	.393	.332
.801	5.84	.393	.331	.853	.812	.636	.564	.466	.393	.331
.900	1.50	.901	.890	.854	.817	.648	.569	.479	.602	.667
.903	2.00	.393	.333	.852	.813	.643	.565	.469	.393	.333
.902	3.01	.393	.334	.853	.810	.640	.565	.468	.393	.334
.901	4.02	.393	.333	.853	.810	.639	.564	.467	.393	.333
.901	6.04	.392	.331	.853	.810	.638	.563	.466	.392	.331
.902	6.31	.393	.331	.853	.811	.638	.564	.466	.393	.331
.943	1.50	.898	.887	.852	.811	.644	.566	.499	.621	.677
.941	2.00	.391	.332	.850	.807	.639	.562	.468	.391	.332
.942	3.00	.391	.332	.850	.806	.638	.563	.466	.391	.332
.942	4.03	.392	.331	.851	.805	.637	.562	.466	.392	.331
.942	6.02	.392	.331	.851	.806	.637	.562	.465	.392	.331
.941	6.51	.392	.331	.852	.806	.637	.563	.465	.392	.331
1.199	1.51	.898	.885	.849	.817	.645	.561	.471	.443	.603
1.200	1.99	.392	.333	.853	.813	.643	.561	.470	.392	.333
1.200	3.01	.391	.334	.853	.810	.639	.563	.469	.391	.334
1.201	4.01	.393	.332	.853	.809	.639	.564	.468	.393	.332
1.201	6.00	.392	.332	.853	.808	.637	.563	.467	.392	.332
1.201	7.99	.392	.332	.853	.808	.636	.563	.466	.392	.332
1.200	8.67	.392	.332	.853	.808	.636	.563	.466	.392	.332

TABLE 16.- STATIC PRESSURES FOR HIGH-EXPANSION-RATIO NOZZLE, ROW 2

M_∞	$\frac{p_{t,j}}{p_\infty}$	$p/p_{t,j}$ for x/d of -	
		0.763	0.942
0.000	1.50	.652	.572
.000	2.01	.398	.398
.000	3.02	.385	.385
.000	4.02	.383	.383
.000	4.12	.383	.383
.601	1.50	.648	.548
.603	2.01	.391	.391
.603	3.01	.383	.383
.601	4.00	.383	.383
.602	5.06	.382	.382
.801	1.49	.649	.592
.802	2.02	.391	.391
.801	3.00	.384	.384
.801	4.01	.383	.383
.801	5.84	.382	.382
.900	1.50	.648	.611
.903	2.00	.390	.390
.902	3.01	.383	.383
.901	4.02	.382	.382
.901	6.04	.382	.382
.902	6.31	.382	.382
.943	1.50	.646	.627
.941	2.00	.391	.391
.942	3.00	.382	.382
.942	4.03	.381	.381
.942	6.02	.381	.381
.941	6.51	.381	.381
1.199	1.51	.647	.487
1.200	1.99	.385	.385
1.200	3.01	.382	.382
1.201	4.01	.381	.381
1.201	6.00	.382	.382
1.201	7.99	.381	.381
1.200	8.67	.382	.382

TABLE 17.- STATIC PRESSURES FOR HIGH-EXPANSION-RATIO NOZZLE, ROW 3

M_∞	$\dfrac{p_{t,j}}{p_\infty}$	$p/p_{t,j}$ for x/d of -		
		0.763	0.942	1.018
0.000	1.50	.666	.658	.661
.000	2.01	.585	.486	.491
.000	3.02	.316	.327	.327
.000	4.02	.258	.245	.245
.000	4.12	.254	.239	.239
.601	1.50	.649	.596	.638
.603	2.01	.574	.463	.469
.603	3.01	.300	.316	.316
.601	4.00	.256	.237	.237
.602	5.06	.239	.190	.190
.801	1.49	.651	.574	.649
.802	2.02	.574	.453	.454
.801	3.00	.304	.310	.310
.801	4.01	.257	.235	.235
.801	5.84	.238	.171	.171
.900	1.50	.653	.577	.661
.903	2.00	.576	.457	.459
.902	3.01	.310	.310	.310
.901	4.02	.258	.238	.238
.901	6.04	.238	.170	.170
.902	6.31	.237	.165	.165
.943	1.50	.654	.603	.672
.941	2.00	.577	.463	.472
.942	3.00	.315	.318	.318
.942	4.03	.257	.242	.242
.942	6.02	.237	.174	.174
.941	6.51	.237	.163	.163
1.199	1.51	.609	.521	.602
1.200	1.99	.323	.411	.323
1.200	3.01	.294	.256	.256
1.201	4.01	.253	.217	.217
1.201	6.00	.237	.173	.173
1.201	7.99	.237	.144	.144
1.200	8.67	.237	.135	.135

TABLE 18.- PRESSURE COEFFICIENTS FOR HIGH-EXPANSION-RATIO NOZZLE, ROW 4

M_∞	$\frac{p_{t,j}}{p_\infty}$	C_p for x/d of -									
		-0.100	0.000	0.100	0.150	0.200	0.250	0.300	0.400	0.450	0.490
0.000	1.50	.000	.000	-.000	-.000	-.000	.000	-.000	.000	-.000	-.000
.000	2.01	-.000	-.000	-.001	-.001	-.001	-.001	-.000	-.000	-.001	-.000
.000	3.02	-.001	-.001	-.001	-.001	-.002	-.002	-.001	-.001	-.001	-.001
.000	4.02	.003	.002	.002	.002	.002	.001	.002	.002	.002	.003
.000	4.12	-.000	-.001	-.001	-.001	-.002	-.001	-.001	-.001	-.001	-.000
.601	1.50	-.167	-.275	-.345	-.348	-.327	-.296	-.229	-.097	.026	.057
.603	2.01	-.169	-.279	-.354	-.356	-.341	-.296	-.233	-.110	.016	.040
.603	3.01	-.170	-.270	-.346	-.358	-.335	-.295	-.244	-.114	.016	.036
.601	4.00	-.171	-.280	-.355	-.356	-.331	-.293	-.228	-.091	.023	.062
.602	5.06	-.168	-.275	-.342	-.339	-.316	-.281	-.217	-.079	.034	.064
.801	1.49	-.179	-.317	-.438	-.446	-.426	-.347	-.251	-.060	.013	.031
.802	2.02	-.185	-.321	-.451	-.462	-.433	-.352	-.259	-.066	.006	.027
.801	3.00	-.184	-.317	-.436	-.444	-.404	-.333	-.243	-.050	.021	.036
.801	4.01	-.180	-.321	-.440	-.449	-.411	-.333	-.240	-.091	.021	.043
.801	5.84	-.170	-.306	-.406	-.415	-.385	-.310	-.216	-.067	.032	.050
.900	1.50	-.146	-.299	-.483	-.577	-.655	-.570	-.262	-.115	-.084	-.074
.903	2.00	-.147	-.297	-.485	-.568	-.658	-.622	-.306	-.162	-.130	-.122
.902	3.01	-.149	-.297	-.482	-.553	-.659	-.620	-.285	-.142	-.115	-.101
.901	4.02	-.151	-.296	-.481	-.541	-.656	-.509	-.233	-.102	-.076	-.058
.901	6.04	-.146	-.296	-.482	-.532	-.621	-.560	-.159	-.038	-.010	.005
.902	6.31	-.143	-.294	-.473	-.519	-.624	-.554	-.171	-.049	-.014	.005
.943	1.50	-.118	-.256	-.431	-.518	-.593	-.660	-.657	-.269	-.232	-.219
.941	2.00	-.110	-.253	-.428	-.517	-.601	-.671	-.650	-.276	-.238	-.239
.942	3.00	-.108	-.251	-.424	-.517	-.598	-.674	-.711	-.286	-.244	-.244
.942	4.03	-.117	-.257	-.431	-.517	-.599	-.669	-.604	-.247	-.201	-.196
.942	6.02	-.124	-.264	-.437	-.523	-.606	-.633	-.312	-.160	-.130	-.115
.941	6.51	-.110	-.260	-.434	-.518	-.594	-.566	-.251	-.133	-.118	-.109
1.199	1.51	-.015	-.094	-.204	-.263	-.291	-.370	-.424	-.482	-.330	-.256
1.200	1.99	-.013	-.090	-.202	-.236	-.316	-.371	-.422	-.482	-.335	-.263
1.200	3.01	-.014	-.092	-.202	-.231	-.317	-.374	-.423	-.477	-.345	-.266
1.201	4.01	-.016	-.095	-.203	-.232	-.314	-.375	-.423	-.473	-.343	-.272
1.201	6.00	-.015	-.096	-.203	-.230	-.290	-.376	-.425	-.472	-.337	-.264
1.201	7.99	-.017	-.098	-.206	-.233	-.287	-.371	-.423	-.451	-.278	-.230
1.200	8.67	-.013	-.093	-.202	-.230	-.267	-.368	-.423	-.450	-.267	-.226

TABLE 18.- Concluded

M_∞	$\frac{p_{t,j}}{p_\infty}$	C_p for x/d of -					
		0.542	0.594	0.699	0.804	0.909	1.018
0.000	1.50	.000	-.000	-.000	-.000	-.000	-.005
.000	2.01	-.001	-.001	-.000	-.001	-.002	-.012
.000	3.02	-.001	-.001	-.002	-.002	-.003	-.017
.000	4.02	.002	.002	.002	.001	.000	-.015
.000	4.12	-.001	-.001	-.001	-.002	-.003	-.015
.601	1.50	.056	.048	.044	.037	.047	.022
.603	2.01	.046	.034	.017	-.018	-.057	-.291
.603	3.01	.034	.027	.010	-.035	-.070	-.211
.601	4.00	.057	.043	.027	.005	-.012	-.064
.602	5.06	.065	.053	.043	.028	.034	.046
.801	1.49	.050	.055	.051	.049	.048	.045
.802	2.02	.039	.039	.027	-.008	-.053	-.255
.801	3.00	.043	.045	.033	-.003	-.042	-.140
.801	4.01	.057	.061	.052	.044	.023	.006
.801	5.84	.075	.083	.086	.090	.105	.156
.900	1.50	-.037	-.019	.050	.069	.079	.070
.903	2.00	-.067	-.035	.024	.028	-.000	-.149
.902	3.01	-.057	-.033	.026	.028	.001	-.094
.901	4.02	-.029	-.004	.062	.064	.055	.028
.901	6.04	.041	.060	.103	.127	.146	.169
.902	6.31	.048	.072	.111	.133	.158	.183
.943	1.50	-.171	-.111	-.013	.052	.084	.095
.941	2.00	-.186	-.127	-.033	.014	.021	-.066
.942	3.00	-.190	-.128	-.033	.011	.018	-.063
.942	4.03	-.150	-.096	-.002	.049	.059	.033
.942	6.02	-.077	-.043	.048	.098	.127	.143
.941	6.51	-.074	-.019	.067	.116	.153	.162
1.199	1.51	-.186	-.158	-.092	-.070	-.059	-.042
1.200	1.99	-.172	-.146	-.094	-.072	-.080	-.338
1.200	3.01	-.212	-.171	-.087	-.057	-.049	-.084
1.201	4.01	-.202	-.166	-.101	-.033	.007	.042
1.201	6.00	-.205	-.161	-.043	.040	.094	.154
1.201	7.99	-.169	-.125	-.020	.090	.136	.195
1.200	8.67	-.173	-.122	-.024	.098	.144	.200

TABLE 19.- PRESSURE COEFFICIENTS FOR HIGH-EXPANSION-RATIO NOZZLE, ROW 5

M_∞	$\frac{p_{t,j}}{p_\infty}$	C_p for x/d of -		
		0.000	0.490	0.804
0.000	1.50	-.000	-.000	-.000
.000	2.01	-.001	-.000	-.001
.000	3.02	-.001	-.001	-.002
.000	4.02	.003	.003	.001
.000	4.12	-.000	-.000	-.002
.601	1.50	-.235	.062	.025
.603	2.01	-.235	.052	-.016
.603	3.01	-.228	.052	-.016
.601	4.00	-.229	.064	.005
.602	5.06	-.221	.069	.028
.801	1.49	-.262	.039	.036
.802	2.02	-.267	.035	.000
.801	3.00	-.269	.036	.004
.801	4.01	-.265	.057	.042
.801	5.84	-.256	.085	.098
.900	1.50	-.251	-.066	.066
.903	2.00	-.248	-.085	.037
.902	3.01	-.243	-.069	.040
.901	4.02	-.251	-.047	.066
.901	6.04	-.240	.003	.122
.902	6.31	-.236	.021	.135
.943	1.50	-.213	-.250	.048
.941	2.00	-.209	-.265	.030
.942	3.00	-.206	-.214	.050
.942	4.03	-.202	-.224	.052
.942	6.02	-.202	-.135	.096
.941	6.51	-.200	-.105	.118
1.199	1.51	-.062	-.210	-.089
1.200	1.99	-.057	-.207	-.082
1.200	3.01	-.059	-.201	-.061
1.201	4.01	-.065	-.203	-.041
1.201	6.00	-.070	-.203	.014
1.201	7.99	-.072	-.194	.073
1.200	8.67	-.075	-.185	.089

TABLE 20.- PRESSURE COEFFICIENTS FOR HIGH-EXPANSION-RATIO NOZZLE, ROW 6

M_∞	$\frac{p_{t,j}}{p_\infty}$	C_p for x/d of -										
		-0.100	0.100	0.200	0.300	0.500	0.650	0.800	1.002	1.224	1.400	1.614
0.000	1.50	-.000	-.002	.001	-.000	-.000	-.000	-.000	-.000	-.000	-.000	-.006
.000	2.01	-.000	-.002	.000	-.000	-.000	-.000	-.001	-.001	-.001	-.001	-.009
.000	3.02	-.001	-.002	-.001	-.001	-.001	-.002	-.002	-.002	-.002	-.001	-.008
.000	4.02	.003	.002	.003	.002	.002	.001	.001	-.000	.002	.005	.034
.000	4.12	-.000	-.001	-.001	-.001	-.001	-.002	-.002	-.003	-.001	.003	.033
.601	1.50	-.118	-.219	-.160	-.124	-.083	-.013	-.051	-.039	.017	.069	.186
.603	2.01	-.126	-.220	-.164	-.125	-.079	-.068	-.059	-.048	.018	.092	.221
.603	3.01	-.129	-.216	-.162	-.121	-.080	-.065	-.046	-.045	.010	.117	.290
.601	4.00	-.121	-.208	-.150	-.106	-.058	-.029	-.015	-.037	-.017	.099	.239
.602	5.06	-.114	-.203	-.150	-.107	-.049	-.015	-.007	-.042	-.077	.027	.261
.801	1.49	-.150	-.270	-.207	-.148	-.088	-.017	-.042	-.009	.045	.098	.201
.802	2.02	-.150	-.276	-.213	-.157	-.094	-.060	-.048	-.032	.038	.110	.237
.801	3.00	-.154	-.269	-.208	-.150	-.084	-.049	-.036	-.046	.011	.120	.294
.801	4.01	-.133	-.253	-.192	-.130	-.050	.001	.007	-.012	-.022	.086	.236
.801	5.84	-.128	-.241	-.175	-.108	-.026	.060	.041	-.015	-.140	-.138	.165
.900	1.50	-.144	-.370	-.359	-.235	-.099	-.029	-.030	-.000	.062	.114	.201
.903	2.00	-.144	-.370	-.372	-.247	-.090	-.024	-.024	-.006	.075	.147	.258
.902	3.01	-.143	-.365	-.367	-.226	-.077	-.016	-.008	-.018	.032	.144	.308
.901	4.02	-.146	-.362	-.333	-.196	-.068	.006	.020	-.002	-.027	.091	.263
.901	6.04	-.134	-.352	-.269	-.144	-.027	.055	.071	.030	-.124	-.183	.136
.902	6.31	-.137	-.346	-.269	-.138	-.016	.060	.074	.026	-.142	-.229	.076
.943	1.50	-.117	-.335	-.389	-.352	-.315	-.085	-.013	.040	.094	.138	.211
.941	2.00	-.113	-.337	-.392	-.362	-.330	-.084	-.010	.030	.101	.170	.265
.942	3.00	-.114	-.327	-.377	-.344	-.251	-.067	-.002	.017	.070	.178	.320
.942	4.03	-.119	-.332	-.390	-.349	-.226	-.031	.037	.031	-.000	.113	.288
.942	6.02	-.112	-.332	-.386	-.325	-.074	.039	.081	.048	-.097	-.153	.165
.941	6.51	-.114	-.336	-.387	-.314	-.052	.060	.099	.057	-.105	-.213	.067
1.199	1.51	-.037	-.129	-.194	-.182	-.172	-.147	-.160	-.189	-.098	-.040	.036
1.200	1.99	-.030	-.130	-.191	-.178	-.170	-.130	-.152	-.155	-.198	-.104	.102
1.200	3.01	-.036	-.132	-.191	-.179	-.170	-.120	-.149	-.088	-.137	-.209	.067
1.201	4.01	-.036	-.131	-.188	-.176	-.171	-.121	-.149	-.045	-.080	-.156	-.016
1.201	6.00	-.029	-.135	-.194	-.180	-.168	-.099	-.155	.014	-.046	-.133	-.228
1.201	7.99	-.027	-.138	-.195	-.180	-.169	-.003	-.123	.027	-.038	-.146	-.252
1.200	8.67	-.034	-.137	-.195	-.180	-.168	-.006	-.101	.028	-.037	-.144	-.246

TABLE 21.- PRESSURE COEFFICIENTS FOR HIGH-EXPANSION-RATIO NOZZLE, ROW 7

M_∞	$\frac{p_{t,j}}{p_\infty}$	C_p for x/d of -		
		0.150	0.500	0.800
0.000	1.50	.000	-.001	.000
.000	2.01	-.000	-.002	.000
.000	3.02	-.001	-.002	-.001
.000	4.02	.004	.001	.001
.000	4.12	.001	-.001	-.002
.601	1.50	-.196	-.101	-.056
.603	2.01	-.192	-.098	-.055
.603	3.01	-.196	-.087	-.034
.601	4.00	-.180	-.070	.007
.602	5.06	-.175	-.063	.023
.801	1.49	-.256	-.107	-.061
.802	2.02	-.251	-.098	-.041
.801	3.00	-.241	-.092	-.023
.801	4.01	-.234	-.070	.025
.801	5.84	-.212	-.043	.066
.900	1.50	-.387	-.096	-.032
.903	2.00	-.396	-.097	-.018
.902	3.01	-.394	-.089	.011
.901	4.02	-.377	-.068	.041
.901	6.04	-.339	-.030	.102
.902	6.31	-.338	-.030	.101
.943	1.50	-.361	-.300	-.038
.941	2.00	-.365	-.305	-.028
.942	3.00	-.368	-.320	-.004
.942	4.03	-.360	-.205	.040
.942	6.02	-.351	-.059	.102
.941	6.51	-.370	-.056	.109
1.199	1.51	-.177	-.187	-.233
1.200	1.99	-.177	-.187	-.220
1.200	3.01	-.177	-.192	-.190
1.201	4.01	-.174	-.190	-.157
1.201	6.00	-.172	-.191	-.086
1.201	7.99	-.175	-.190	-.051
1.200	8.67	-.177	-.191	-.060

TABLE 22.- PRESSURE COEFFICIENTS FOR HIGH-EXPANSION-RATIO NOZZLE, ROW 8

M_∞	$\frac{p_{t,j}}{p_\infty}$	C_p for x/d of -							
		0.000	0.100	0.200	0.300	0.400	0.500	0.600	0.800
0.000	1.50	.000	.000	-.000	-.000	-.000	-.000	-.000	-.001
.000	2.01	-.000	-.000	-.001	-.000	-.000	-.001	-.001	-.008
.000	3.02	-.001	-.001	-.001	-.002	-.002	-.002	-.002	-.007
.000	4.02	-.001	-.002	-.002	.002	.001	.001	.001	-.009
.000	4.12	-.001	-.002	-.002	-.001	-.002	-.002	-.002	-.011
.601	1.50	-.148	-.192	-.219	-.231	-.281	-.220	-.099	-.073
.603	2.01	-.151	-.197	-.224	-.234	-.283	-.231	-.103	-.029
.603	3.01	-.151	-.197	-.225	-.233	-.287	-.230	-.089	.035
.601	4.00	-.146	-.192	-.217	-.237	-.280	-.231	-.077	.098
.602	5.06	-.142	-.186	-.211	-.227	-.265	-.198	-.046	.149
.801	1.49	-.183	-.248	-.281	-.276	-.304	-.205	-.081	-.047
.802	2.02	-.185	-.251	-.286	-.280	-.321	-.216	-.084	.002
.801	3.00	-.183	-.248	-.282	-.282	-.307	-.214	-.067	.057
.801	4.01	-.178	-.241	-.271	-.265	-.300	-.191	-.040	.119
.801	5.84	-.167	-.226	-.252	-.240	-.262	-.142	.003	.191
.900	1.50	-.191	-.303	-.424	-.467	-.306	-.173	-.089	-.034
.903	2.00	-.189	-.302	-.427	-.496	-.334	-.176	-.087	.007
.902	3.01	-.189	-.302	-.425	-.459	-.303	-.157	-.069	.070
.901	4.02	-.188	-.300	-.418	-.419	-.275	-.132	-.030	.143
.901	6.04	-.183	-.295	-.392	-.329	-.236	-.086	.024	.217
.902	6.31	-.182	-.291	-.390	-.298	-.224	-.074	.035	.224
.943	1.50	-.154	-.261	-.388	-.480	-.682	-.349	-.174	-.019
.941	2.00	-.156	-.264	-.390	-.478	-.692	-.368	-.163	.016
.942	3.00	-.154	-.262	-.388	-.484	-.703	-.389	-.168	.049
.942	4.03	-.154	-.261	-.388	-.475	-.578	-.220	-.124	.140
.942	6.02	-.152	-.261	-.387	-.475	-.257	-.106	-.037	.224
.941	6.51	-.152	-.261	-.387	-.470	-.202	-.090	-.043	.217
1.199	1.51	-.036	-.091	-.172	-.237	-.391	-.612	-.415	-.154
1.200	1.99	-.036	-.091	-.171	-.236	-.394	-.613	-.414	-.104
1.200	3.01	-.036	-.091	-.171	-.240	-.396	-.610	-.402	-.044
1.201	4.01	-.035	-.090	-.171	-.239	-.394	-.614	-.402	.003
1.201	6.00	-.035	-.091	-.171	-.238	-.390	-.605	-.376	.051
1.201	7.99	-.035	-.090	-.171	-.243	-.393	-.608	-.339	.069
1.200	8.67	-.036	-.091	-.171	-.238	-.392	-.604	-.332	.066

TABLE 23.- PRESSURE COEFFICIENTS FOR HIGH-EXPANSION-RATIO NOZZLE, ROW 9

M_∞	$\frac{p_{t,j}}{p_\infty}$	C_p for x/d of -				
		0.750	0.920	1.002	1.200	1.400
0.000	1.50	.662	.570	.642	.658	.659
.000	2.01	.378	.378	.419	.483	.493
.000	3.02	.312	.197	.296	.330	.330
.000	4.02	.316	.202	.197	.240	.240
.000	4.12	.310	.209	.192	.232	.232
.601	1.50	.663	.520	.611	.672	.681
.603	2.01	.332	.353	.353	.499	.509
.603	3.01	.317	.197	.281	.343	.343
.601	4.00	.316	.196	.185	.228	.228
.602	5.06	.308	.196	.141	.147	.147
.801	1.49	.665	.529	.619	.694	.705
.802	2.02	.323	.346	.346	.506	.527
.801	3.00	.310	.198	.283	.351	.351
.801	4.01	.309	.196	.179	.226	.226
.801	5.84	.308	.196	.120	.121	.121
.900	1.50	.662	.544	.631	.701	.715
.903	2.00	.323	.377	.377	.516	.546
.902	3.01	.309	.197	.292	.355	.355
.901	4.02	.309	.196	.179	.235	.235
.901	6.04	.308	.196	.118	.115	.115
.902	6.31	.311	.196	.116	.112	.112
.943	1.50	.659	.562	.649	.712	.729
.941	2.00	.323	.323	.409	.527	.559
.942	3.00	.308	.196	.310	.368	.368
.942	4.03	.307	.195	.186	.261	.261
.942	6.02	.308	.196	.118	.116	.116
.941	6.51	.308	.196	.116	.109	.109
1.199	1.51	.654	.464	.531	.592	.622
1.200	1.99	.315	.209	.209	.410	.471
1.200	3.01	.308	.195	.219	.258	.258
1.201	4.01	.309	.196	.153	.169	.169
1.201	6.00	.308	.197	.117	.117	.117
1.201	7.99	.307	.197	.111	.102	.102
1.200	8.67	.307	.197	.111	.100	.100

TABLE 24.- STATIC PRESSURES FOR HIGH-EXPANSION-RATIO NOZZLE, ROW 10

M_∞	$\frac{p_{t,j}}{p_\infty}$	$p/p_{t,j}$ for x/d of -									
		0.573	0.591	0.650	0.700	0.750	0.800	0.850	0.912	0.950	1.002
0.000	1.50	.392	.898	.805	.712	.615	.509	.392	.490	.489	.528
.000	2.01	.387	.252	.254	.382	.392	.506	.387	.252	.254	.382
.000	3.02	.386	.251	.223	.211	.201	.189	.279	.318	.328	.334
.000	4.02	.393	.251	.223	.212	.201	.189	.172	.158	.141	.228
.000	4.12	.396	.251	.223	.212	.201	.189	.172	.158	.141	.133
.601	1.50	.388	.905	.803	.708	.613	.506	.388	.413	.480	.550
.603	2.01	.386	.252	.224	.366	.376	.395	.386	.252	.224	.366
.603	3.01	.386	.252	.225	.213	.201	.190	.285	.317	.325	.331
.601	4.00	.386	.252	.225	.213	.201	.190	.172	.158	.142	.181
.602	5.06	.385	.251	.224	.213	.202	.190	.174	.159	.142	.128
.801	1.49	.389	.906	.804	.708	.615	.506	.389	.443	.506	.568
.802	2.02	.385	.253	.225	.344	.373	.391	.385	.253	.225	.344
.801	3.00	.386	.253	.225	.213	.201	.191	.299	.321	.328	.331
.801	4.01	.386	.252	.225	.212	.201	.190	.172	.158	.141	.216
.801	5.84	.385	.251	.224	.212	.201	.190	.175	.160	.143	.129
.900	1.50	.391	.906	.803	.707	.614	.505	.391	.478	.530	.582
.903	2.00	.385	.253	.226	.337	.380	.503	.385	.253	.226	.337
.902	3.01	.386	.253	.226	.213	.201	.193	.303	.323	.328	.331
.901	4.02	.386	.253	.225	.213	.201	.190	.172	.158	.141	.237
.901	6.04	.385	.251	.225	.212	.201	.188	.174	.159	.143	.128
.902	6.31	.385	.251	.224	.213	.201	.189	.174	.160	.143	.129
.943	1.50	.392	.903	.801	.705	.613	.502	.392	.496	.550	.603
.941	2.00	.383	.251	.226	.355	.393	.500	.383	.251	.226	.355
.942	3.00	.384	.252	.224	.212	.200	.192	.311	.326	.331	.335
.942	4.03	.385	.252	.225	.213	.201	.190	.171	.157	.143	.250
.942	6.02	.384	.251	.225	.212	.201	.189	.174	.160	.143	.128
.941	6.51	.385	.251	.224	.212	.200	.189	.175	.160	.143	.129
1.199	1.51	.987	.904	.800	.707	.611	.499	.404	.467	.501	.517
1.200	1.99	.384	.255	.225	.215	.206	.244	.311	.357	.225	.215
1.200	3.01	.385	.254	.224	.213	.199	.195	.169	.166	.267	.280
1.201	4.01	.384	.254	.226	.213	.200	.191	.172	.157	.142	.127
1.201	6.00	.385	.254	.226	.214	.201	.190	.175	.160	.144	.129
1.201	7.99	.384	.254	.225	.213	.200	.188	.174	.159	.144	.129
1.200	8.67	.384	.253	.225	.213	.200	.188	.175	.159	.144	.129

TABLE 24.- Concluded

M_∞	$\frac{p_{t,j}}{p_\infty}$	$p/p_{t,j}$ for x/d of -							
		1.050	1.100	1.155	1.200	1.250	1.300	1.400	1.500
0.000	1.50	.593	.646	.674	.684	.689	.692	.692	.705
.000	2.01	.392	.406	.430	.455	.483	.506	.530	.549
.000	3.02	.352	.377	.279	.318	.328	.334	.352	.377
.000	4.02	.257	.265	.172	.158	.141	.228	.257	.265
.000	4.12	.242	.249	.172	.158	.141	.133	.242	.249
.601	1.50	.604	.644	.671	.686	.695	.701	.691	.720
.603	2.01	.376	.395	.433	.474	.513	.537	.544	.570
.603	3.01	.346	.376	.285	.317	.325	.331	.346	.376
.601	4.00	.247	.251	.172	.158	.142	.181	.247	.251
.602	5.06	.140	.196	.174	.159	.142	.128	.140	.196
.801	1.49	.615	.652	.681	.700	.711	.718	.709	.739
.802	2.02	.373	.391	.441	.495	.538	.557	.553	.581
.801	3.00	.348	.383	.299	.321	.328	.331	.348	.383
.801	4.01	.249	.252	.172	.158	.141	.216	.249	.252
.801	5.84	.113	.154	.175	.160	.143	.129	.113	.154
.900	1.50	.622	.652	.682	.698	.711	.721	.722	.749
.903	2.00	.380	.411	.473	.521	.555	.569	.565	.594
.902	3.01	.348	.395	.303	.323	.328	.331	.348	.395
.901	4.02	.256	.262	.172	.158	.141	.237	.256	.262
.901	6.04	.114	.146	.174	.159	.143	.128	.114	.146
.902	6.31	.113	.103	.174	.160	.143	.129	.113	.103
.943	1.50	.643	.675	.700	.715	.726	.734	.749	.758
.941	2.00	.393	.440	.498	.539	.564	.577	.586	.602
.942	3.00	.366	.192	.311	.326	.331	.335	.366	.409
.942	4.03	.264	.270	.171	.157	.143	.250	.264	.270
.942	6.02	.107	.153	.174	.160	.143	.128	.107	.153
.941	6.51	.107	.092	.175	.160	.143	.129	.107	.092
1.199	1.51	.526	.547	.560	.578	.594	.611	.629	.666
1.200	1.99	.206	.244	.311	.357	.403	.446	.494	.557
1.200	3.01	.290	.312	.169	.166	.267	.280	.290	.312
1.201	4.01	.222	.222	.172	.157	.142	.127	.222	.222
1.201	6.00	.119	.077	.175	.160	.144	.129	.119	.077
1.201	7.99	.106	.072	.174	.159	.144	.129	.106	.072
1.200	8.67	.102	.072	.175	.159	.144	.129	.102	.072

TABLE 25.- STATIC PRESSURES FOR HIGH-EXPANSION-RATIO NOZZLE, ROW 11

M_∞	$\frac{p_{t,j}}{p_\infty}$	$p/p_{t,j}$ for x/d of -					
		0.912	1.002	1.050	1.100	1.155	1.200
0.000	1.50	.483	.561	.611	.652	.674	.683
.000	2.01	.332	.378	.390	.408	.426	.454
.000	3.02	.269	.207	.196	.187	.200	.298
.000	4.02	.251	.253	.207	.186	.169	.155
.000	4.12	.253	.230	.207	.185	.169	.155
.601	1.50	.451	.555	.615	.653	.676	.688
.603	2.01	.310	.355	.383	.403	.439	.478
.603	3.01	.261	.208	.199	.188	.229	.306
.601	4.00	.252	.208	.199	.186	.169	.155
.602	5.06	.238	.209	.199	.186	.170	.156
.801	1.49	.476	.569	.623	.661	.686	.699
.802	2.02	.327	.249	.378	.415	.460	.503
.801	3.00	.274	.209	.199	.191	.259	.314
.801	4.01	.253	.209	.199	.185	.168	.155
.801	5.84	.232	.209	.199	.185	.171	.157
.900	1.50	.495	.578	.624	.661	.688	.708
.903	2.00	.311	.261	.383	.437	.489	.531
.902	3.01	.271	.209	.199	.192	.267	.317
.901	4.02	.253	.210	.199	.187	.168	.155
.901	6.04	.233	.208	.199	.185	.171	.157
.902	6.31	.232	.209	.199	.183	.171	.156
.943	1.50	.511	.601	.646	.683	.707	.720
.941	2.00	.290	.303	.397	.456	.508	.545
.942	3.00	.265	.209	.197	.191	.291	.322
.942	4.03	.249	.209	.198	.186	.167	.154
.942	6.02	.232	.208	.199	.185	.171	.157
.941	6.51	.230	.209	.199	.183	.171	.157
1.199	1.51	.436	.512	.528	.547	.564	.582
1.200	1.99	.314	.212	.208	.255	.310	.353
1.200	3.01	.289	.210	.197	.189	.165	.153
1.201	4.01	.234	.210	.198	.186	.168	.155
1.201	6.00	.232	.210	.199	.182	.172	.157
1.201	7.99	.218	.210	.199	.182	.171	.156
1.200	8.67	.211	.209	.199	.182	.171	.157

TABLE 26.- STATIC PRESSURES FOR HIGH-EXPANSION-RATIO NOZZLE, ROW 12

M_∞	$\frac{p_{t,j}}{p_\infty}$	$p/p_{t,j}$ for x/d of -									
		0.573	0.591	0.650	0.750	0.850	0.950	1.002	1.050	1.100	1.155
0.000	1.50	.389	.973	.802	.618	.389	.482	.574	.641	.673	.678
.000	2.01	.377	.220	.349	.365	.377	.220	.349	.365	.402	.488
.000	3.02	.375	.214	.200	.185	.177	.155	.277	.370	.291	.155
.000	4.02	.388	.229	.226	.201	.173	.156	.146	.120	.302	.156
.000	4.12	.390	.230	.217	.212	.173	.156	.146	.118	.292	.156
.601	1.50	.384	.916	.804	.612	.384	.469	.573	.636	.668	.683
.603	2.01	.376	.217	.361	.373	.390	.217	.361	.373	.390	.437
.603	3.01	.376	.213	.201	.189	.177	.154	.278	.330	.316	.154
.601	4.00	.376	.213	.201	.189	.173	.156	.146	.118	.286	.156
.602	5.06	.375	.212	.202	.190	.174	.156	.147	.119	.160	.156
.801	1.49	.384	.916	.804	.612	.384	.493	.580	.637	.672	.689
.802	2.02	.375	.218	.318	.369	.375	.218	.318	.369	.400	.466
.801	3.00	.376	.213	.201	.190	.178	.176	.284	.315	.369	.176
.801	4.01	.376	.213	.201	.189	.172	.156	.146	.118	.261	.156
.801	5.84	.375	.212	.201	.189	.175	.157	.147	.119	.069	.157
.900	1.50	.385	.914	.802	.613	.385	.516	.588	.640	.674	.695
.903	2.00	.375	.218	.283	.379	.375	.218	.283	.379	.434	.505
.902	3.01	.376	.213	.202	.190	.178	.235	.301	.319	.178	.235
.901	4.02	.376	.213	.201	.189	.172	.155	.145	.127	.261	.155
.901	6.04	.375	.212	.201	.189	.174	.157	.147	.119	.069	.157
.902	6.31	.375	.212	.201	.189	.174	.157	.147	.119	.069	.157
.943	1.50	.386	.911	.797	.611	.386	.539	.616	.665	.695	.710
.941	2.00	.372	.217	.335	.397	.372	.217	.335	.397	.460	.524
.942	3.00	.373	.212	.200	.189	.177	.277	.306	.333	.177	.277
.942	4.03	.374	.212	.201	.189	.171	.155	.144	.187	.277	.155
.942	6.02	.374	.212	.201	.189	.174	.157	.147	.119	.069	.157
.941	6.51	.375	.212	.201	.189	.174	.157	.147	.119	.069	.157
1.199	1.51	.955	.917	.800	.606	.401	.492	.506	.520	.539	.558
1.200	1.99	.370	.215	.204	.199	.255	.318	.359	.199	.255	.318
1.200	3.01	.372	.211	.202	.190	.168	.155	.144	.259	.334	.155
1.201	4.01	.373	.212	.202	.190	.172	.157	.145	.119	.210	.157
1.201	6.00	.375	.212	.202	.190	.174	.158	.148	.120	.070	.158
1.201	7.99	.374	.212	.202	.189	.174	.157	.147	.121	.070	.157
1.200	8.67	.374	.212	.202	.189	.174	.157	.147	.121	.070	.157

TABLE 26.- Concluded

M_∞	$\frac{p_{t,j}}{p_\infty}$	$p/p_{t,j}$ for x/d of -		
		1.200	1.300	1.500
0.000	1.50	.682	.683	.688
.000	2.01	.533	.525	.526
.000	3.02	.277	.370	.291
.000	4.02	.146	.120	.302
.000	4.12	.146	.118	.292
.601	1.50	.690	.698	.716
.603	2.01	.500	.556	.559
.603	3.01	.278	.330	.316
.601	4.00	.146	.118	.286
.602	5.06	.147	.119	.160
.801	1.49	.701	.716	.740
.802	2.02	.523	.560	.574
.801	3.00	.284	.315	.369
.801	4.01	.146	.118	.261
.801	5.84	.147	.119	.069
.900	1.50	.719	.726	.752
.903	2.00	.547	.570	.591
.902	3.01	.301	.319	.429
.901	4.02	.145	.127	.261
.901	6.04	.147	.119	.069
.902	6.31	.147	.119	.069
.943	1.50	.720	.734	.758
.941	2.00	.558	.577	.598
.942	3.00	.306	.333	.449
.942	4.03	.144	.187	.277
.942	6.02	.147	.119	.069
.941	6.51	.147	.119	.069
1.199	1.51	.578	.619	.676
1.200	1.99	.359	.455	.562
1.200	3.01	.144	.259	.334
1.201	4.01	.145	.119	.210
1.201	6.00	.148	.120	.070
1.201	7.99	.147	.121	.070
1.200	8.67	.147	.121	.070

TABLE 27.- STATIC PRESSURES FOR HIGH-EXPANSION-RATIO NOZZLE, ROW 13

M_∞	$\frac{p_{t,j}}{p_\infty}$	$p/p_{t,j}$ for x/d of -					
		0.912	1.002	1.050	1.100	1.155	1.200
0.000	1.50	.372	.643	.667	.673	.675	.675
.000	2.01	.238	.321	.413	.537	.532	.516
.000	3.02	.230	.190	.181	.166	.166	.276
.000	4.02	.232	.191	.196	.167	.146	.135
.000	4.12	.232	.201	.191	.167	.146	.135
.601	1.50	.363	.618	.661	.678	.684	.687
.603	2.01	.234	.297	.386	.449	.515	.541
.603	3.01	.230	.189	.178	.167	.147	.270
.601	4.00	.231	.188	.177	.167	.146	.134
.602	5.06	.231	.188	.177	.164	.148	.135
.801	1.49	.396	.608	.662	.687	.698	.704
.802	2.02	.233	.264	.381	.440	.505	.543
.801	3.00	.229	.189	.179	.172	.148	.275
.801	4.01	.230	.188	.177	.167	.146	.135
.801	5.84	.230	.188	.177	.162	.149	.136
.900	1.50	.416	.618	.666	.690	.702	.709
.903	2.00	.233	.283	.383	.459	.517	.554
.902	3.01	.228	.189	.180	.177	.170	.284
.901	4.02	.230	.189	.178	.167	.146	.134
.901	6.04	.230	.188	.177	.162	.149	.135
.902	6.31	.230	.188	.177	.162	.149	.136
.943	1.50	.426	.647	.685	.702	.715	.720
.941	2.00	.231	.303	.411	.476	.528	.560
.942	3.00	.227	.189	.179	.177	.230	.298
.942	4.03	.229	.188	.178	.166	.145	.134
.942	6.02	.229	.188	.178	.161	.148	.135
.941	6.51	.230	.188	.177	.162	.149	.136
1.199	1.51	.454	.511	.527	.539	.554	.574
1.200	1.99	.228	.196	.204	.257	.320	.380
1.200	3.01	.227	.186	.178	.174	.147	.135
1.201	4.01	.228	.187	.178	.167	.148	.135
1.201	6.00	.229	.188	.179	.161	.149	.136
1.201	7.99	.229	.187	.177	.161	.149	.136
1.200	8.67	.229	.187	.177	.162	.149	.136

TABLE 28.- STATIC PRESSURES FOR HIGH-EXPANSION-RATIO NOZZLE, ROW 14

M_∞	$\frac{p_{t,j}}{p_\infty}$	$p/p_{t,j}$ for x/d of -									
		0.573	0.591	0.650	·0.750	0.850	0.912	0.950	1.002	1.050	1.100
0.000	1.50	1.001	.915	.817	.624	.423	.499	.559	.644	.677	.675
.000	2.01	.381	.248	.225	.388	.381	.248	.225	.388	.429	.509
.000	3.02	.373	.234	.200	.184	.173	.171	.289	.339	.353	.324
.000	4.02	.373	.237	.202	.188	.173	.154	.140	.153	.234	.266
.000	4.12	.374	.239	.204	.182	.172	.154	.140	.145	.222	.257
.601	1.50	.985	.915	.811	.612	.413	.476	.498	.594	.662	.684
.603	2.01	.380	.242	.235	.358	.355	.242	.235	.358	.355	.448
.603	3.01	.375	.233	.201	.182	.169	.162	.246	.328	.369	.345
.601	4.00	.375	.233	.200	.181	.168	.154	.139	.134	.198	.273
.602	5.06	.374	.233	.200	.181	.168	.155	.140	.130	.114	.182
.801	1.49	.986	.915	.811	.613	.414	.475	.507	.605	.668	.693
.802	2.02	.380	.241	.283	.345	.346	.241	.283	.345	.346	.419
.801	3.00	.376	.233	.201	.183	.170	.162	.233	.321	.377	.365
.801	4.01	.375	.232	.200	.181	.168	.154	.139	.132	.178	.282
.801	5.84	.374	.233	.200	.181	.167	.155	.140	.130	.107	.127
.900	1.50	.985	.915	.812	.612	.415	.480	.521	.623	.675	.695
.903	2.00	.381	.245	.342	.357	.368	.245	.342	.357	.368	.424
.902	3.01	.376	.232	.201	.182	.171	.164	.241	.312	.385	.385
.901	4.02	.376	.232	.201	.182	.168	.154	.139	.132	.175	.287
.901	6.04	.374	.233	.200	.181	.168	.155	.140	.130	.107	.113
.902	6.31	.375	.233	.200	.182	.167	.155	.140	.130	.106	.107
.943	1.50	.981	.911	.806	.610	.420	.502	.548	.642	.691	.707
.941	2.00	.378	.261	.365	.370	.385	.261	.365	.370	.385	.438
.942	3.00	.373	.230	.200	.181	.170	.171	.274	.318	.399	.171
.942	4.03	.374	.231	.199	.181	.168	.153	.138	.132	.206	.299
.942	6.02	.374	.232	.199	.181	.167	.155	.139	.129	.106	.115
.941	6.51	.374	.232	.199	.181	.168	.156	.140	.129	.107	.103
1.199	1.51	.982	.912	.808	.604	.405	.461	.497	.514	.532	.547
1.200	1.99	.379	.237	.208	.192	.192	.278	.326	.390	.192	.278
1.200	3.01	.377	.233	.201	.182	.169	.153	.142	.165	.276	.302
1.201	4.01	.377	.233	.201	.182	.168	.154	.140	.131	.133	.198
1.201	6.00	.377	.234	.202	.183	.169	.156	.141	.131	.108	.113
1.201	7.99	.376	.234	.201	.182	.169	.155	.141	.132	.108	.093
1.200	8.07	.376	.234	.201	.182	.169	.156	.141	.133	.108	.092

TABLE 28.- Concluded

M_∞	$\frac{p_{t,j}}{p_\infty}$	$p/p_{t,j}$ for x/d of -			
		1.155	1.200	1.300	1.500
0.000	1.50	.673	.673	.670	.673
.000	2.01	.517	.510	.501	.507
.000	3.02	.289	.339	.353	.324
.000	4.02	.140	.153	.234	.266
.000	4.12	.140	.145	.222	.257
.601	1.50	.685	.684	.683	.695
.603	2.01	.527	.542	.524	.529
.603	3.01	.246	.328	.369	.345
.601	4.00	.139	.134	.198	.273
.602	5.06	.140	.130	.114	.182
.801	1.49	.699	.703	.706	.726
.802	2.02	.505	.547	.545	.551
.801	3.00	.233	.321	.377	.365
.801	4.01	.139	.132	.178	.282
.801	5.84	.140	.130	.107	.127
.900	1.50	.706	.711	.717	.757
.903	2.00	.500	.548	.568	.572
.902	3.01	.241	.312	.385	.385
.901	4.02	.139	.132	.175	.287
.901	6.04	.140	.130	.107	.113
.902	6.51	.140	.130	.106	.107
.943	1.50	.714	.720	.726	.748
.941	2.00	.512	.560	.579	.581
.942	3.00	.274	.318	.399	.401
.942	4.03	.138	.132	.206	.299
.942	6.02	.139	.129	.106	.115
.941	6.51	.140	.129	.107	.103
1.199	1.51	.565	.583	.625	.668
1.200	1.99	.326	.390	.467	.533
1.200	3.01	.142	.165	.276	.302
1.201	4.01	.140	.131	.133	.198
1.201	6.00	.141	.131	.108	.113
1.201	7.99	.141	.132	.108	.093
1.200	8.67	.141	.133	.108	.092

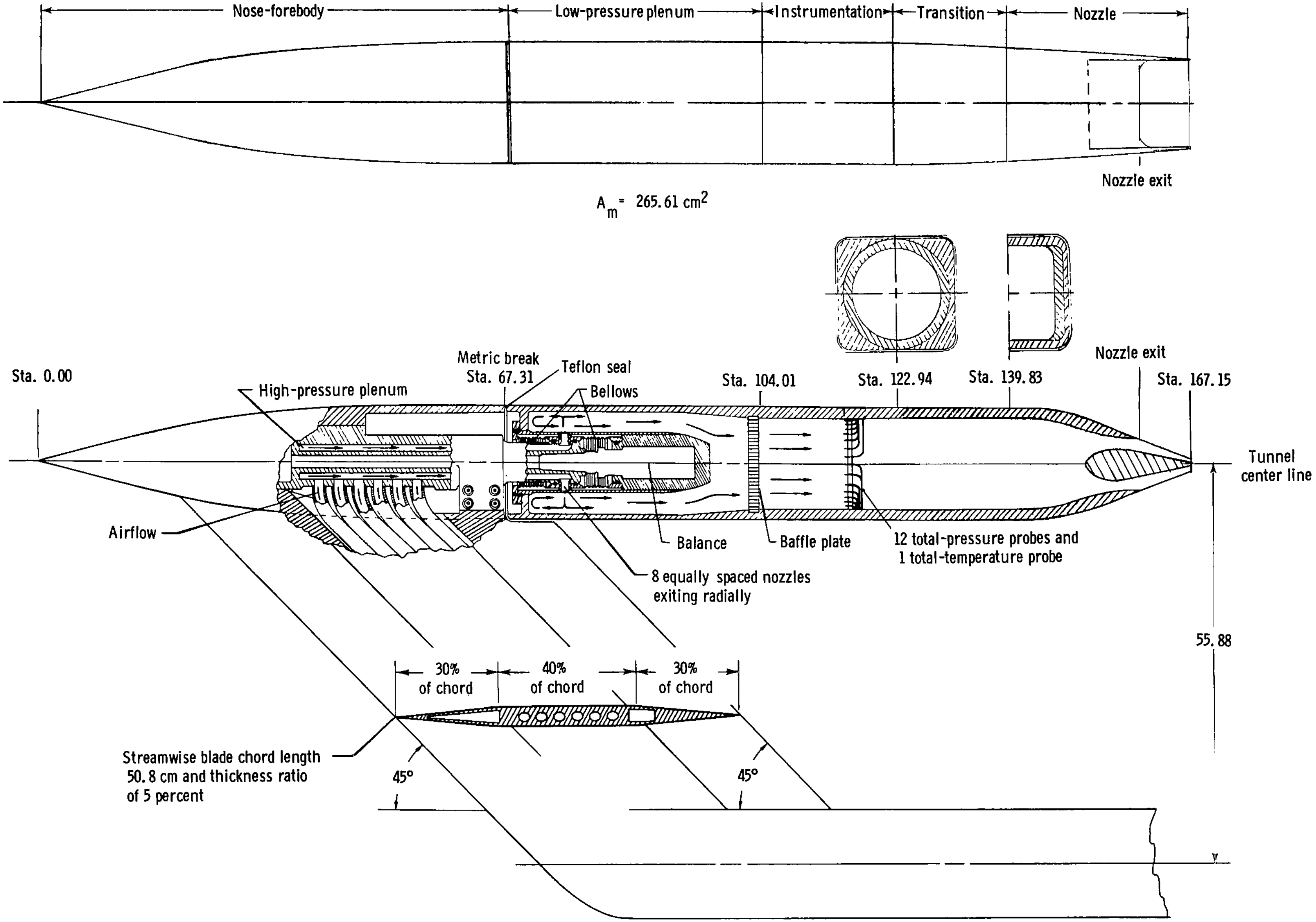

Figure 1.- Air-powered nacelle model with nonaxisymmetric plug nozzle installed. All dimensions are in centimeters unless otherwise noted.

$$ {\frac{z'(x')}{a(x')}}^{\eta(x')} + {\frac{y'(x')}{b(x')}}^{\eta(x')} = 1 $$

$0.0 \leq x' \leq 15.2654$

$$a(x') = x' \tan\left(\frac{14\pi}{180}\right)$$

$$b(x') = x' \tan\left(\frac{14.}{180}\right)$$

$$\eta(x') = 2.00$$

$15.2654 \leq x' \leq 67.31$

$$a(x') = a_1 x' + a_2 + \sqrt{a_3(x')^2 + a_4 x' + a_5}$$

$$b(x') = b_1 x' + b_2 + \sqrt{b_3(x')^2 + b_4 x' + b_5}$$

$$\eta(x') = 3.5 \sin\left(\frac{x' - 41.2877}{52.0446}\right)\pi + 5.50$$

n	a_n	b_n
1	-0.363118	-0.209539
2	-25.208332	-5.578971
3	$-.834887 \times 10^{-13}$	$-.213163 \times 10^{-13}$
4	42.329327	11.548538
5	548.051732	-17.942117

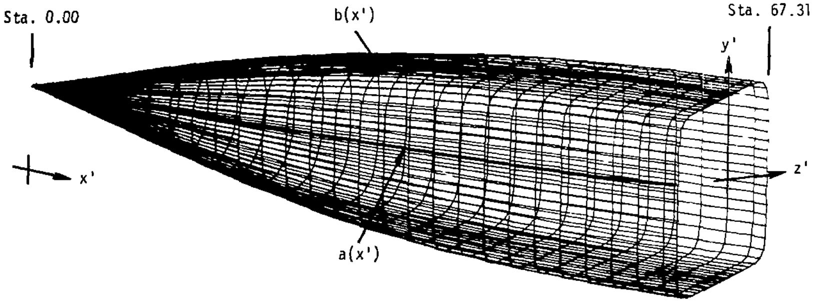

Nose-forebody external geometry parameters

x'	a(x')	b(x')	η(x')	x'	a(x')	b(x')	η(x')
0.00	0.0000	0.0000	2.0000	34.29	7.0564	6.6797	4.0652
1.27	.3167	.3167	2.0000	35.56	7.1923	6.7871	4.3139
2.54	.6332	.6332	2.0000	36.83	7.3205	6.8877	4.5695
3.81	.9500	.9500	2.0000	38.10	7.4412	6.9817	4.8307
5.08	1.2667	1.2667	2.0000	39.37	7.5547	7.0693	5.0957
6.35	1.5832	1.5832	2.0000	40.64	7.6614	7.1514	5.3632
7.62	1.8999	1.8999	2.0000	41.91	7.7612	7.2276	5.6314
8.89	2.2164	2.2164	2.0000	43.18	7.8547	7.2984	5.8989
10.16	2.5331	2.5331	2.0000	44.45	7.9418	7.3645	6.1641
11.43	2.8499	2.8499	2.0000	45.72	8.0231	7.4254	6.4253
12.70	3.1664	3.1664	2.0000	46.99	8.0985	7.4816	6.6811
13.97	3.4831	3.4831	2.0000	48.26	8.1681	7.5334	6.9299
15.24	3.7998	3.7998	2.0000	49.53	8.2324	7.5809	7.1704
15.26	3.8062	3.8062	2.0000	50.80	8.2913	7.6243	7.4011
16.51	4.1082	4.1041	2.0098	52.07	8.3449	7.6639	7.6205
17.78	4.4003	4.3845	2.0402	53.34	8.3937	7.6995	7.8276
19.05	4.6769	4.6441	2.0909	54.61	8.4376	7.7313	8.0209
20.32	4.9388	4.8847	2.1617	55.88	8.4767	7.7597	8.1995
21.59	5.1872	5.1087	2.2520	57.15	8.5113	7.7848	8.3622
22.86	5.4229	5.3172	2.3614	58.42	8.5413	7.8064	8.5080
24.13	5.6459	5.5118	2.4892	59.69	8.5669	7.8250	8.6362
25.40	5.8577	5.6937	2.6348	60.96	8.5885	7.8402	8.7460
26.67	6.0582	5.8636	2.7971	62.23	8.6058	7.6433	8.8367
27.94	6.2481	6.0228	2.9754	63.50	8.6192	7.8621	8.9078
29.21	6.4282	6.1719	3.1684	64.77	8.6286	7.8687	8.9598
30.48	6.5987	6.3116	3.3752	66.04	8.6342	7.8727	8.9897
31.75	6.7600	6.4422	3.5944	67.31	8.6360	7.8740	9.0000
33.02	6.9124	6.5649	3.8249				

(a) Nose-forebody section, with equations and table defining the external geometry.

Figure 2.- External geometry of nose-forebody section. All dimensions are in centimeters unless otherwise noted.

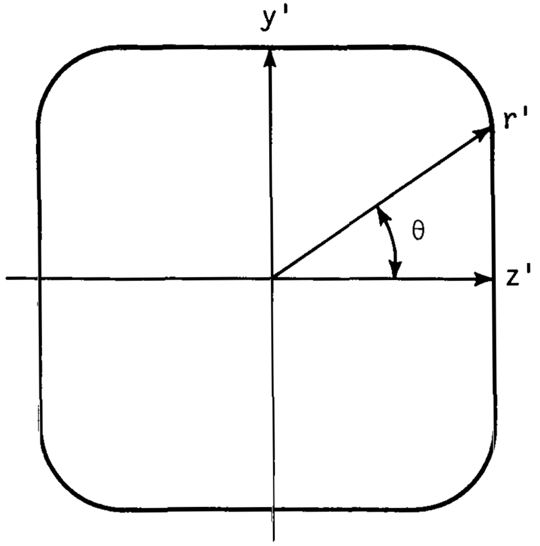

$$z'(x') = r'(x') \cos \theta \qquad y'(x') = r'(x') \sin \theta$$

$$r'(x') = \left\{ \left[\frac{\cos \theta}{a(x')} \right]^{\eta(x')} + \left[\frac{\sin \theta}{b(x')} \right]^{\eta(x')} \right\}^{-1/\eta(x')}$$

(b) Superellipse cross section at constant value of x', looking upstream.

Figure 2.- Concluded.

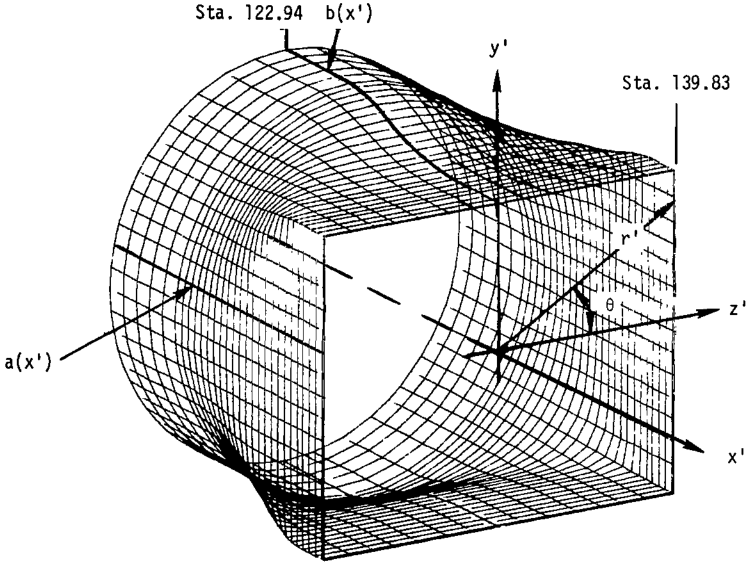

$122.94 \leq x' \leq 134.29$

$${\frac{z'(x')}{a(x')}}^{n(x')} + {\frac{y'(x')}{b(x')}}^{n(x')} = 1$$

$$r'(x') = \left\{ \left[\frac{\sin\theta}{b(x')}\right]^{n(x')} + \left[\frac{\cos\theta}{a(x')}\right]^{n(x')} \right\}^{-1/n(x')}$$

$$y'(x') = r'(x') \sin\theta$$

$$z'(x') = r'(x') \cos\theta$$

$134.29 \leq x' \leq 139.83$

$0° \leq \theta \leq 38.1460°$

$$y'(x') = a(x') \tan\theta$$

$$z'(x') = a(x')$$

$38.1460° \leq \theta \leq 90°$

$$y'(x') = b(x')$$

$$z'(x') = \frac{b(x')}{\tan\theta}$$

Transition-section internal-geometry parameters			
x'	a(x')	b(x')	n(x')
122.94	6.2865	6.2865	2.0000
126.75	6.2865	6.2865	2.0000
127.13	6.2865	6.2675	2.0151
127.51	6.2865	6.2144	2.0612
127.89	6.2865	6.1303	2.1406
128.27	6.2865	6.0216	2.2576
128.65	6.2865	5.8953	2.4187
129.03	6.2865	5.7595	2.6338
129.41	6.2865	5.6215	2.9173
129.79	6.2865	5.4882	3.2908
130.18	6.2865	5.3647	3.7863
130.56	6.2865	5.2553	4.4539
130.94	6.2865	5.1623	5.3737
131.32	6.2865	5.0874	6.6810
131.70	6.2865	5.0302	8.6176
132.08	6.2865	4.9893	11.6511
132.46	6.2865	4.9627	16.7835
132.84	6.2865	4.9474	26.4952
133.22	6.2865	4.9403	48.4106
133.60	6.2865	4.9378	116.5000
133.99	6.2865	4.9375	587.9680
134.29	6.2865	4.9375	
139.83	6.2865	4.9375	

Figure 3.- Transition section with equations and table defining the internal geometry. All dimensions are in centimeters unless otherwise specified.

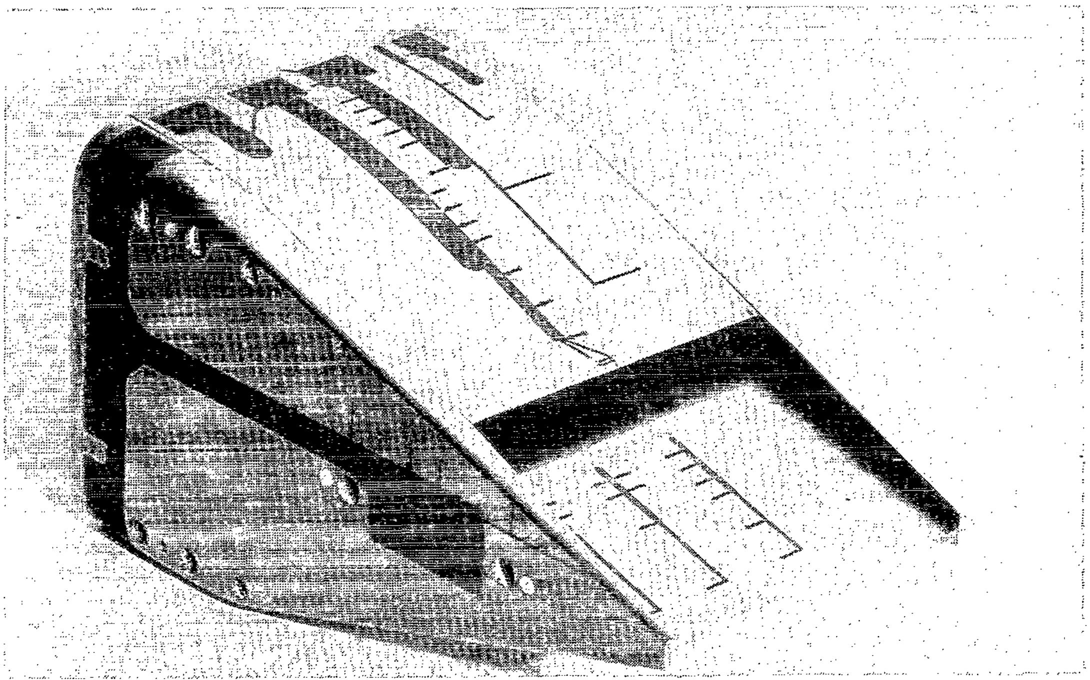

L-81-6332

(a) Low-expansion-ratio configuration.

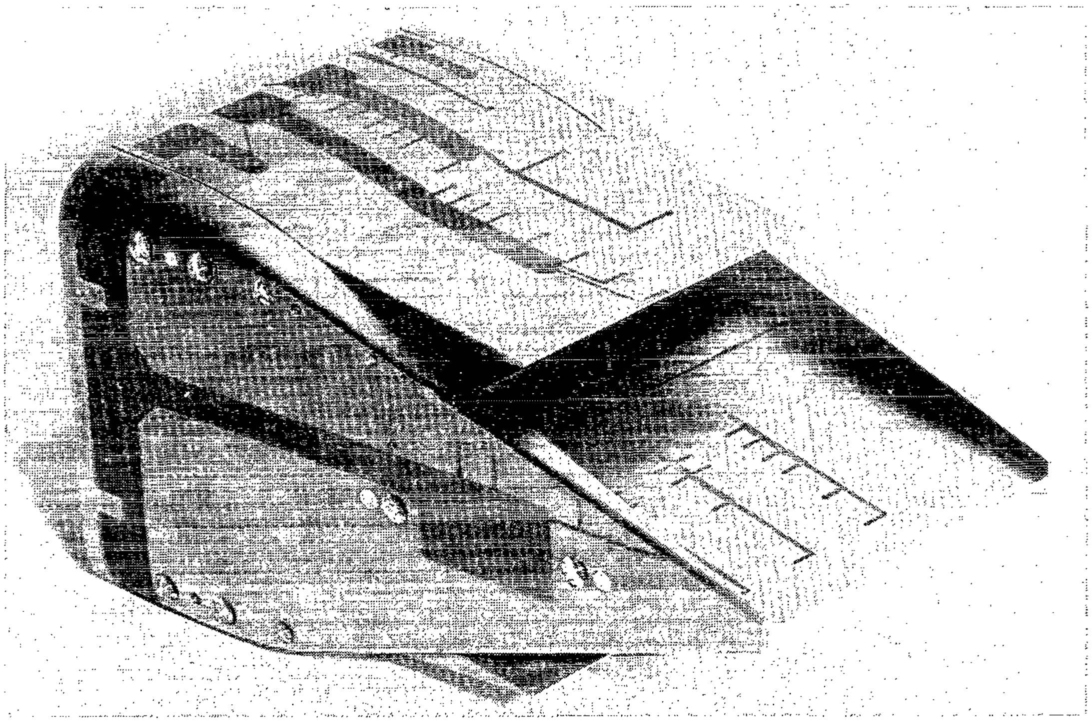

L-81-6334

(b) High-expansion-ratio configuration.

Figure 4.- Nonaxisymmetric wedge nozzles.

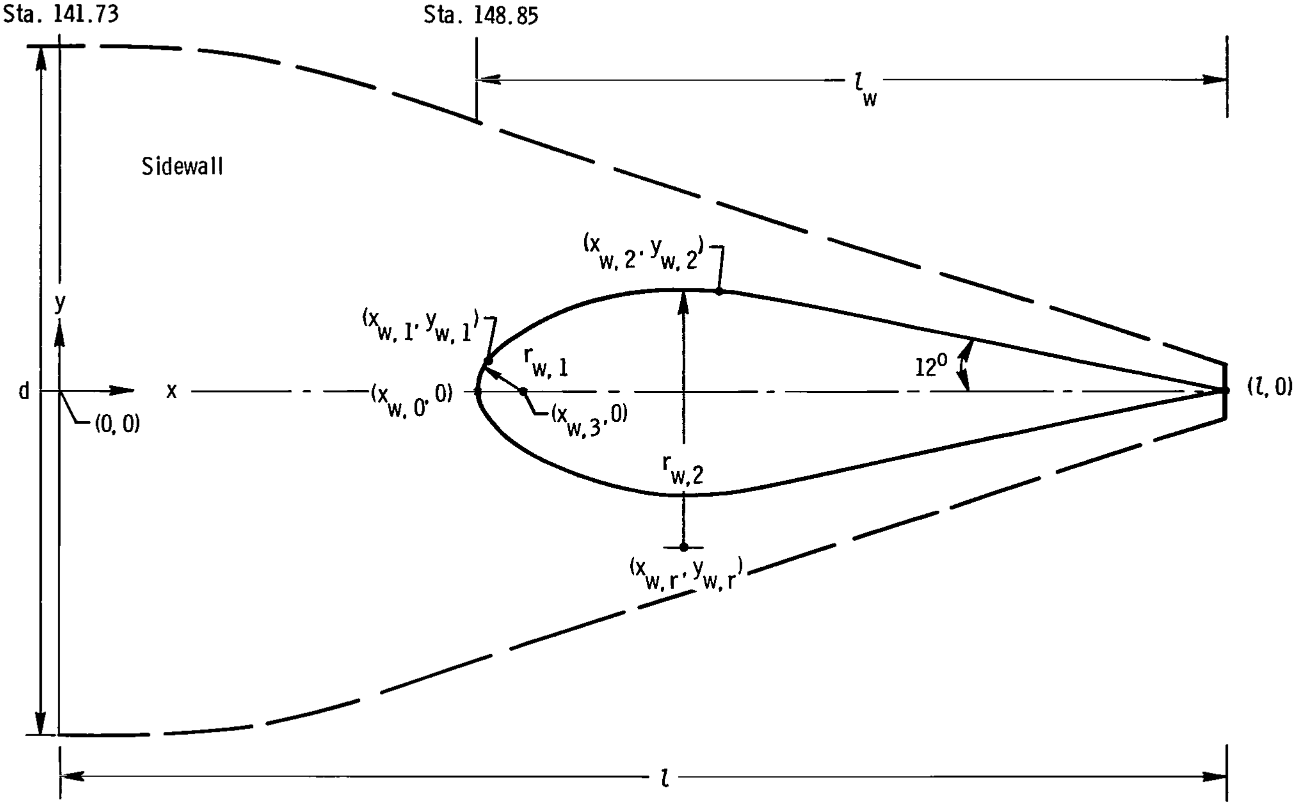

d	15.748
l	25.417
l_w . . .	16.398
$r_{w,1}$ . .	0.958
$r_{w,2}$ . .	5.955
$x_{w,0}$ . .	9.019
$x_{w,1}$ . .	9.303
$x_{w,2}$ . .	14.729
$x_{w,3}$ . .	9.477
$x_{w,r}$ . .	13.491
$y_{w,1}$ . .	0.681
$y_{w,2}$ . .	2.272
$y_{w,r}$ . .	-3.553

(a) Wedge geometry.

Figure 5.- Internal and external geometry for both nozzle configurations. All dimensions are in centimeters unless otherwise noted.

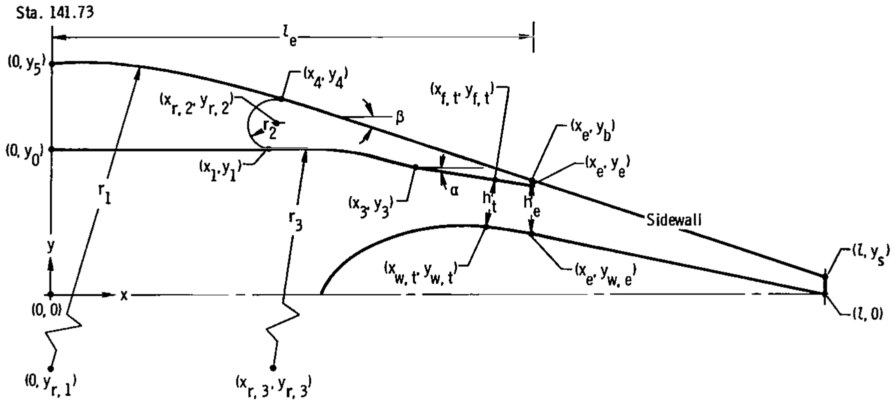

Low-expansion-ratio configuration

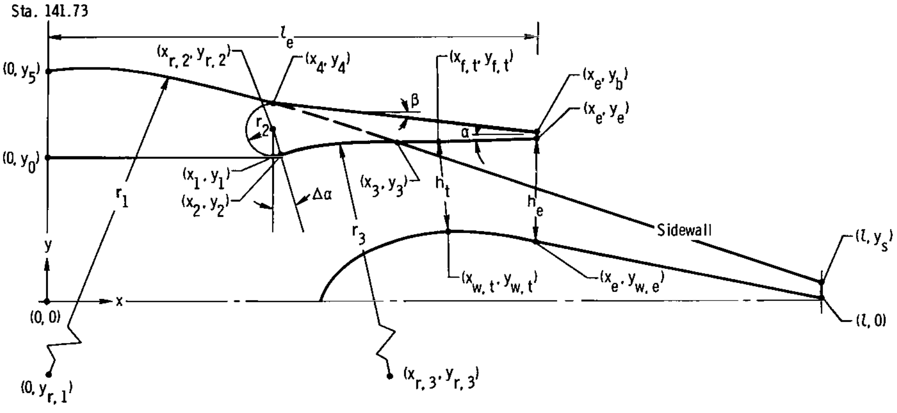

High-expansion-ratio configuration

	Low expansion ratio	High expansion ratio
A_e/A_t . .	1.060	1.200
h_e. . . .	1.707	3.652
h_t. . . .	1.611	3.044
l	25.417	25.417
l_e	15.782	16.025
r_1. . . .	23.622	23.622
r_2. . . .	0.871	0.871
r_3. . . .	18.220	18.220
x_e	15.782	16.025
$x_{f,t}$ . . .	14.603	12.852
$x_{r,2}$ . . .	7.274	7.274
$x_{r,3}$ . . .	7.274	11.413

	Low expansion ratio	High expansion ratio
$x_{w,t}$ . .	14.366	13.068
x_1. . . .	7.274	7.274
x_2. . . .		7.463
x_3. . . .	11.973	12.183
x_4. . . .	7.553	7.553
y_b. . . .	3.856	5.750
y_e. . . .	3.755	5.649
$y_{f,t}$ . . .	3.931	5.423
$y_{r,1}$ . . .	-15.748	-15.748
$y_{r,2}$ . . .	5.809	5.809
$y_{r,3}$ . . .	-13.282	-12.828
y_s	0.606	0.606

	Low expansion ratio	High expansion ratio
$y_{w,e}$ . . .	2.048	1.997
$y_{w,t}$ . . .	2.337	2.387
y_0	4.937	4.937
y_1	4.937	4.937
y_2		4.958
y_3	4.321	5.375
y_4	6.634	6.634
y_5	7.874	7.874
α, deg . .	8.448	4.073
β, deg . .	18.647	5.955
Δα, deg . .	0.000	12.521

(b) Flap geometry.

Figure 5.- Continued.

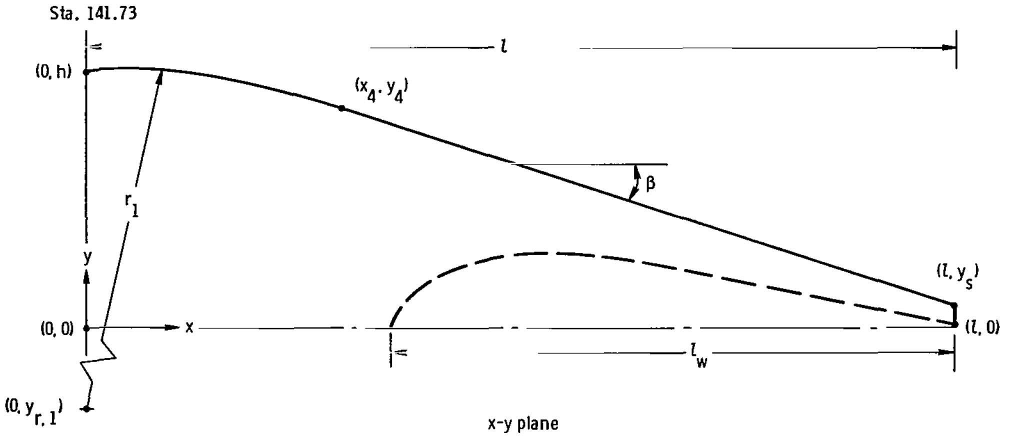

x-y plane

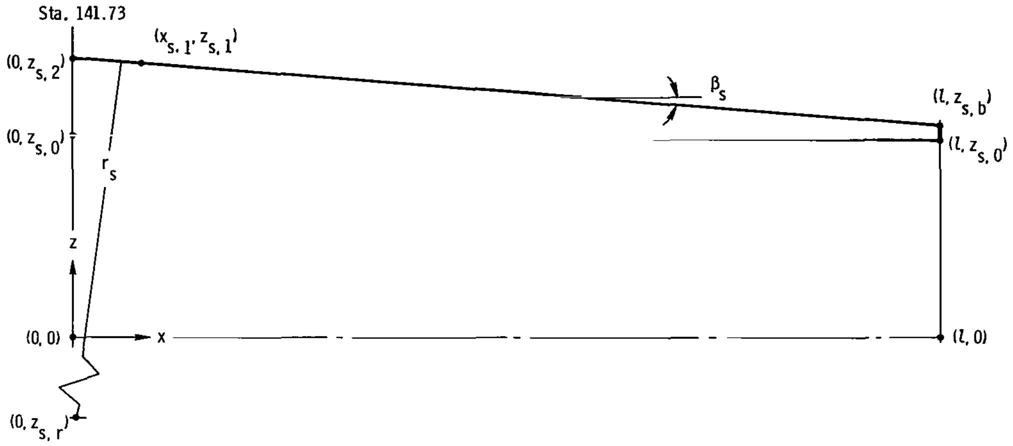

x-z plane

h	7.874
l	25.417
l_w . . .	16.398
r_1 . . .	23.622
r_s . . .	23.622
x_4 . . .	7.553
$x_{s,1}$ . .	1.957
y_4 . . .	6.634
$y_{r,1}$ . .	23.622
y_s . . .	0.606
$z_{s,0}$ . .	6.287
$z_{s,1}$ . .	8.555
$z_{s,2}$ . .	8.636
$z_{s,b}$ . .	6.604
$z_{s,r}$ . .	-23.622
β, deg .	18.647
β_s, deg.	4.753

(c) Sidewall geometry.

Figure 5.- Concluded.

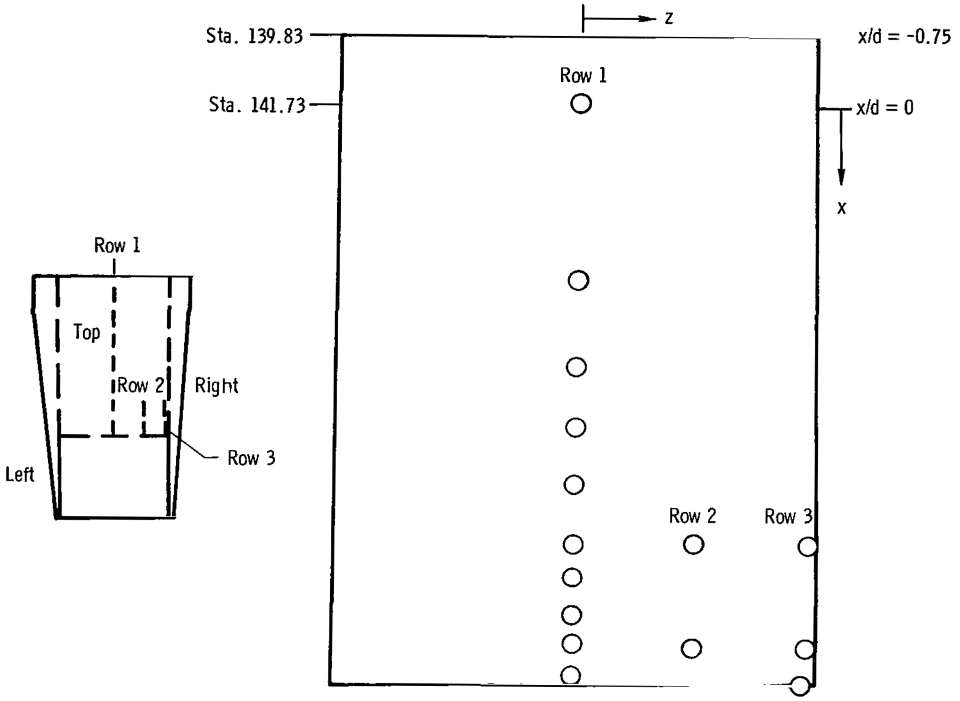

Internal orifice coordinates						
x/d	Row 1		Row 2		Row 3	
	y	z	y	z	y	z
Low expansion ratio						
0.000	4.938	0.000		3.144		6.033
.300	4.938					
.450	4.938					
.550	4.884					
.650	4.695					
.750	4.364		4.364		4.364	
.800	4.228					
.875	4.053					
.927	3.931		3.931		3.931	
.975	3.819					
1.002					[a]3.806	
High expansion ratio						
0.000	4.938	0.000		3.144		6.033
.300	4.938					
.450	4.938					
.560	5.206					
.661	5.363					
.763	5.381		5.381		5.381	
.814	5.420					
.889	5.505					
.942	5.564		5.564		5.564	
.990	5.616					
1.018					[a]5.649	

[a] Base pressure.

(a) Internal flap pressure orifices.

Figure 6.- Pressure orifice locations. All flap pressure orifices are located on top flap; all wedge pressure orifices are located on top of wedge. All dimensions are in centimeters unless otherwise noted.

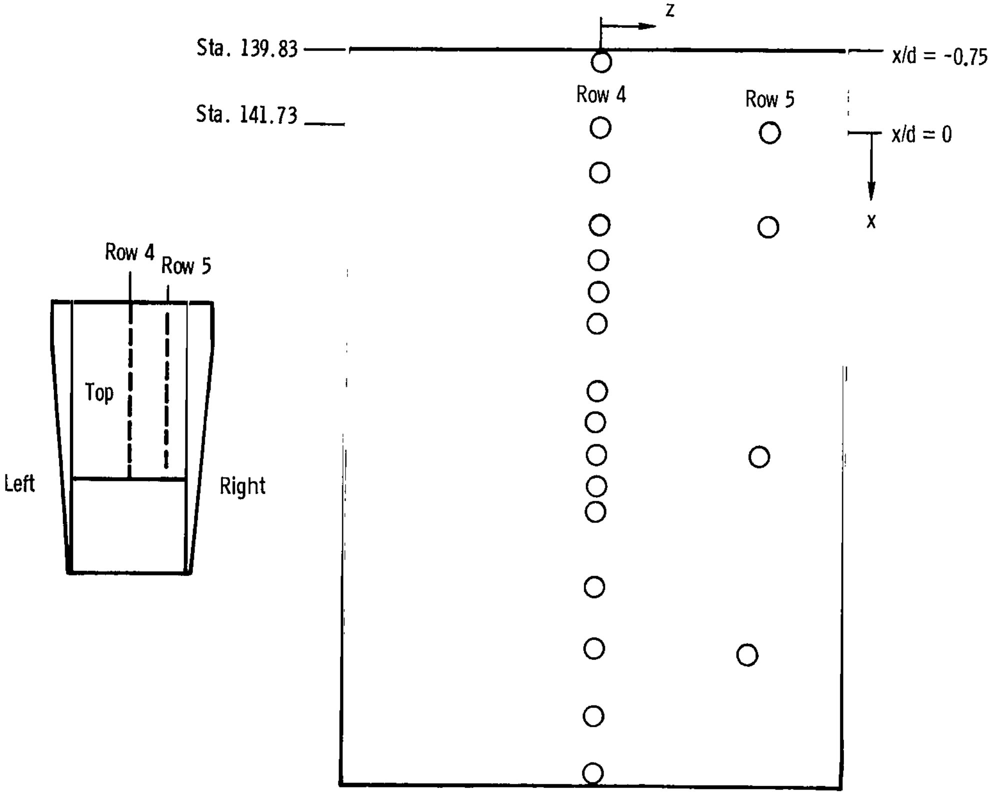

External orifice coordinates

x/d	Row 4		Row 5	
	y	z	y	z
Low expansion ratio				
-0.100	7.874	0.000		
.000	7.874		7.872	4.318
.100	7.821			
.150	7.756		7.755	5.023
.200	7.663			
.250	7.544			
.300	7.397			
.400	7.019			
.450	6.786			
.500	6.526			
.550	6.260			
.600	5.994			
.700	5.463			
.800	4.931		4.931	3.835
.900	4.400			
1.002	[a]3.806			
High expansion ratio				
-0.100	7.874	0.000		
.000	7.874		7.872	4.318
.100	7.821			
.150	7.756			
.200	7.663			
.250	7.544			
.300	7.397			
.400	7.019			
.450	6.786			
.490	6.618		6.618	4.032
.542	6.532			
.594	6.446			
.699	6.273			
.804	6.109		6.101	3.835
.909	5.928			
1.018	[a]5.750			

[a] Base pressure.

(b) External flap pressure orifices.

Figure 6.- Continued.

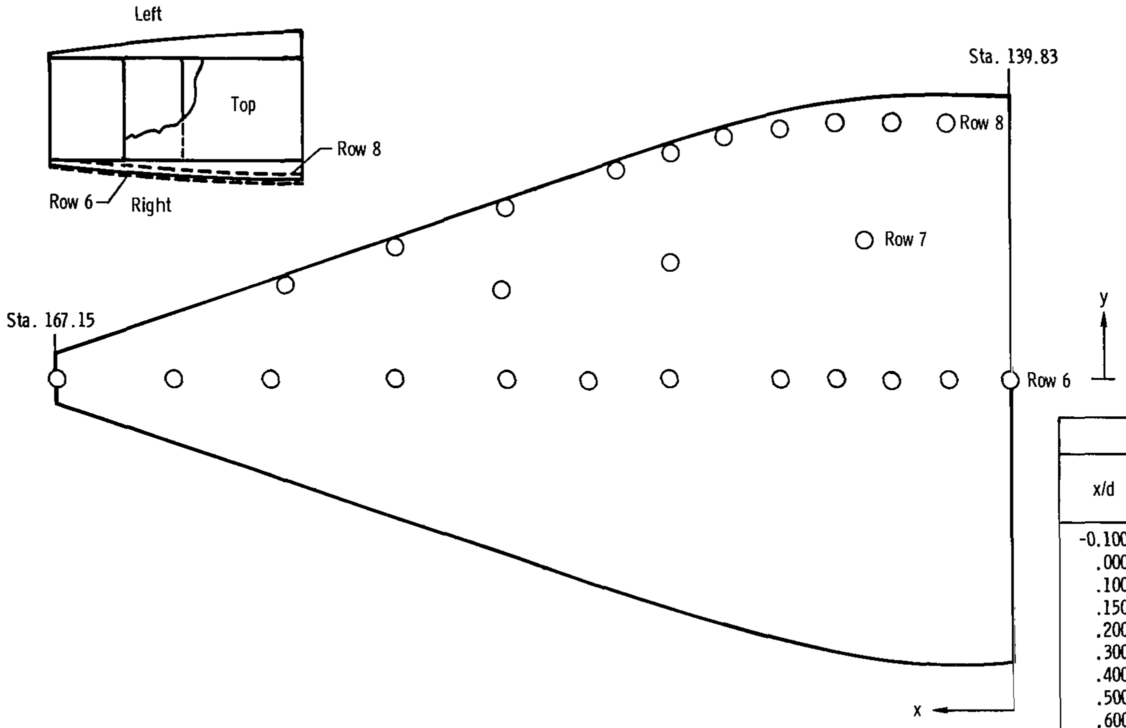

Sidewall external orifice coordinates						
x/d	Row 6		Row 7		Row 8	
	y	z	y	z	y	z
-0.100	0.000	8.636				
.000		8.636			7.189	8.096
.100		8.583			7.185	8.081
.150			3.878	8.521		
.200		8.456			7.150	8.055
.300		8.325			7.031	8.054
.400					6.812	8.065
.500		8.063	3.253	8.063	6.408	8.011
.600					5.869	7.885
.650		7.866				
.800		7.670	2.466	7.670	4.790	7.635
1.002		7.405			3.696	7.382
1.200					2.620	7.133
1.224		7.146				
1.400		6.884				
1.614		[a]6.445				

[a]Base pressure.

(c) External sidewall (right sidewall) pressure orifices.

Figure 6.- Continued.

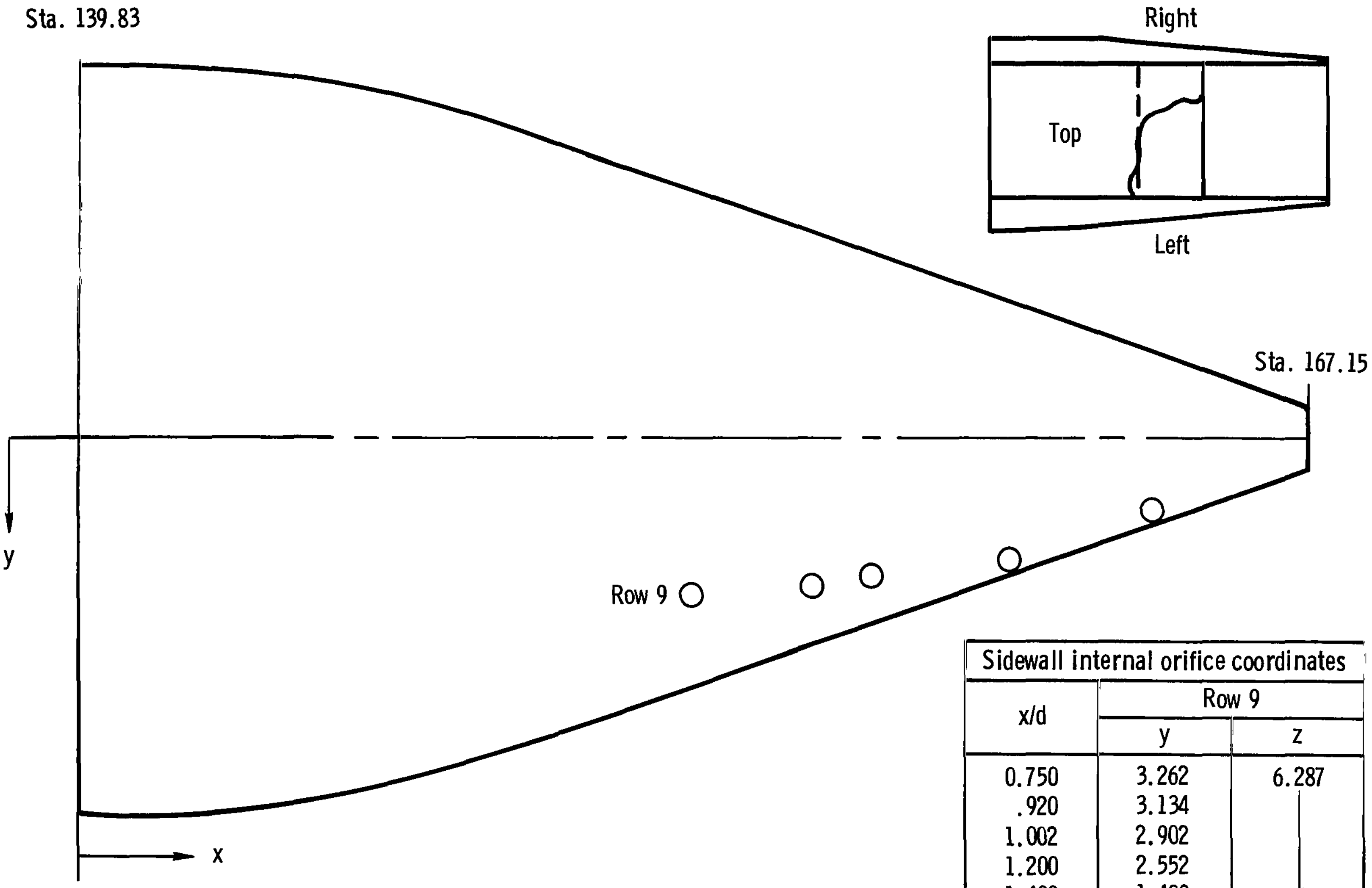

Sidewall internal orifice coordinates		
x/d	Row 9	
	y	z
0.750	3.262	6.287
.920	3.134	↓
1.002	2.902	
1.200	2.552	
1.400	1.489	

(d) Internal sidewall (left sidewall) pressure orifices.

Figure 6.- Continued.

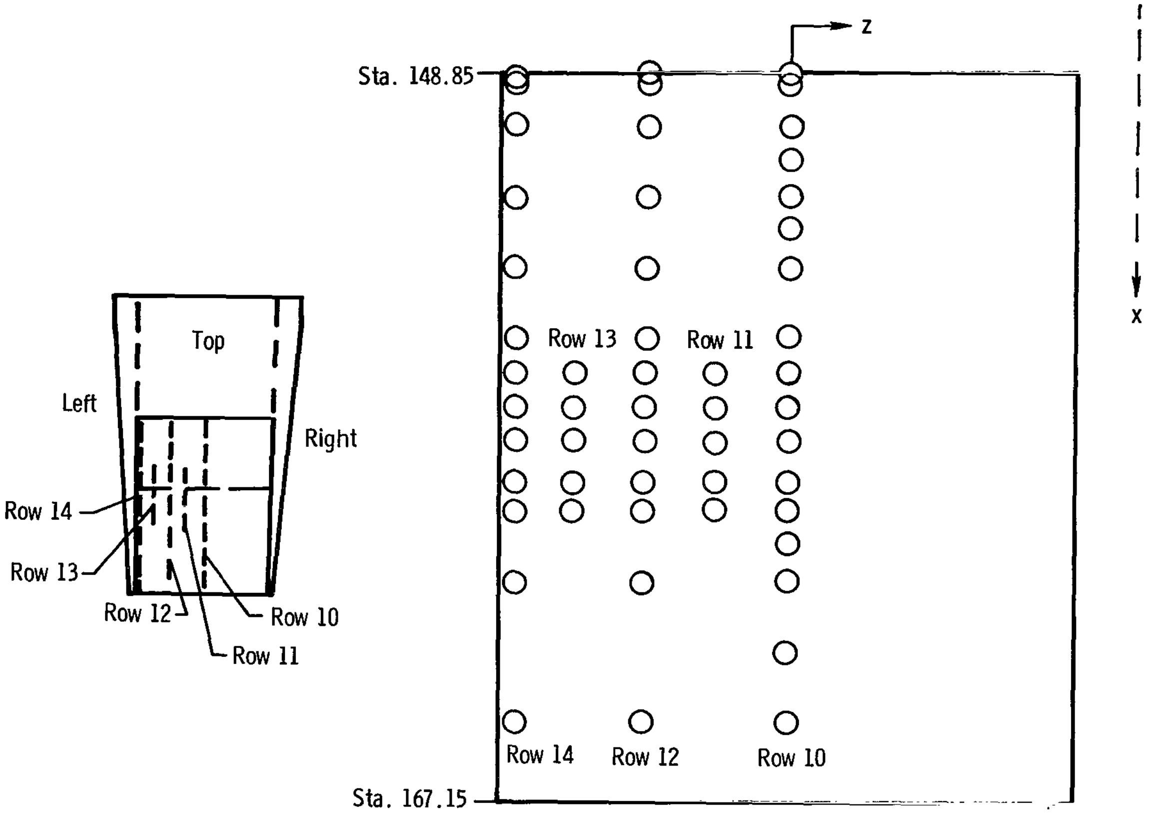

Wedge internal and external orifice coordinates					
x/d	y at –				
	Row 10 (z = 0.000)	Row 11 (z = -1.572)	Row 12 (z = -3.144)	Row 13 (z = -4.715)	Row 14 (z = -6.033)
0.573	0.000		0.000		0.000
.591	.681		.681		.681
.650	1.434		1.434		1.434
.700	1.867				
.750	2.160		2.160		2.160
.800	2.335				
.850	2.401		2.401		2.401
.950	2.223		2.223		2.223
1.002	2.048	2.048	2.048	2.048	2.048
1.050	1.888	1.888	1.888	1.888	1.888
1.100	1.721	1.721	1.721	1.721	1.721
1.155	1.536	1.536	1.536	1.536	1.536
1.200	1.721	1.721	1.721	1.721	1.721
1.250	1.218				
1.300	1.051		1.051		1.051
1.400	.716				
1.500	.382		.382		.382

(e) Wedge pressure orifices.

Figure 6.- Concluded.

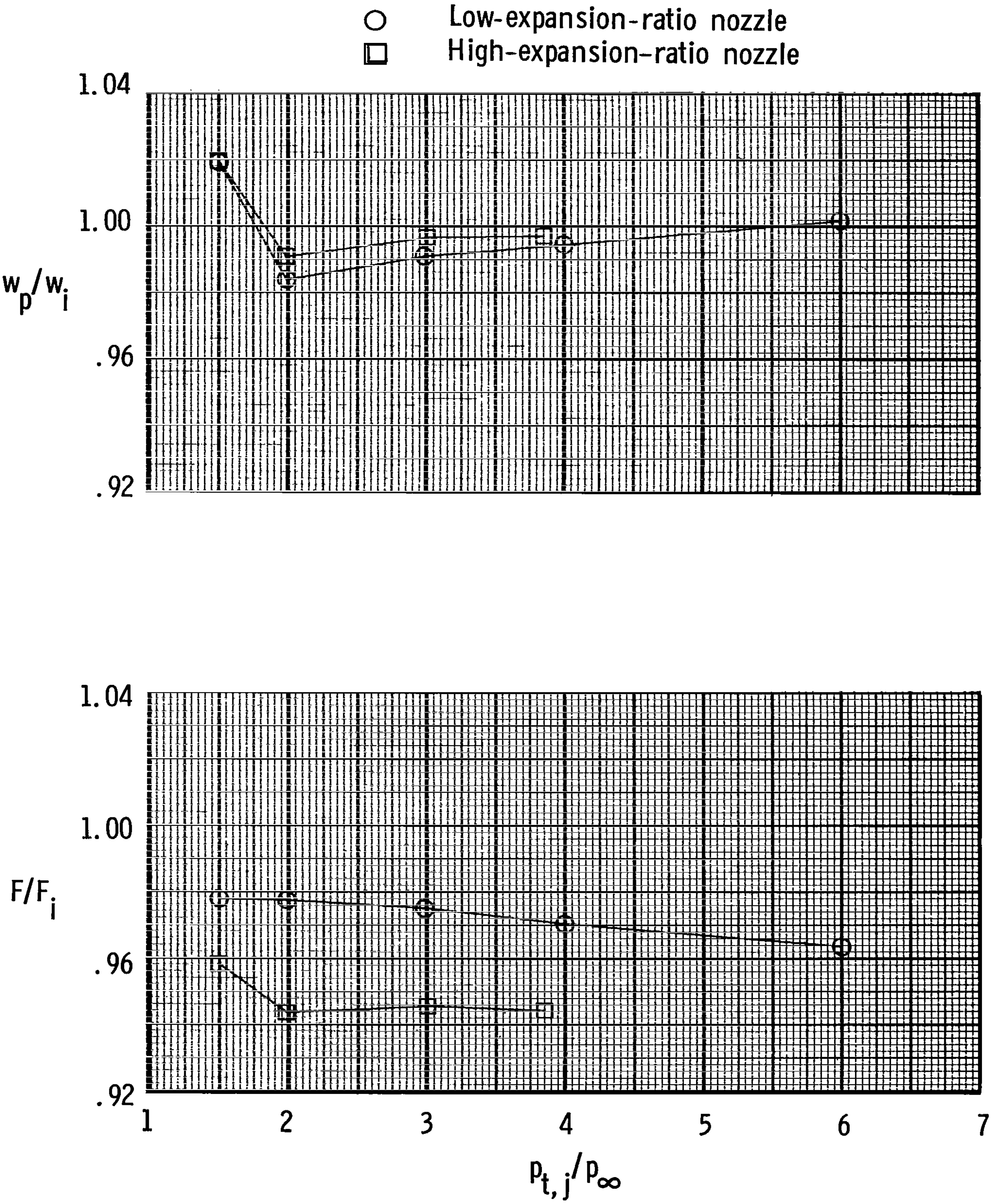

Figure 7.- Static performance data.

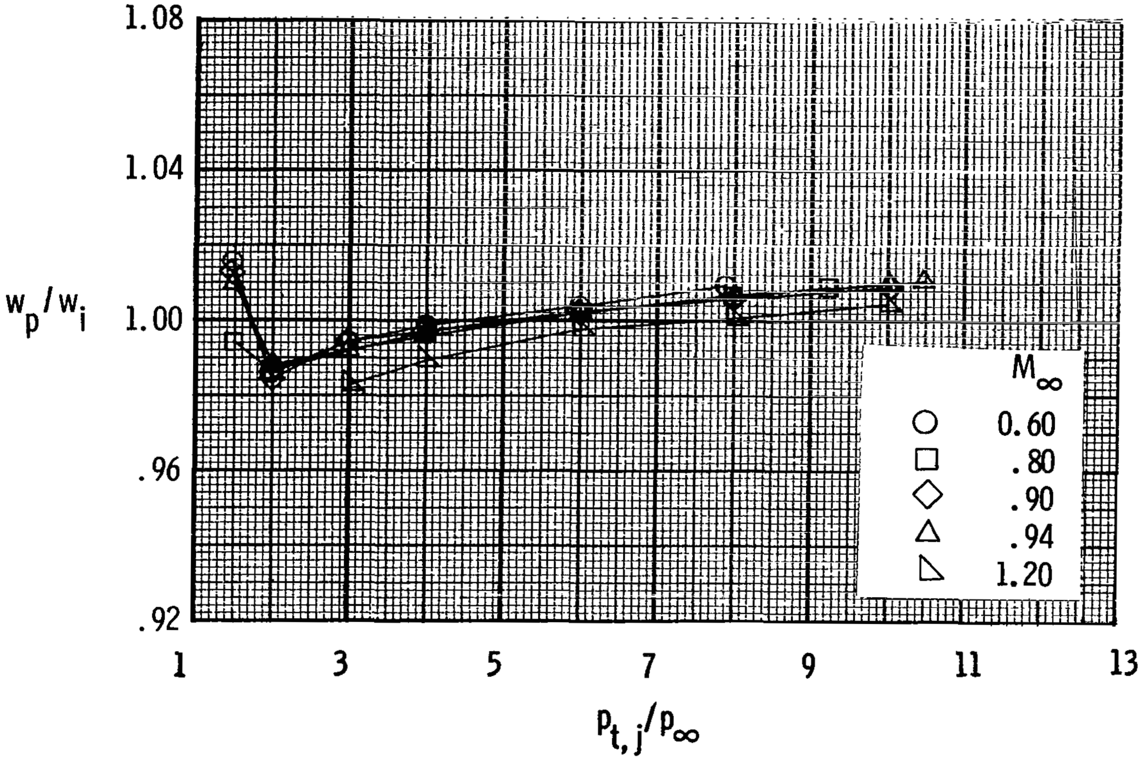

(a) Low-expansion-ratio nozzle.

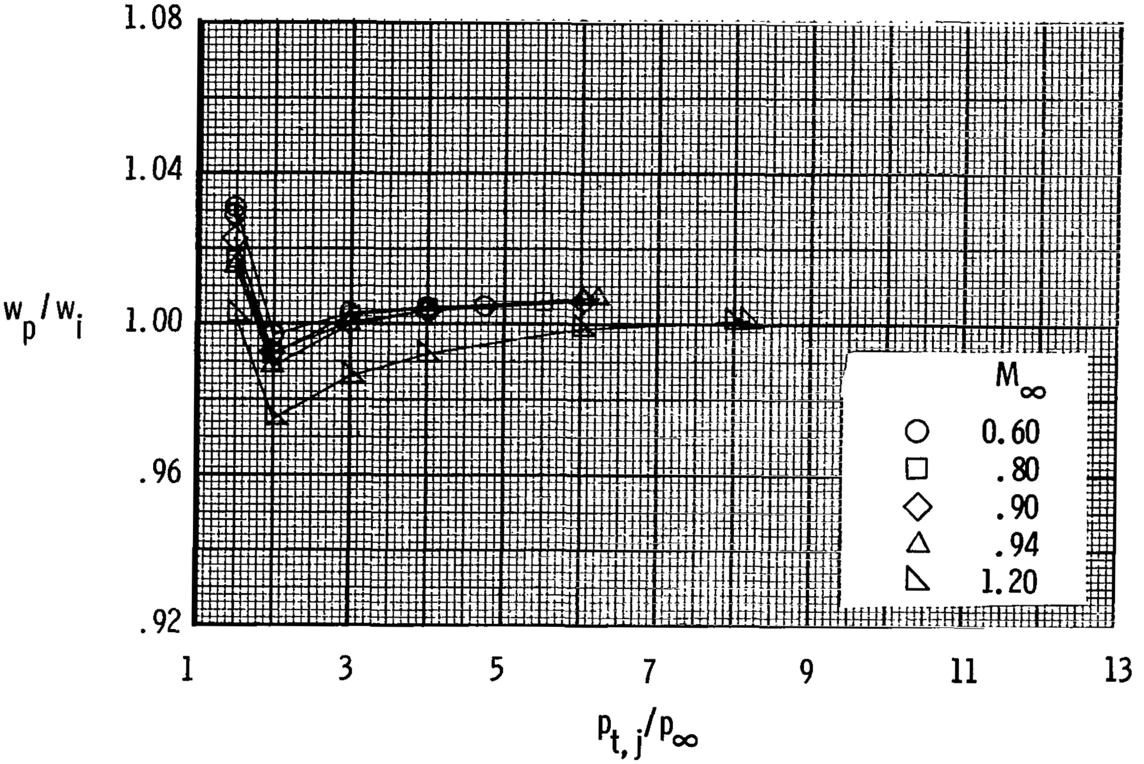

(b) High-expansion-ratio nozzle.

Figure 8.- Variation of discharge coefficient with free-stream Mach number.

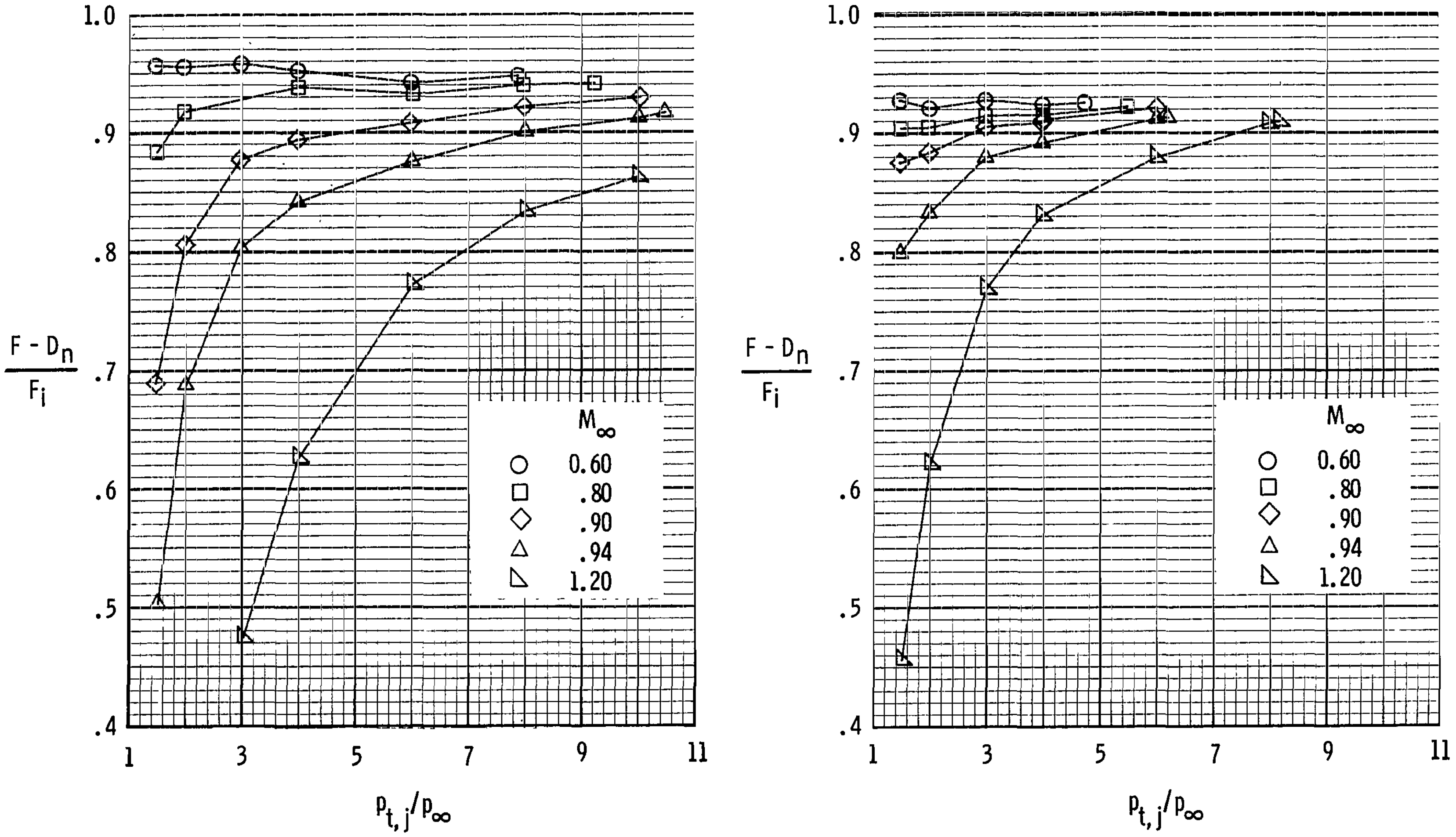

(a) Low-expansion-ratio nozzle.

(b) High-expansion-ratio nozzle.

Figure 9.- Variation of thrust-minus-nozzle drag ratio with free-stream Mach number.

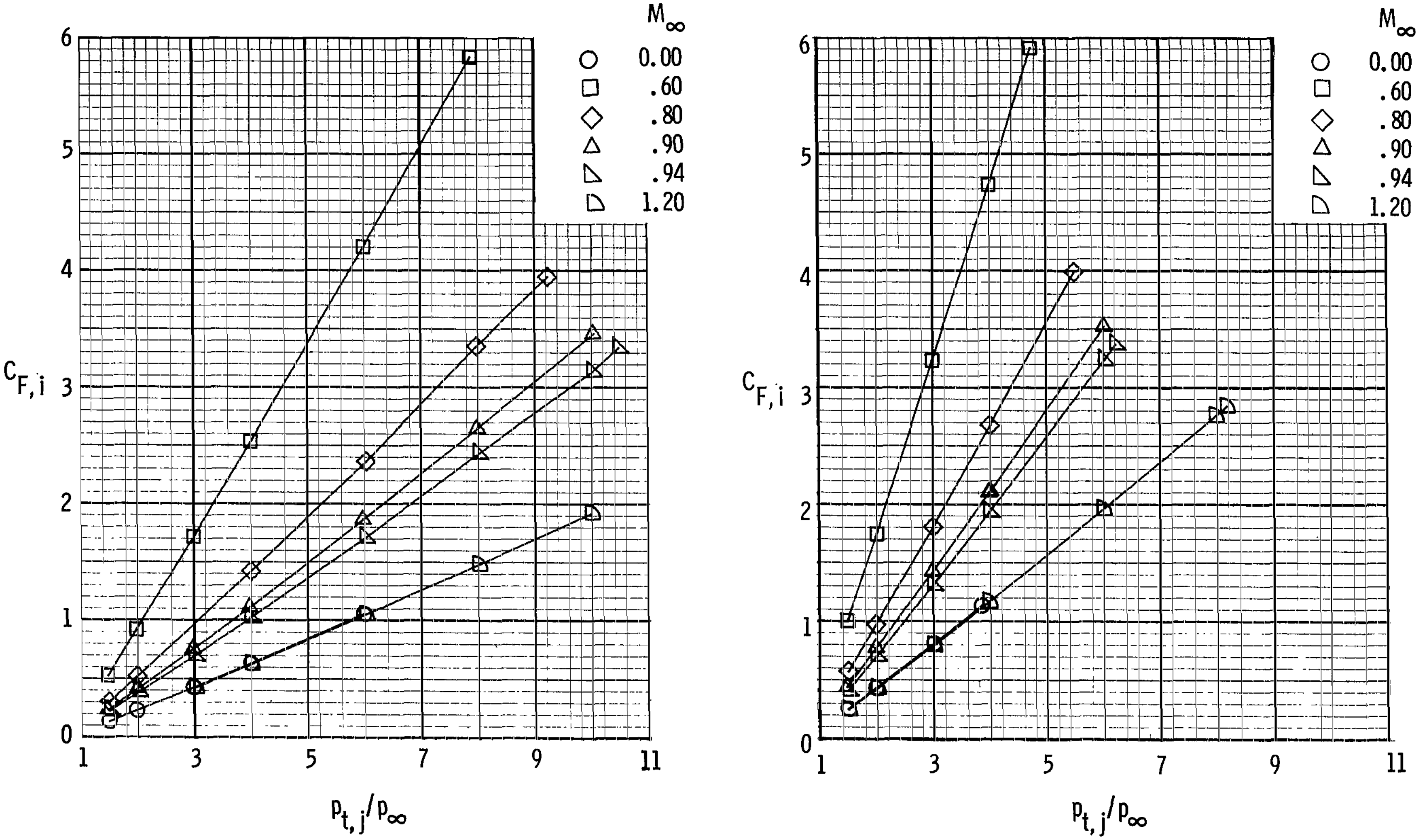

(a) Low-expansion-ratio nozzle.

(b) High-expansion-ratio nozzle.

Figure 10.- Variation of thrust coefficient with free-stream Mach number.

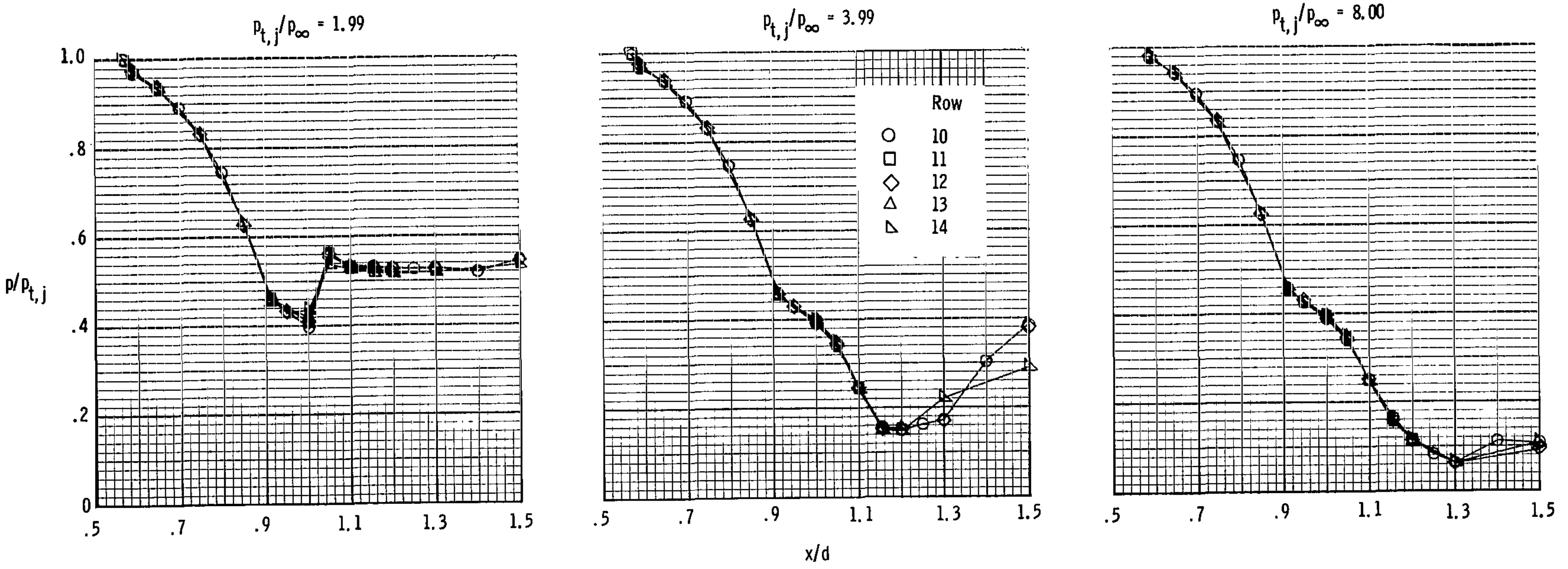

(a) M_∞ = 0.60.

Figure 11.- Static-pressure distributions along wedge surface at selected test conditions for low-expansion-ratio nozzle.

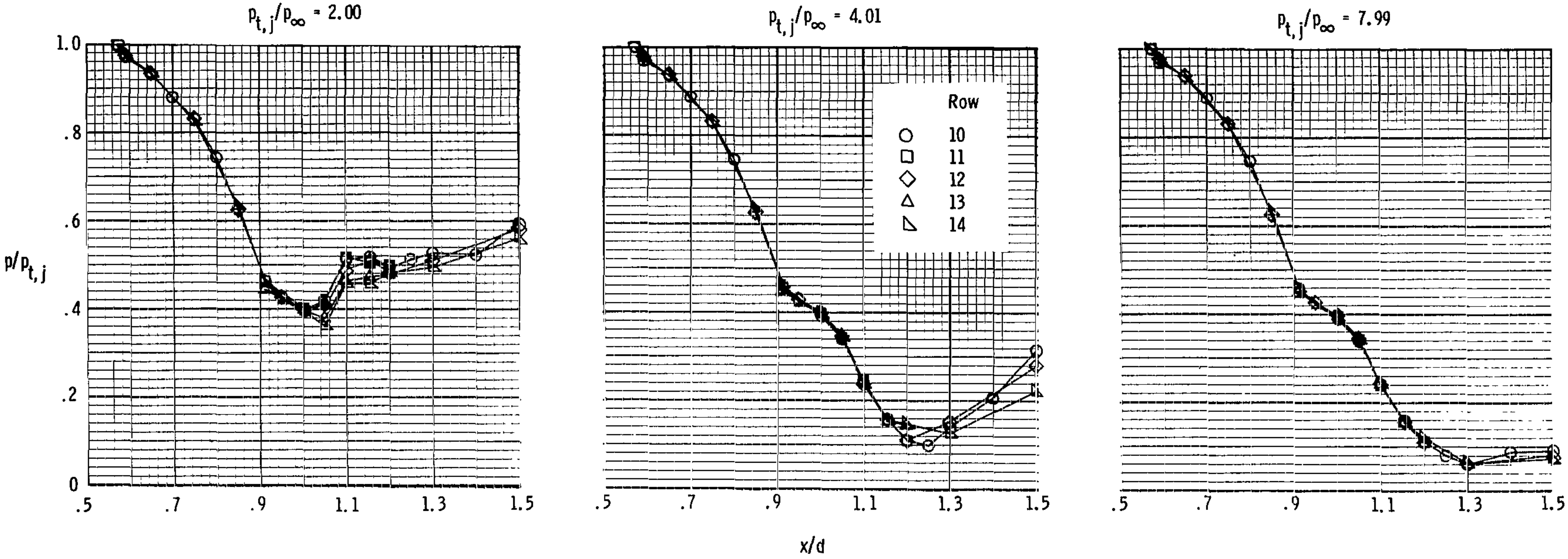

(b) $M_\infty = 1.20$.

Figure 11.- Concluded.

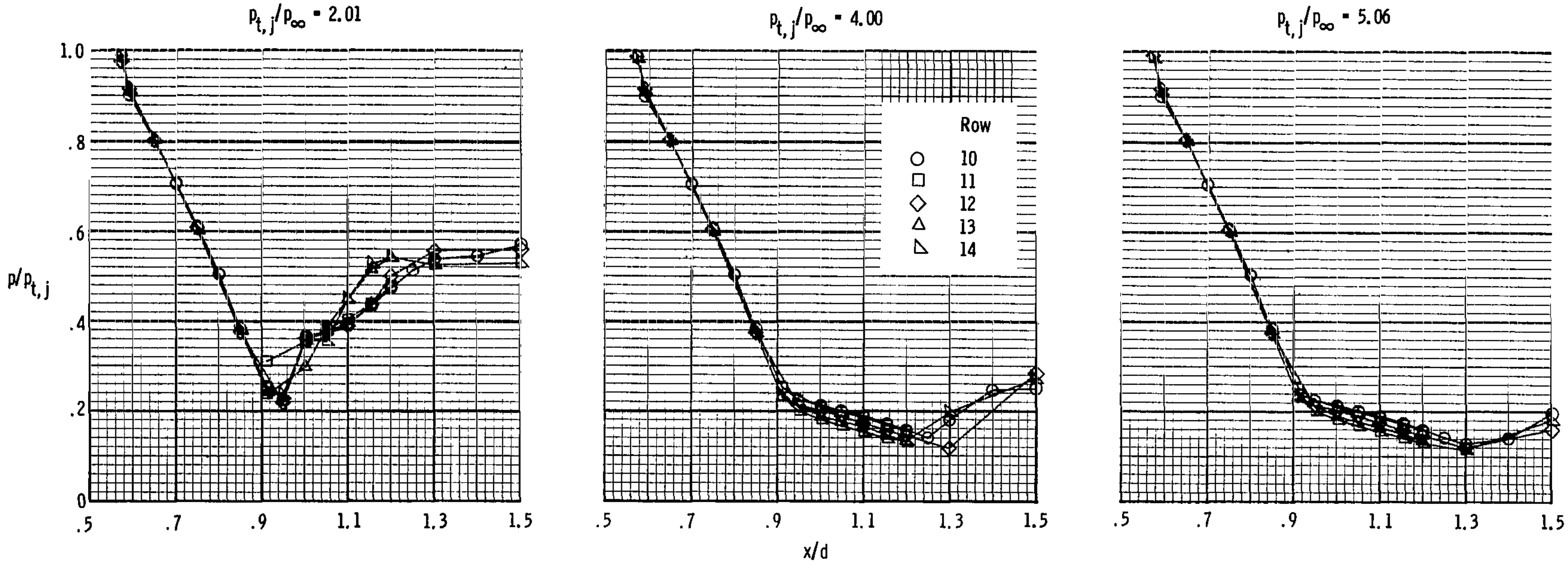

(a) M_∞ = 0.60.

Figure 12.- Static-pressure distributions along wedge surface at selected test conditions for high-expansion-ratio nozzle.

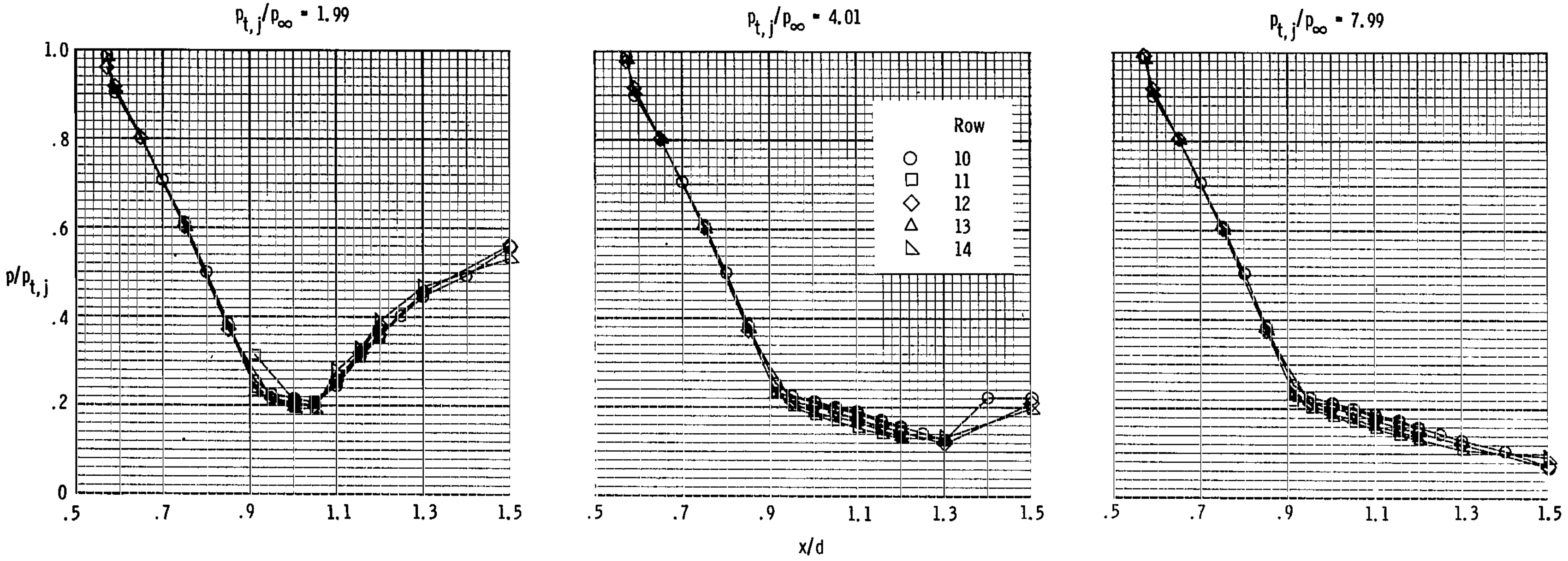

(b) $M_\infty = 1.20$.

Figure 12.- Concluded.

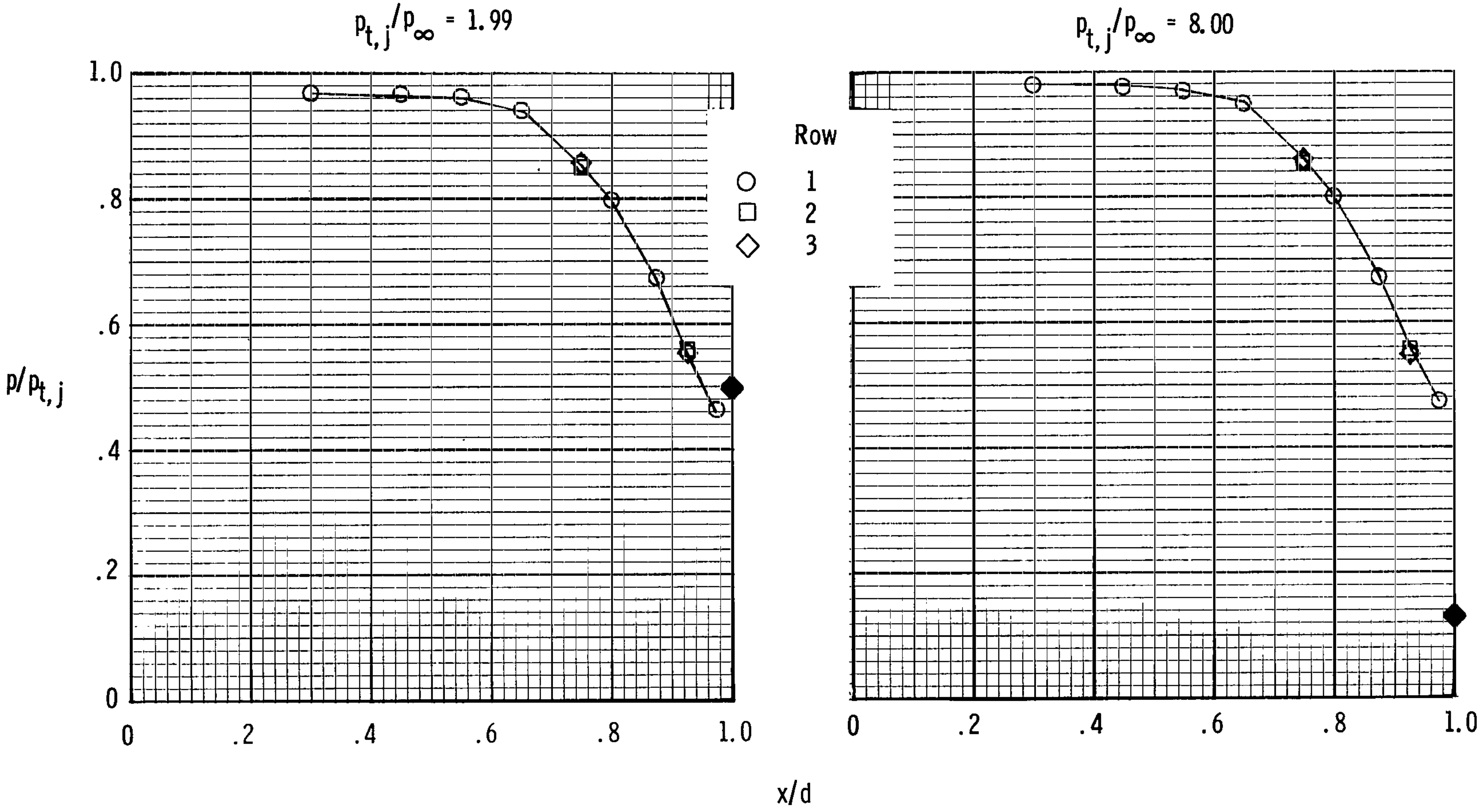

(a) $M_\infty = 0.60$.

Figure 13.- Internal static-pressure distributions along the upper flap at selected test conditions for low-expansion-ratio nozzle. Base pressure is indicated by solid symbol.

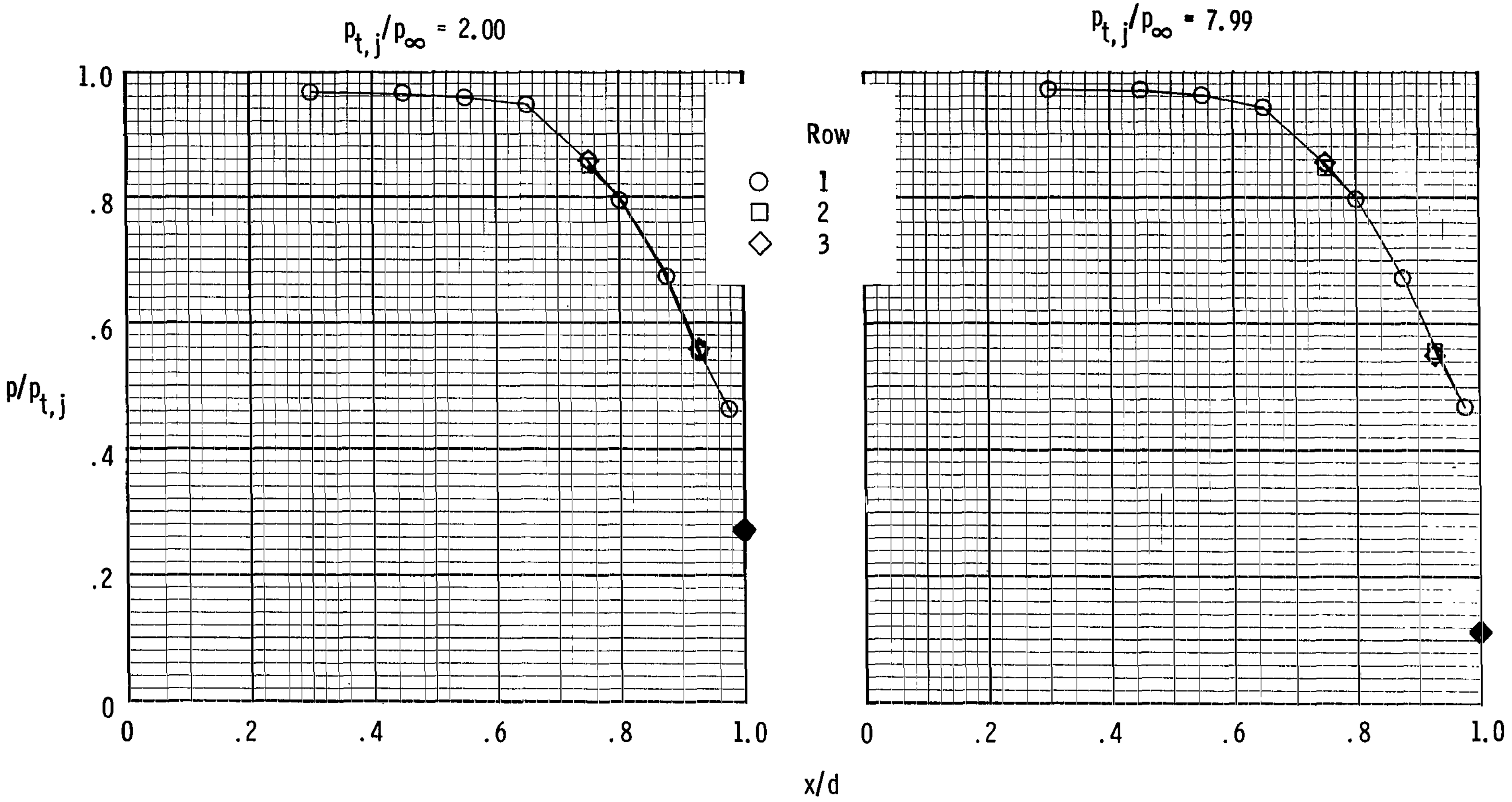

(b) $M_\infty = 1.20$.

Figure 13.- Concluded.

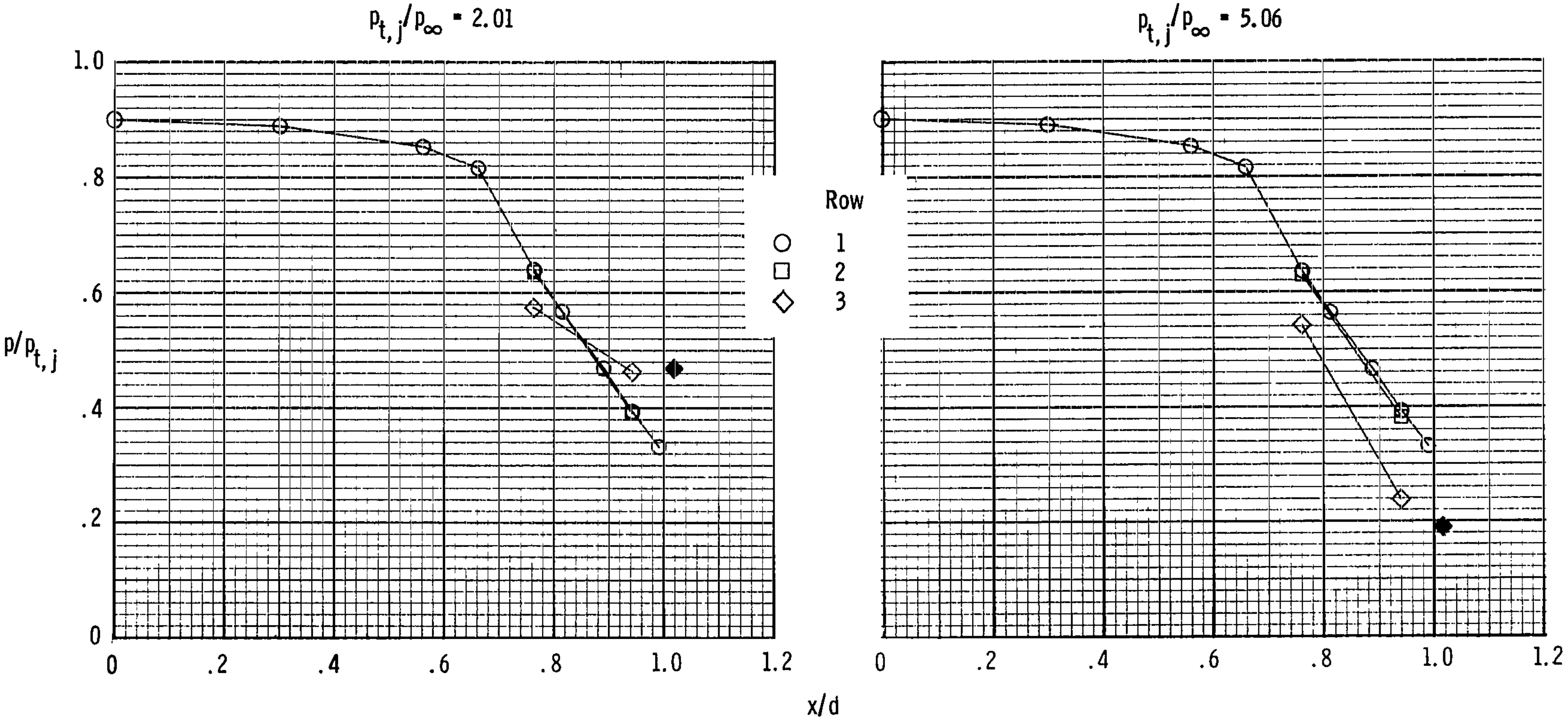

(a) $M_\infty = 0.60$.

Figure 14.- Internal static-pressure distributions along upper flap at selected test conditions for high-expansion-ratio nozzle. Base pressure is indicated by solid symbol.

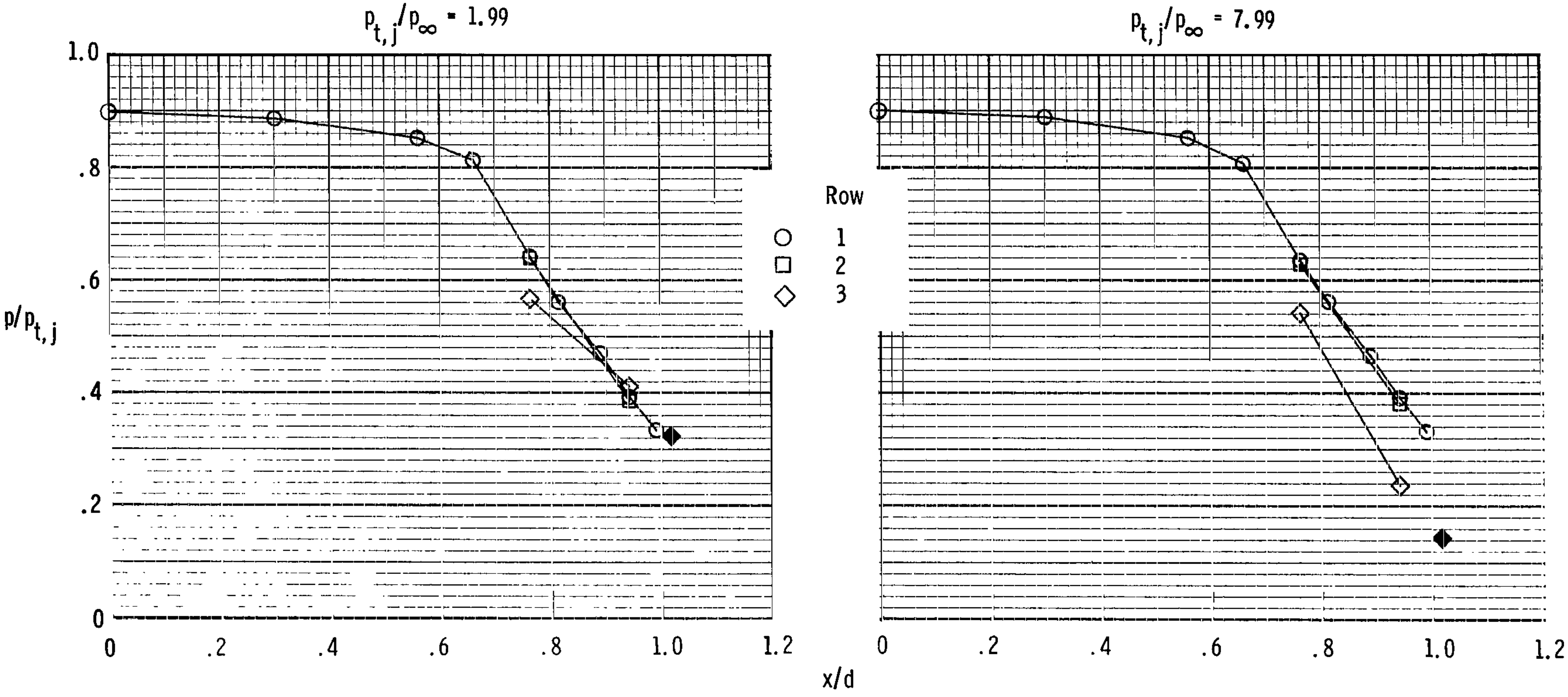

(b) M_∞ = 1.20.

Figure 14.- Concluded.

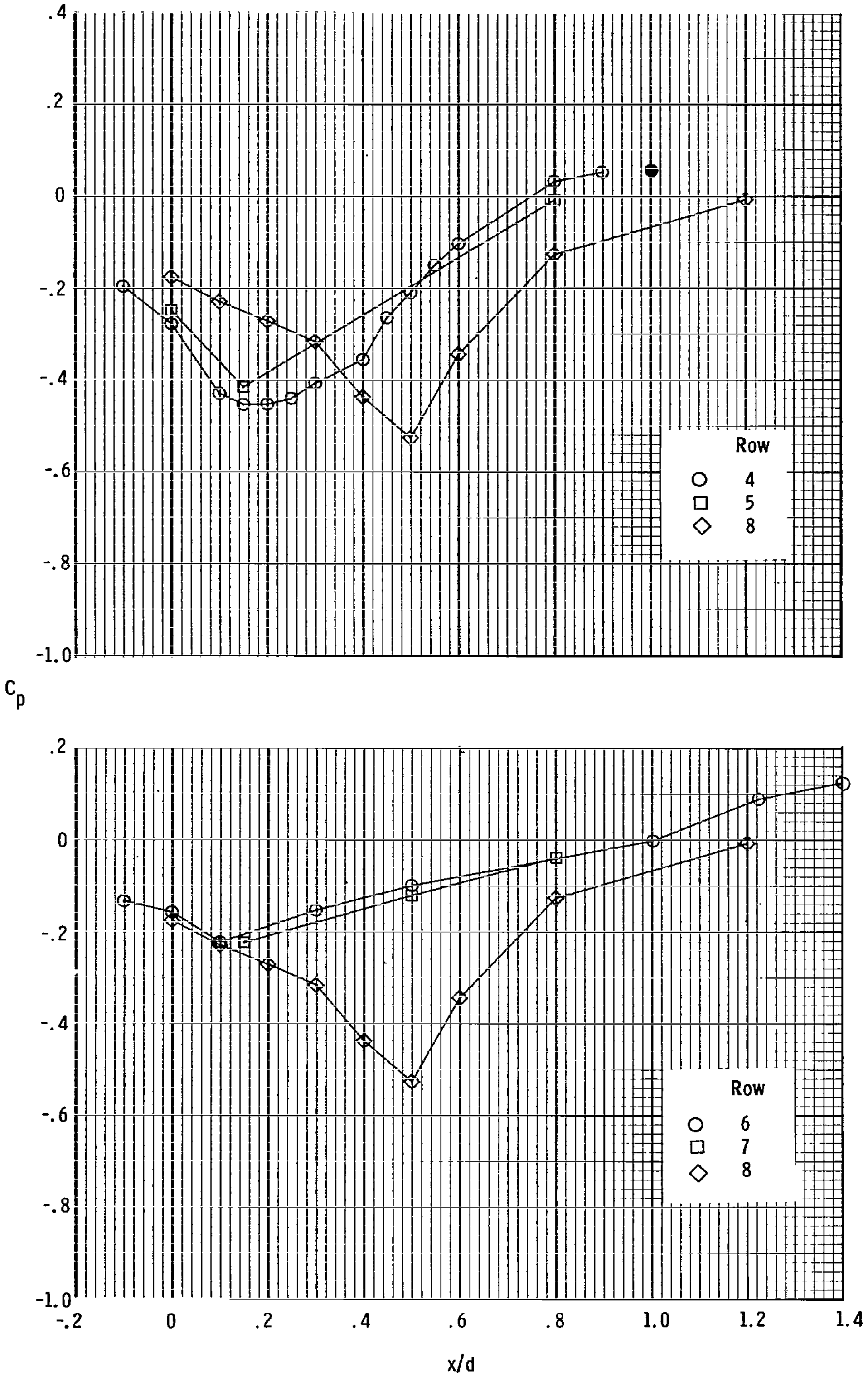

(a) $M_\infty = 0.60$; $p_{t,j}/p_\infty = 1.99$.

Figure 15.- External pressure distributions along upper flap and right sidewall at selected test conditions for low-expansion-ratio nozzle. Base pressure is indicated by solid symbol.

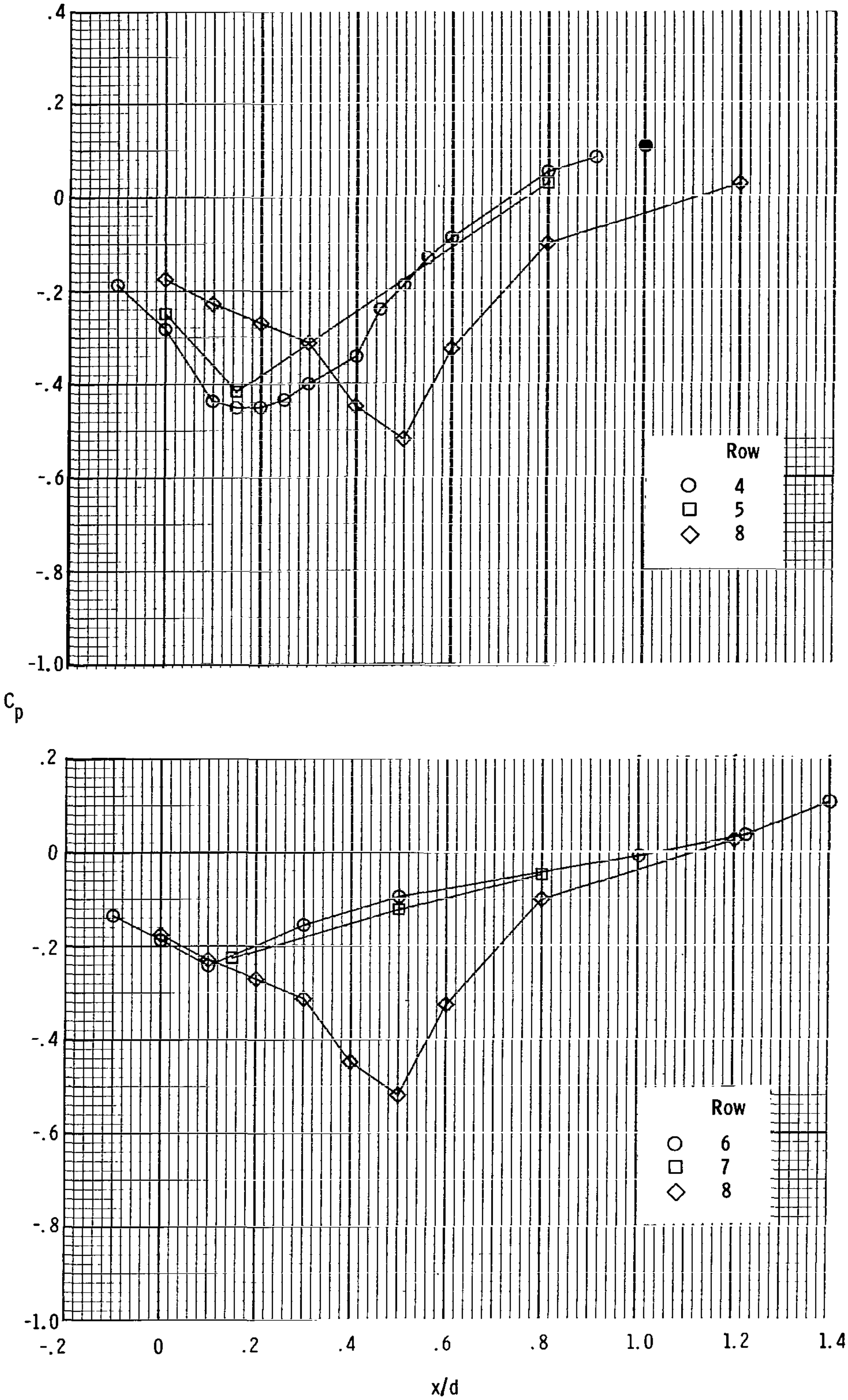

(b) $M_\infty = 0.60$; $p_{t,j}/p_\infty = 3.99$.

Figure 15.- Continued.

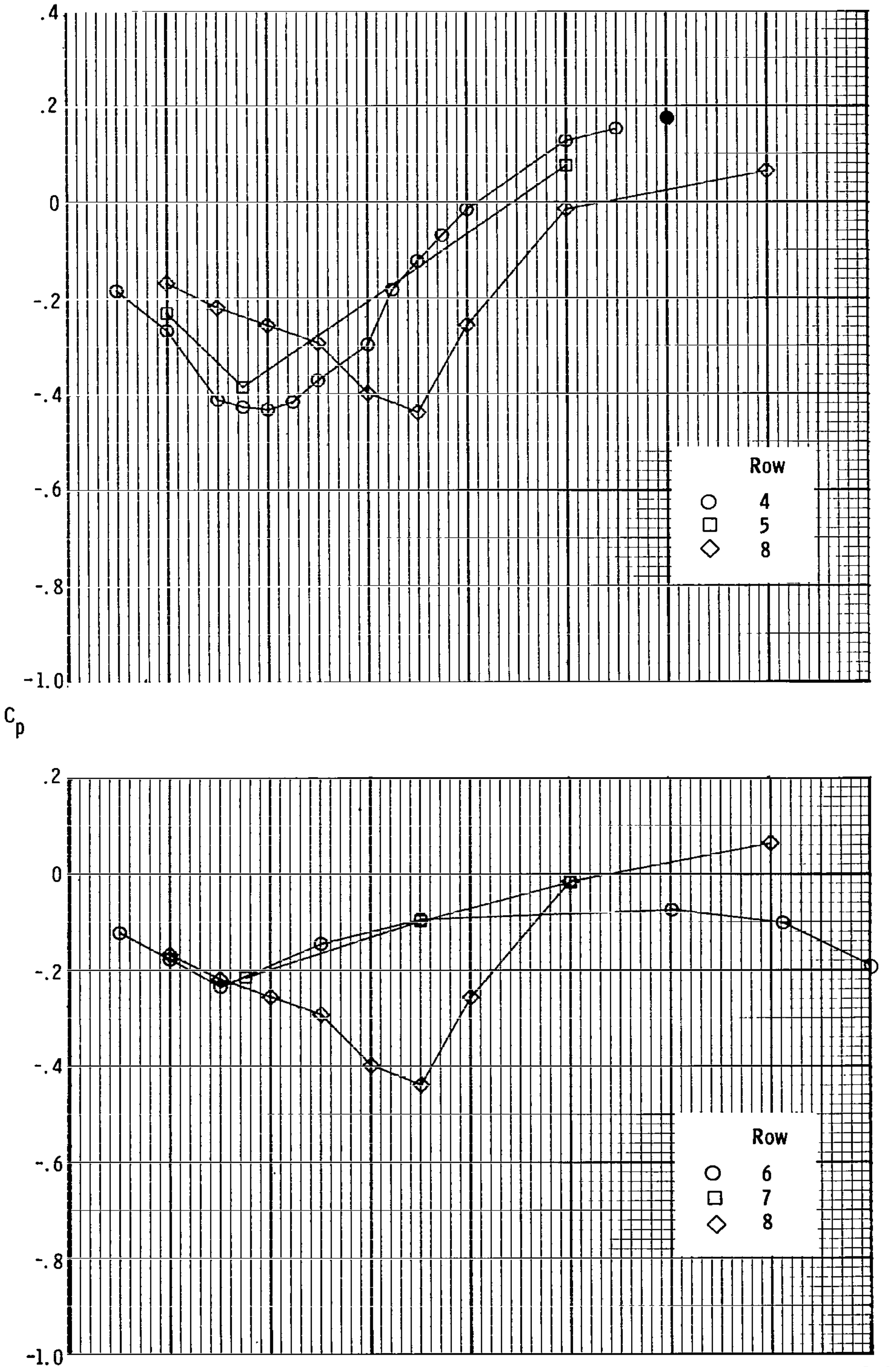

(c) $M_\infty = 0.60$; $p_{t,j}/p_\infty = 8.00$.

Figure 15.- Continued.

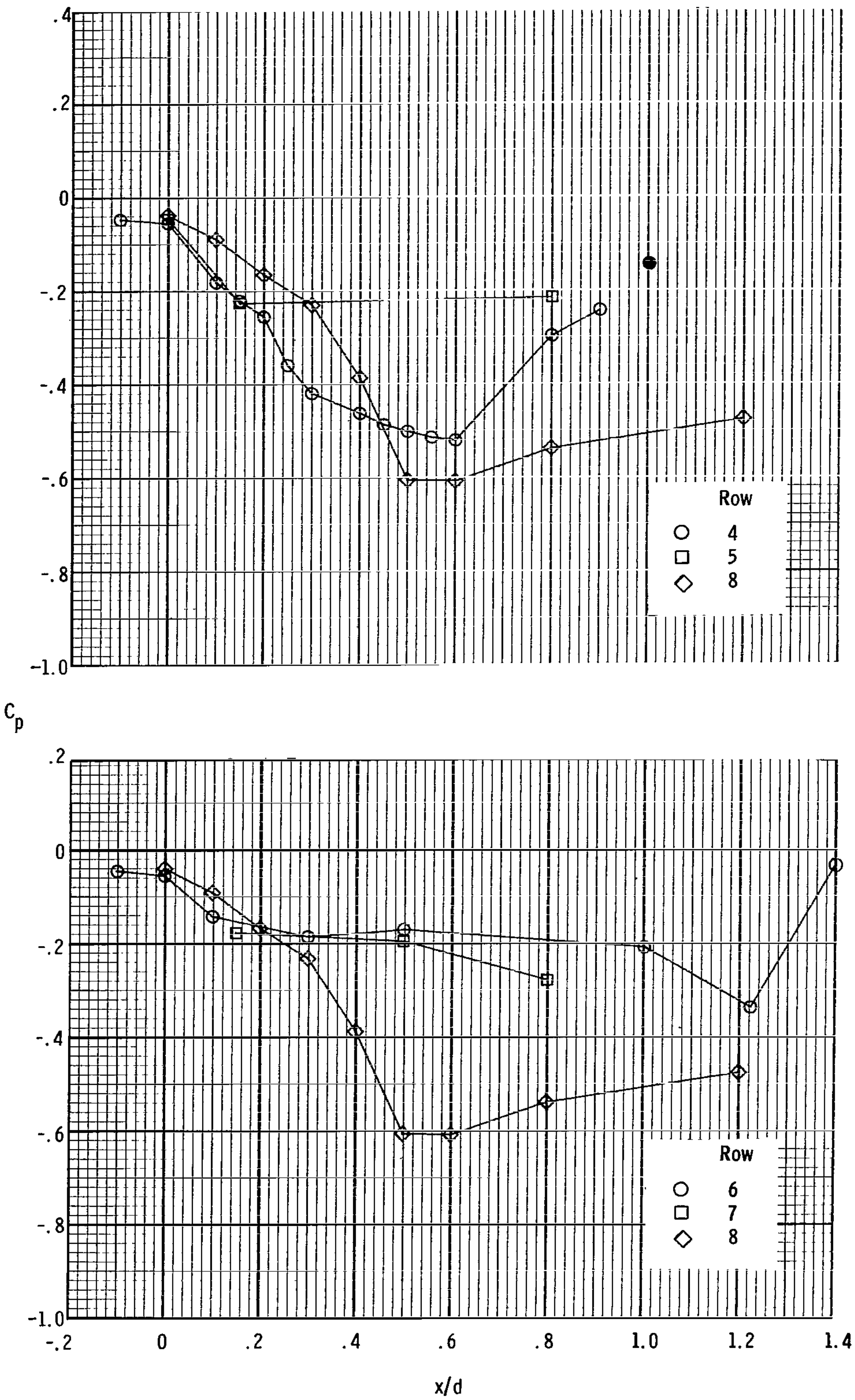

(d) $M_\infty = 1.20$; $p_{t,j}/p_\infty = 2.00$.

Figure 15.- Continued.

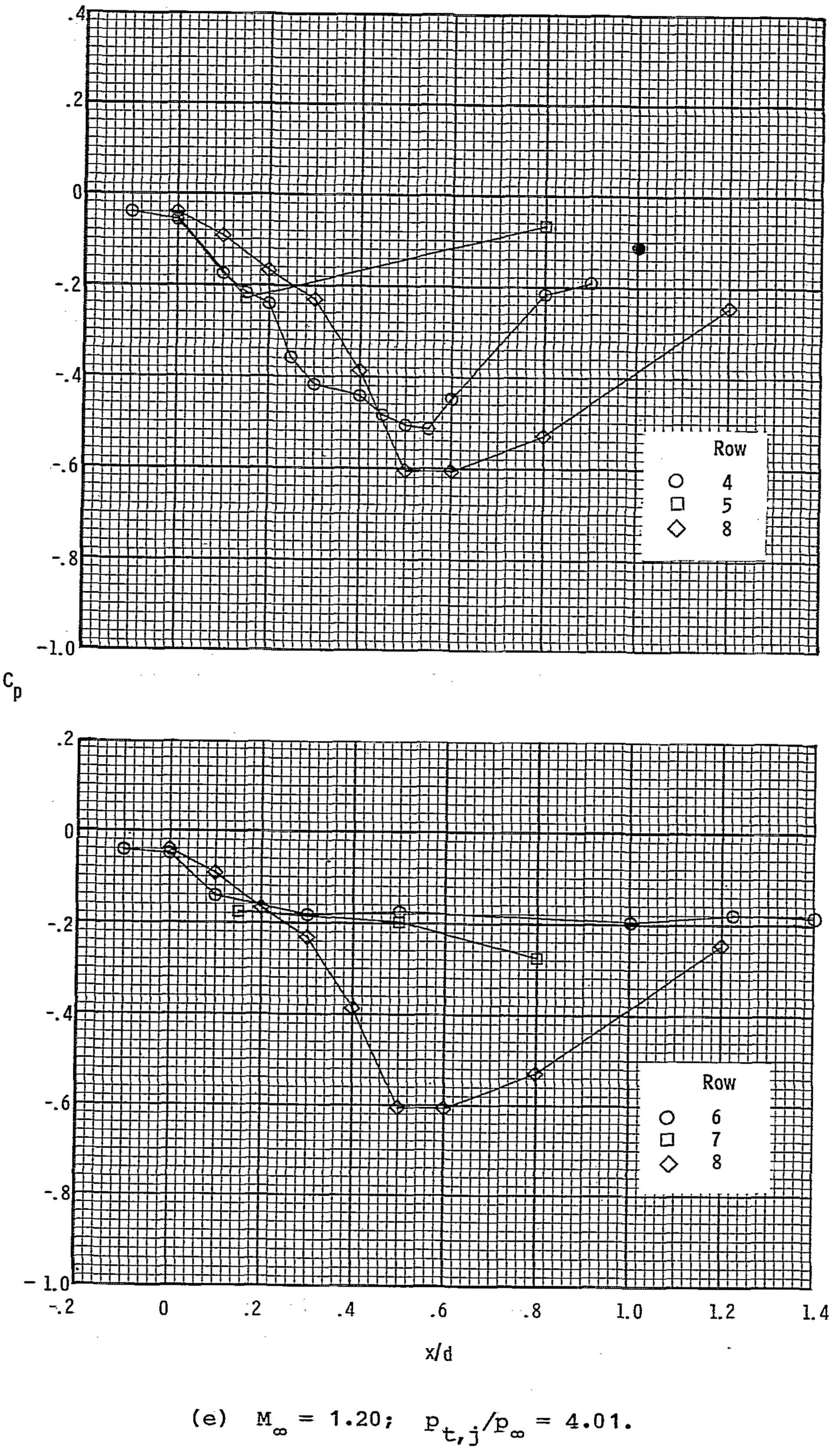

(e) $M_\infty = 1.20$; $p_{t,j}/p_\infty = 4.01$.

Figure 15.- Continued.

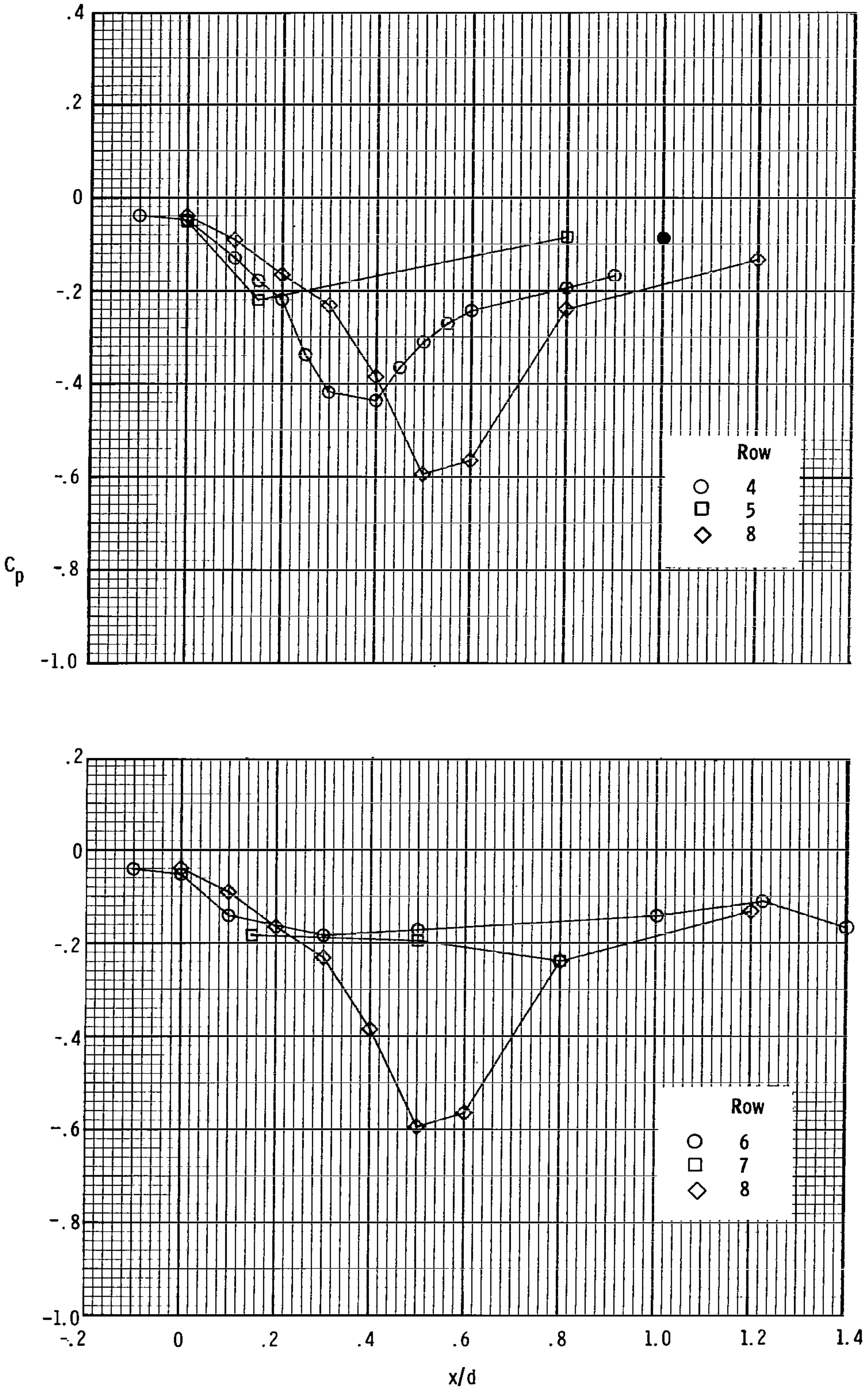

(f) $M_\infty = 1.20$; $p_{t,j}/p_\infty = 7.99$.

Figure 15.- Concluded.

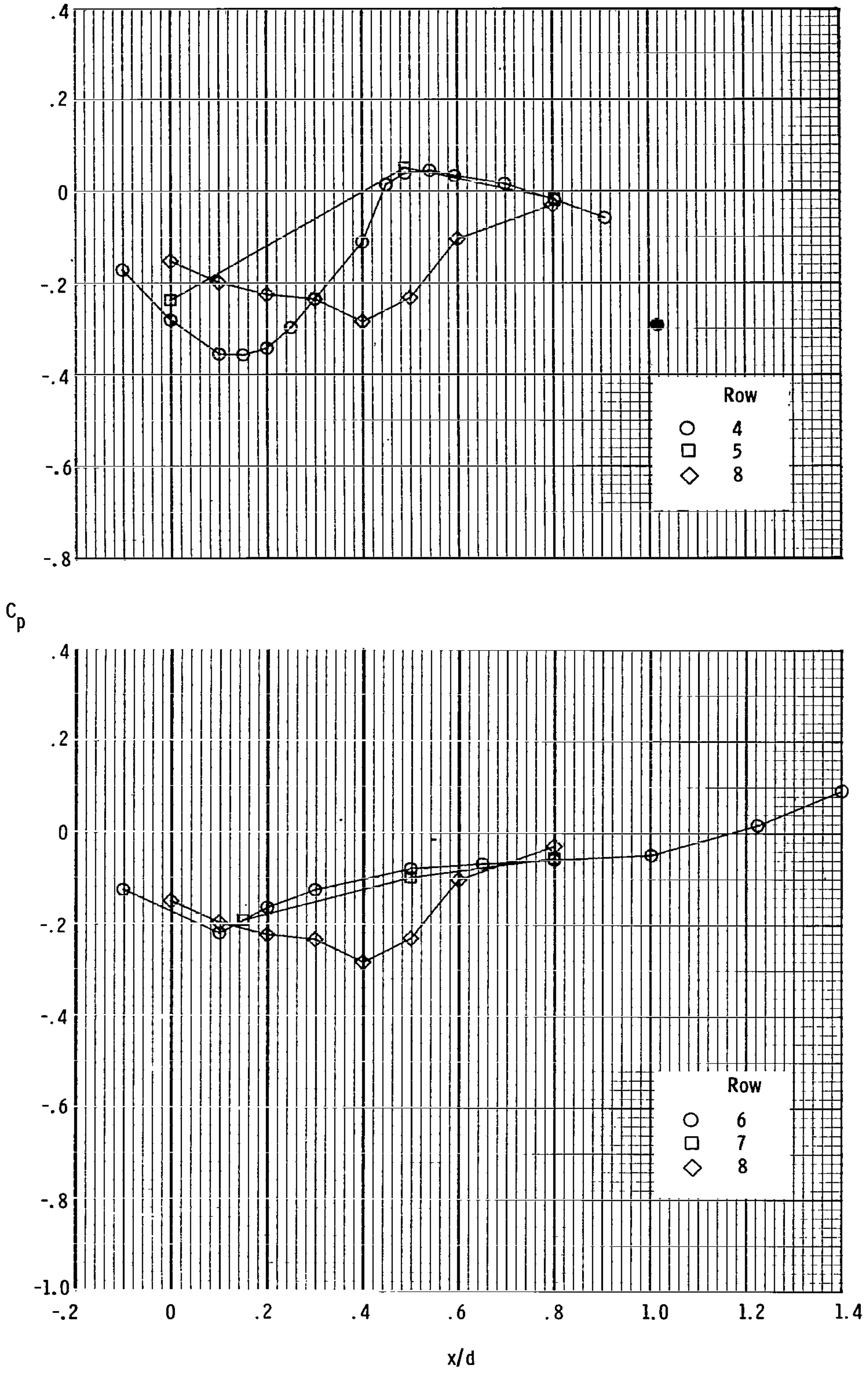

(a) $M_\infty = 0.60$; $p_{t,j}/p_\infty = 2.01$.

Figure 16.- External pressure distributions along upper flap and right sidewall at selected test conditions for high-expansion-ratio nozzle. Base pressure is indicated by solid symbol.

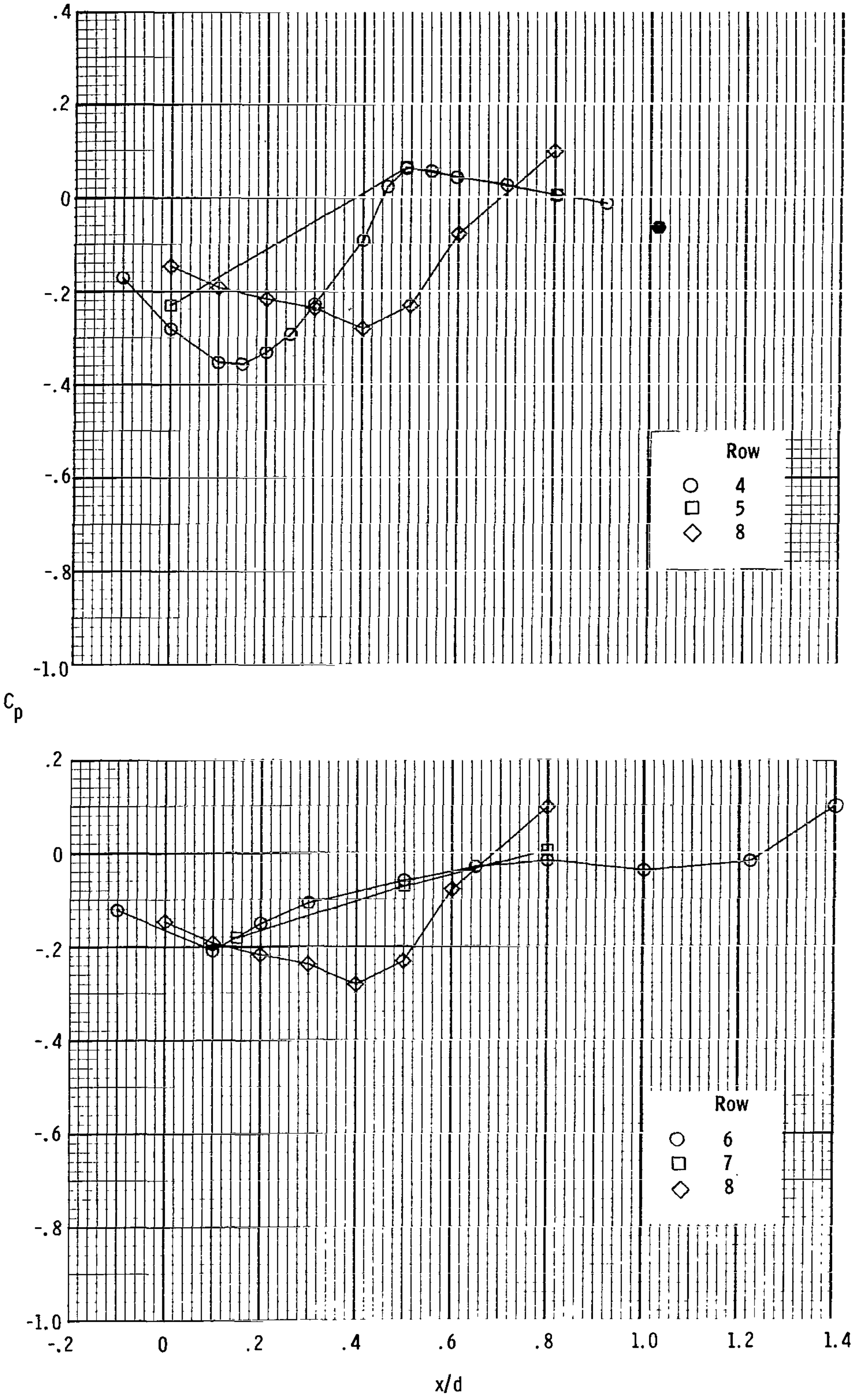

(b) $M_\infty = 0.60$; $p_{t,j}/p_\infty = 4.00$.

Figure 16.- Continued.

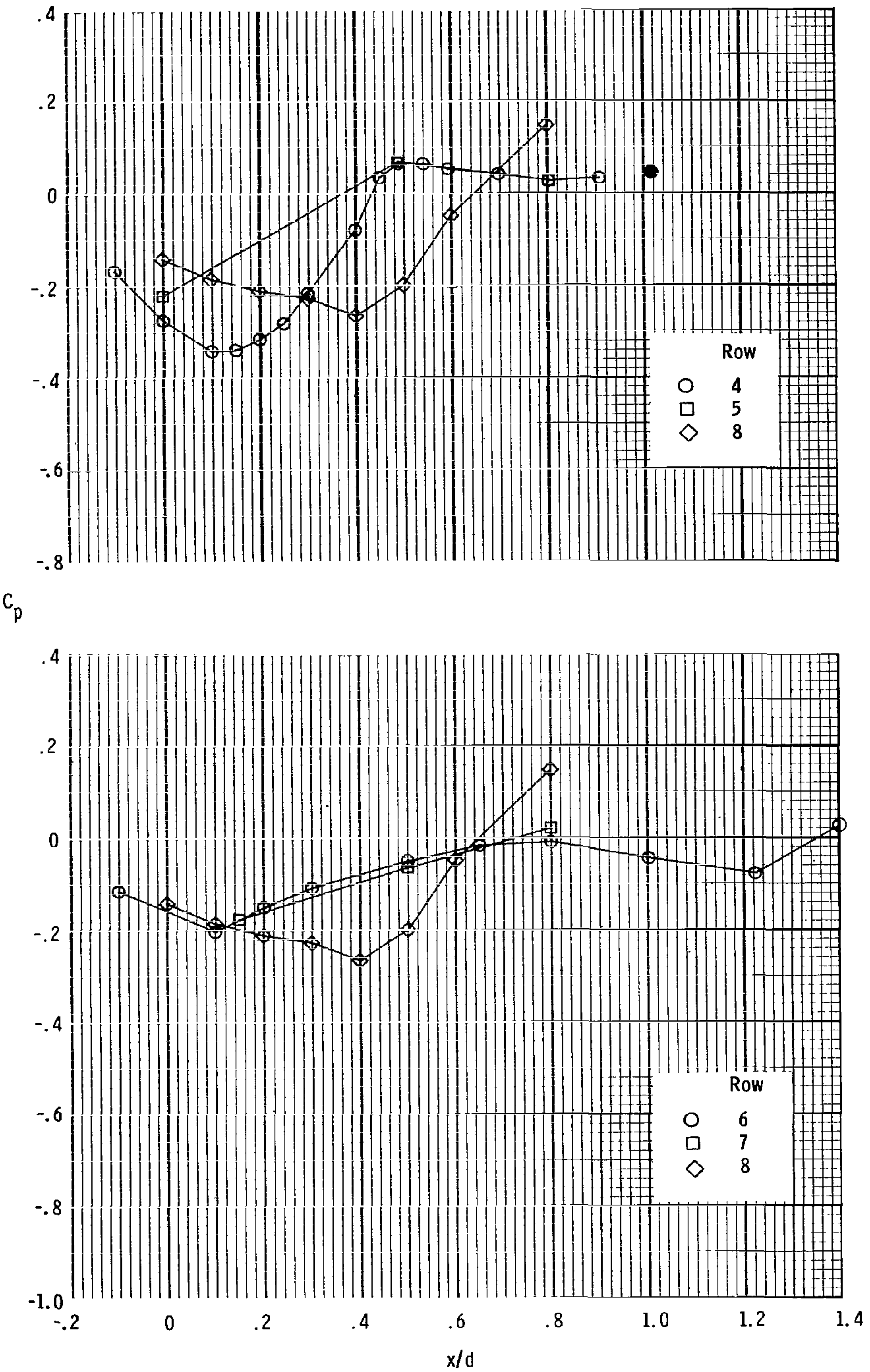

(c) $M_\infty = 0.60$; $p_{t,j}/p_\infty = 5.06$.

Figure 16.- Continued.

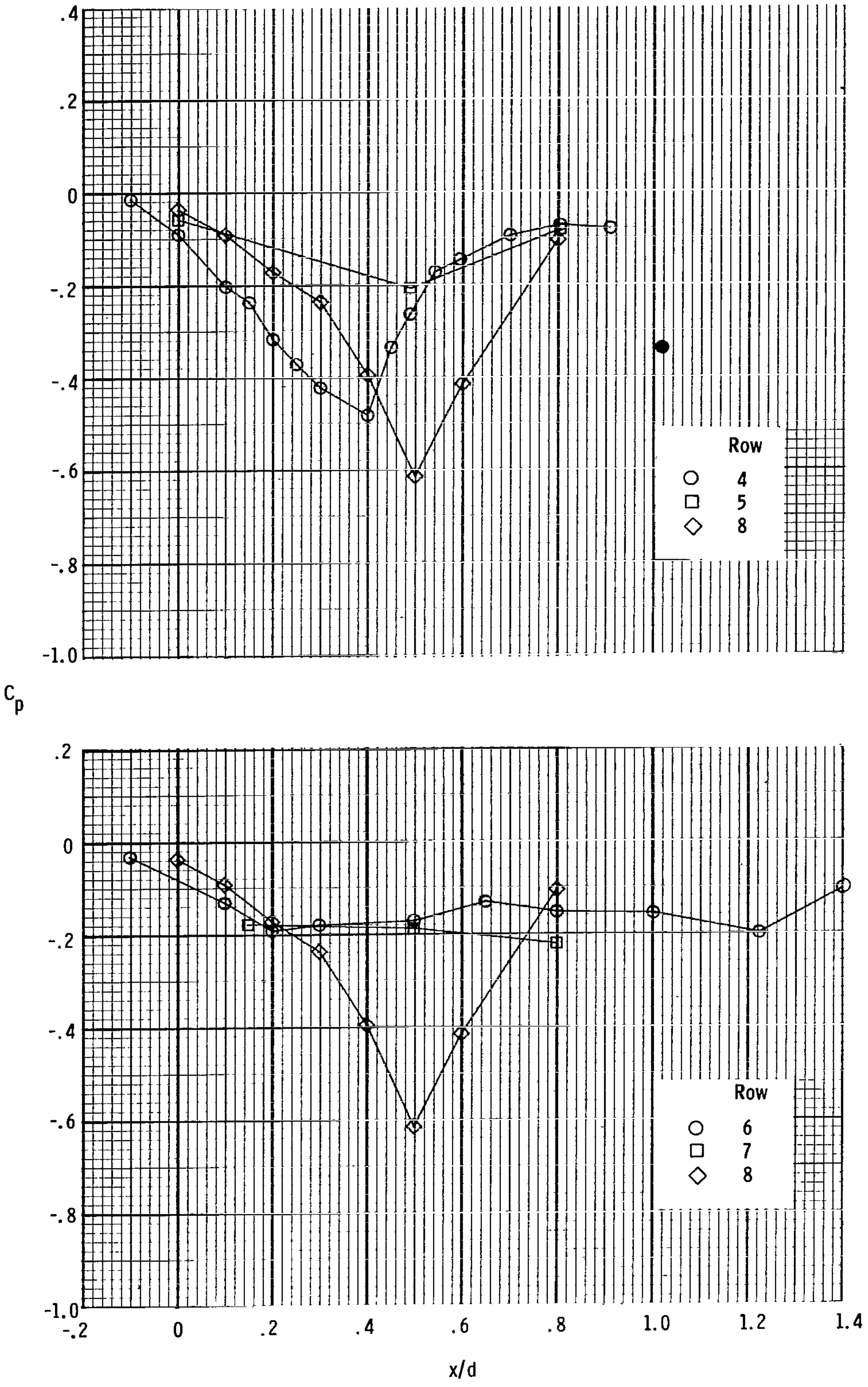

(d) $M_\infty = 1.20;\ p_{t,j}/p_\infty = 1.99.$

Figure 16.- Continued.

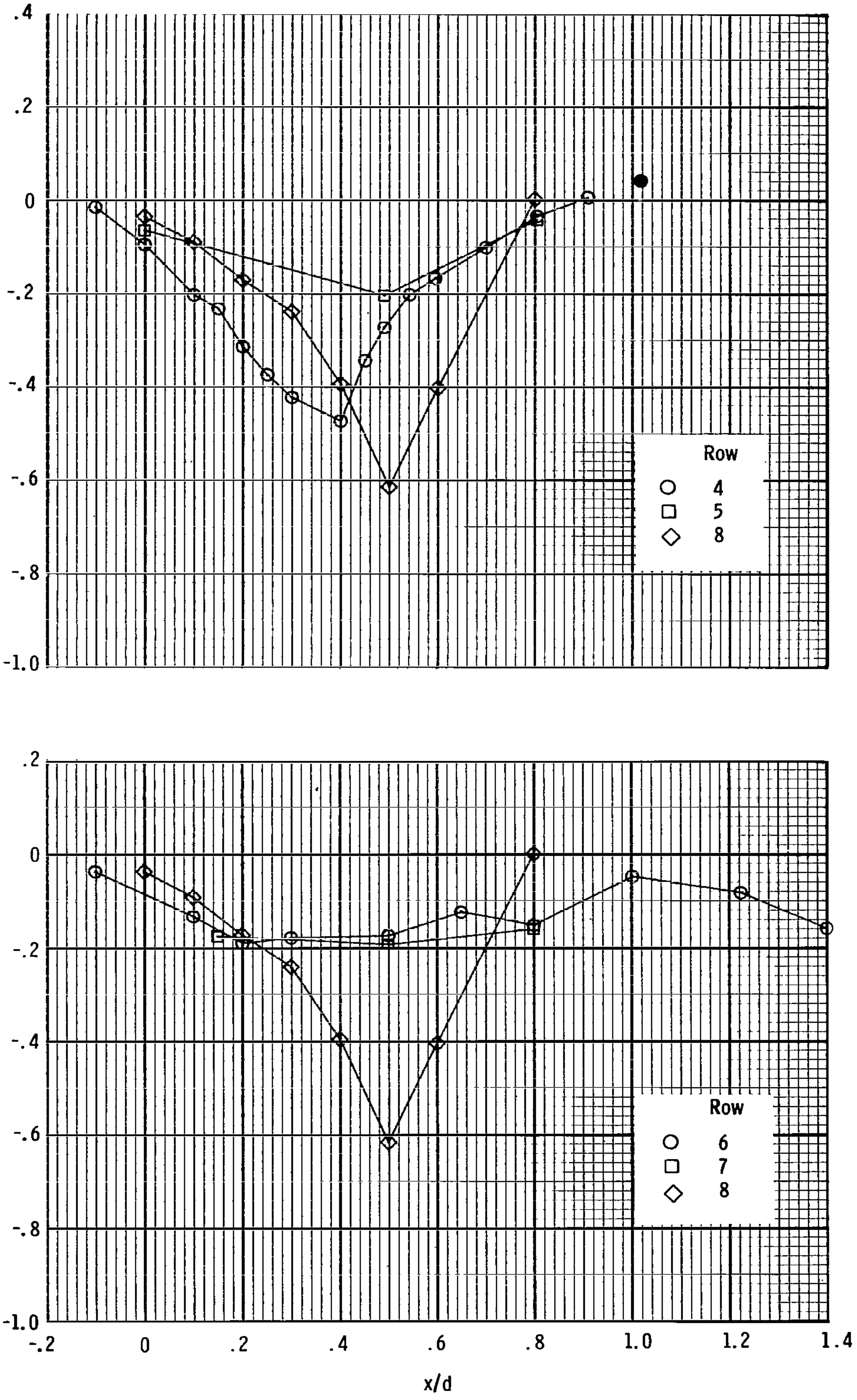

(e) $M_\infty = 1.20$; $p_{t,j}/p_\infty = 4.01$.

Figure 16.- Continued.

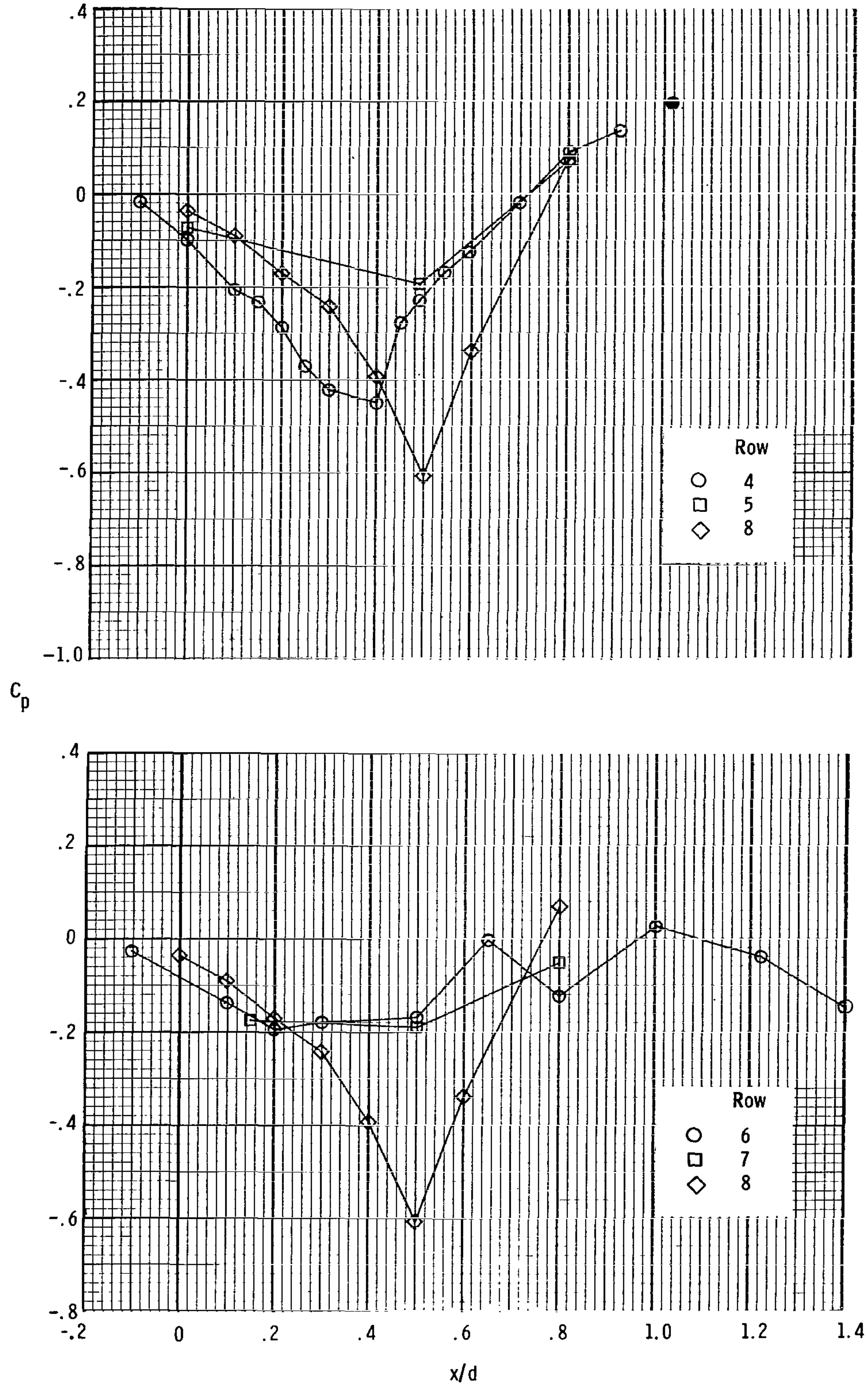

(f) $M_\infty = 1.20$; $p_{t,j}/p_\infty = 7.99$.

Figure 16.- Concluded.

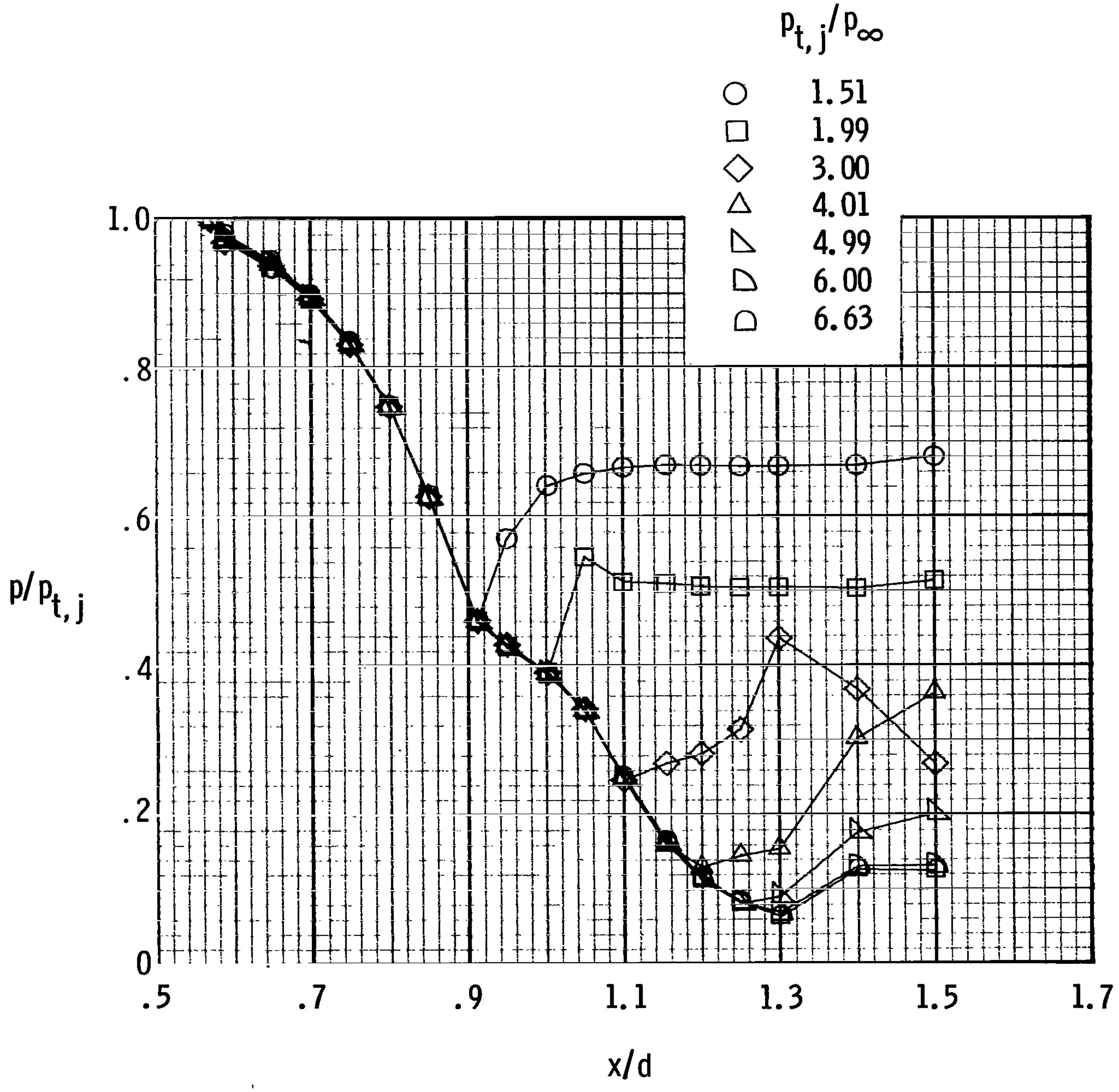

(a) $M_\infty = 0$.

Figure 17.- Effect of nozzle pressure ratio on center-line wedge static-pressure profiles for low-expansion-ratio nozzle.

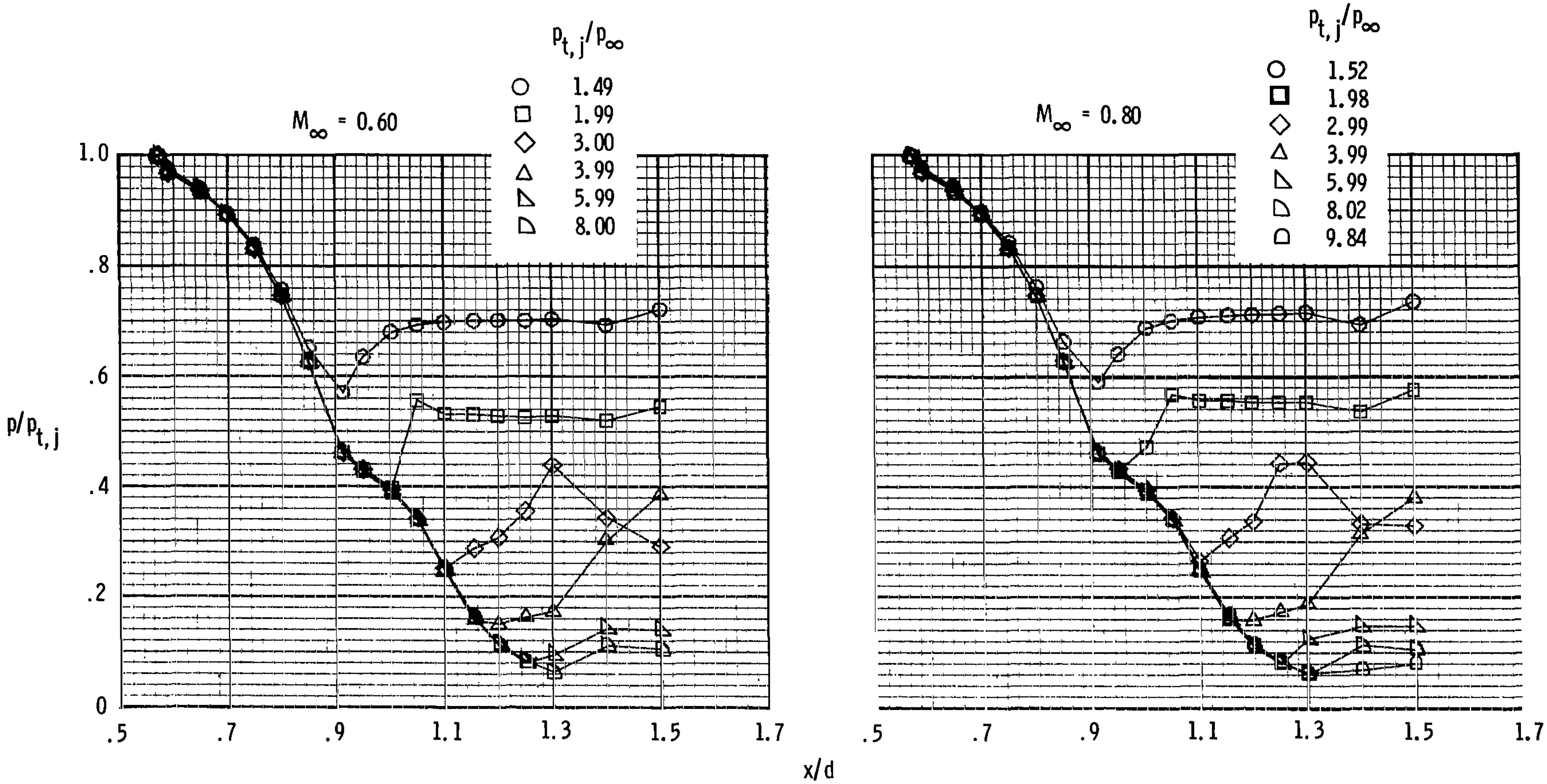

(b) M_∞ = 0.60 and 0.80.

Figure 17.- Continued.

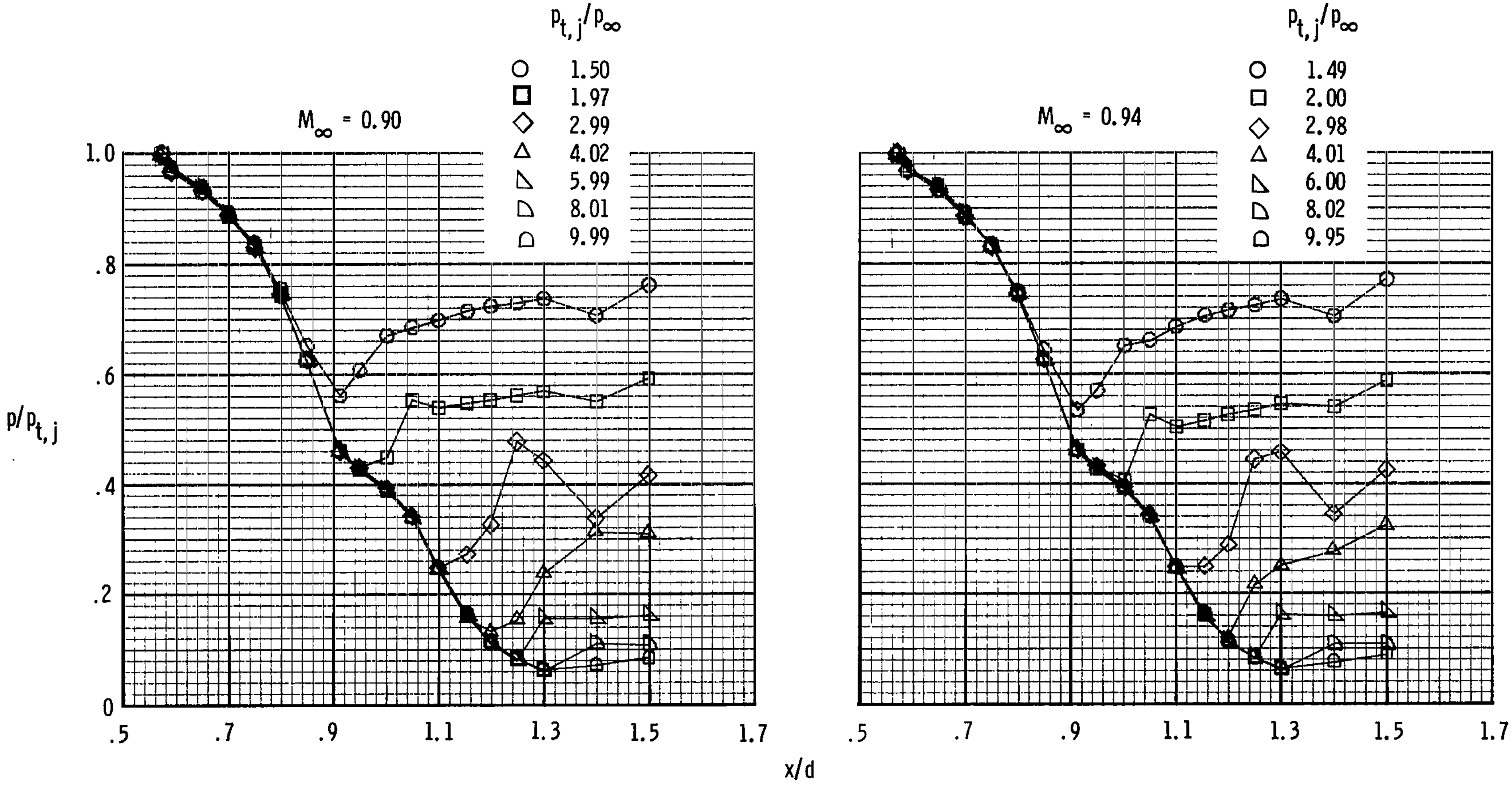

(c) M_∞ = 0.90 and 0.94.

Figure 17.- Continued.

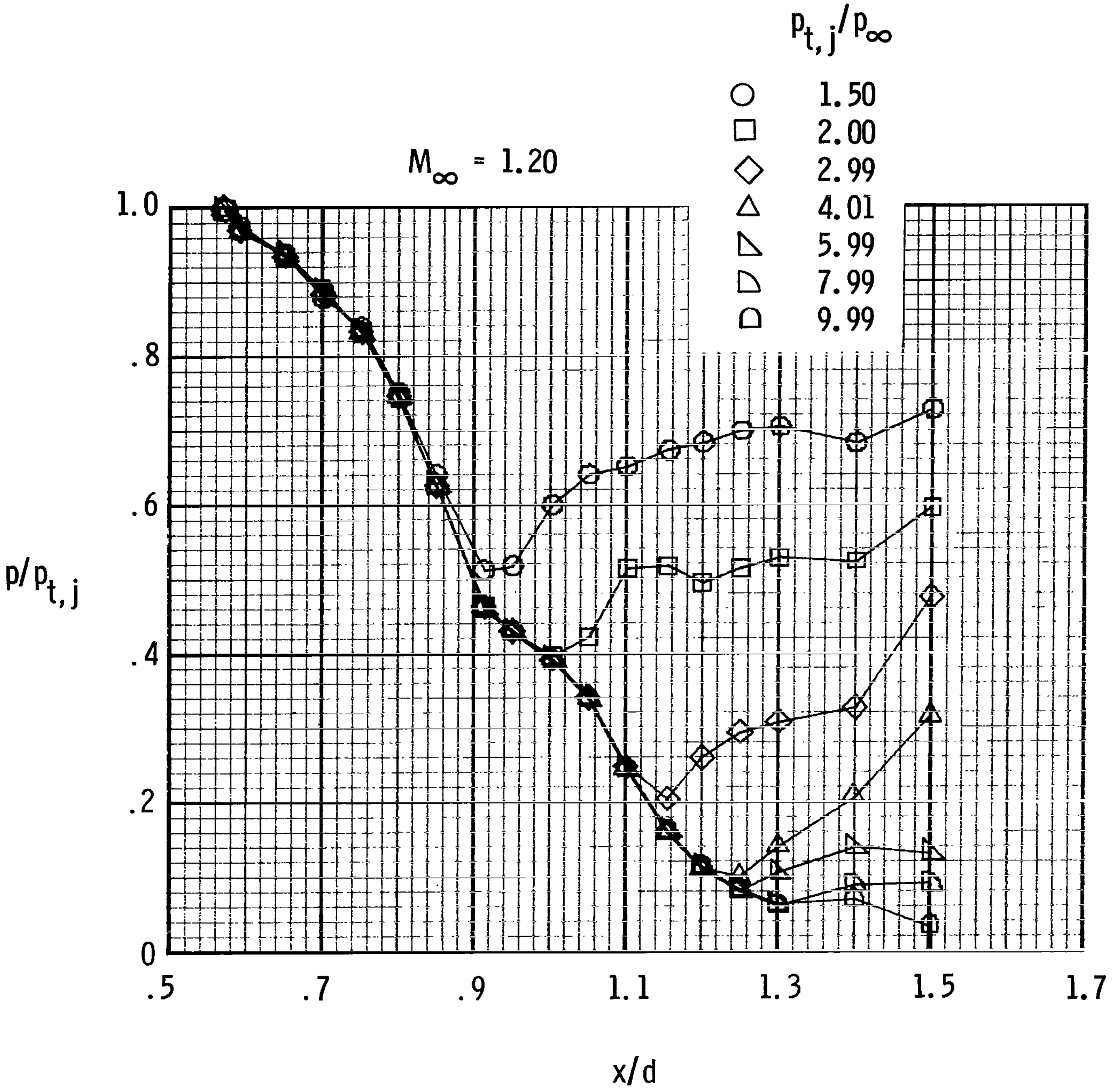

(d) M_∞ = 1.20.

Figure 17.- Concluded.

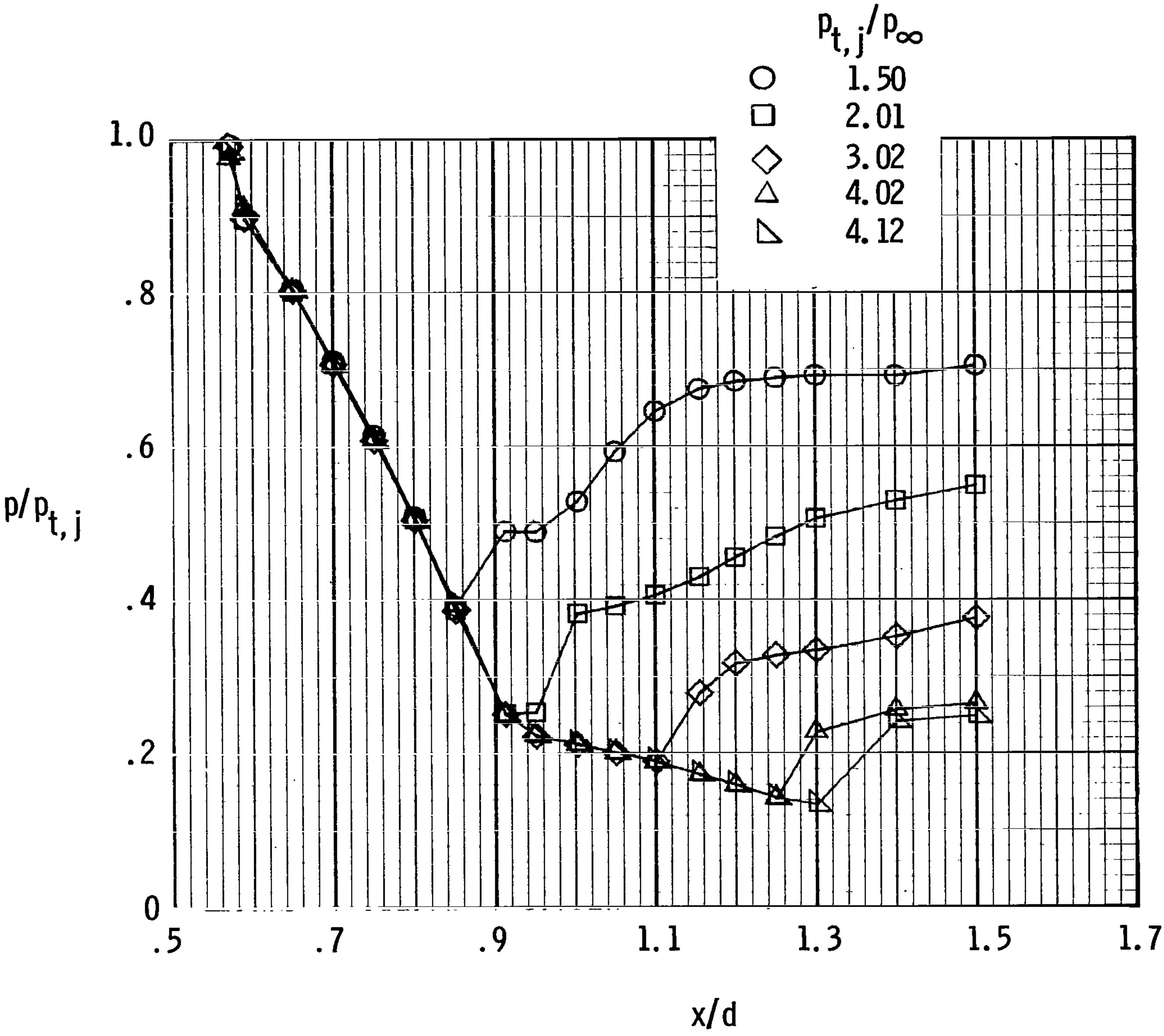

(a) $M_\infty = 0$.

Figure 18.- Effect of nozzle pressure ratio on center-line wedge static-pressure profiles for high-expansion-ratio nozzle.

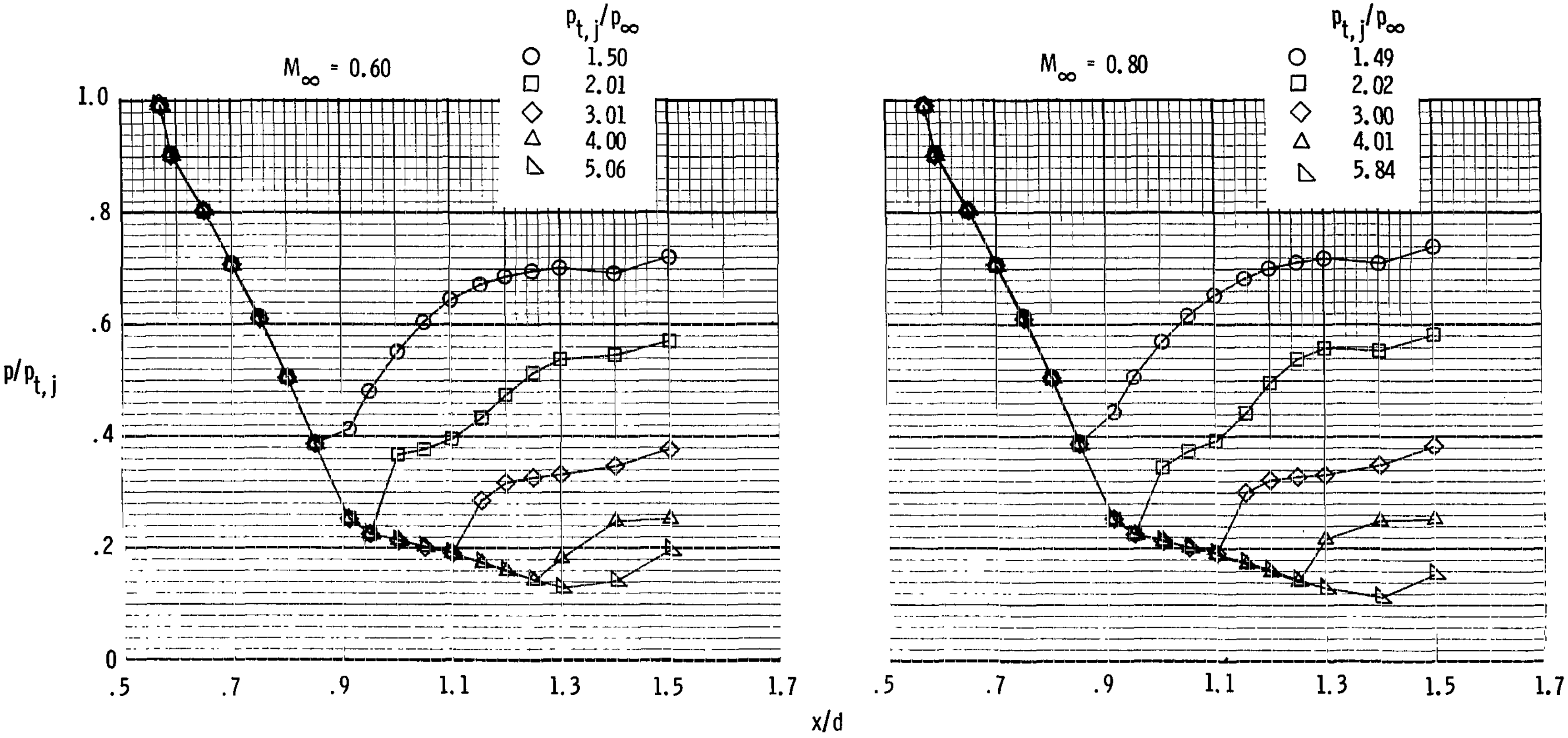

(b) M_∞ = 0.60 and 0.80.

Figure 18.- Continued.

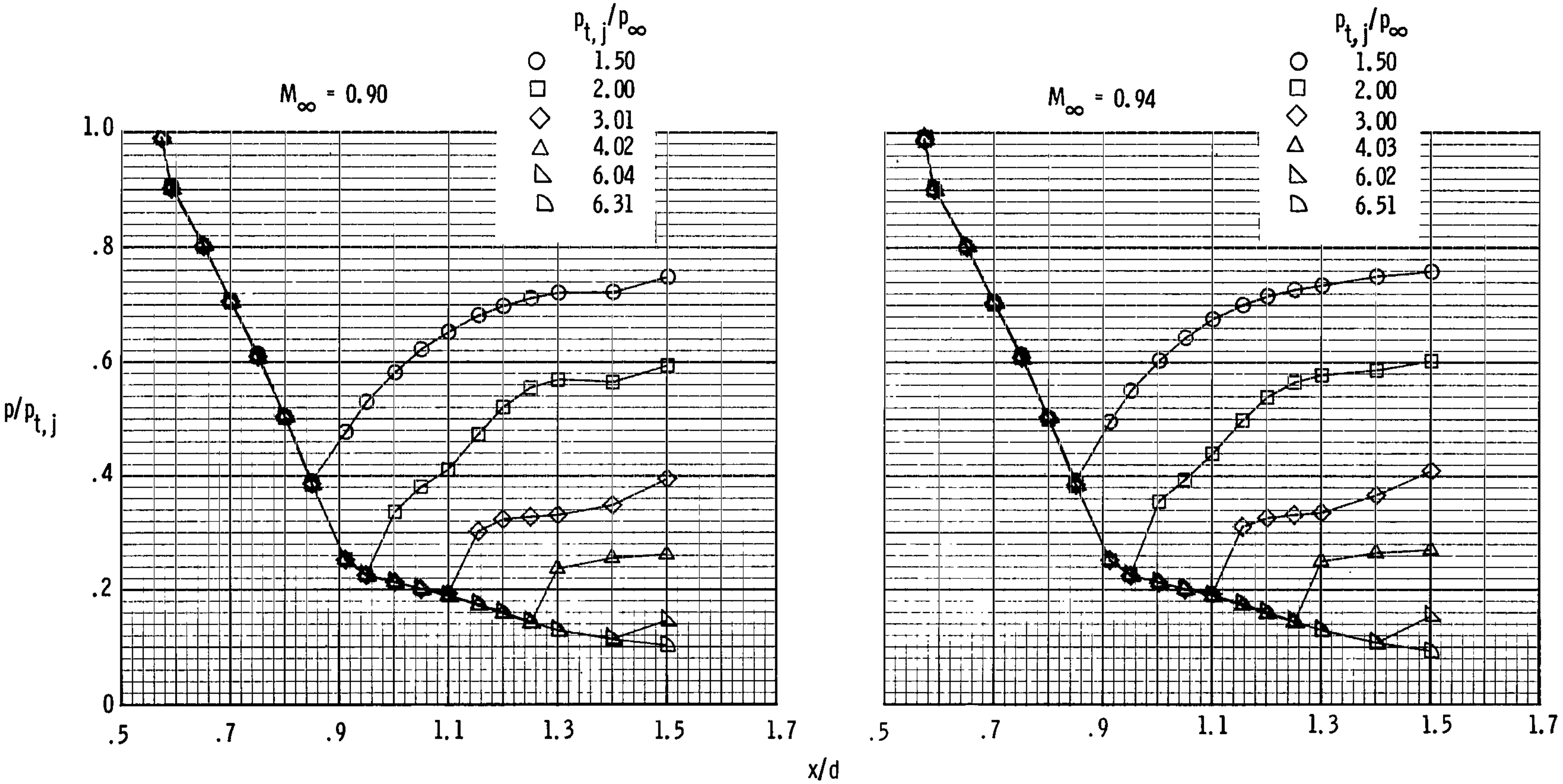

(c) M_∞ = 0.90 and 0.94.

Figure 18.- Continued.

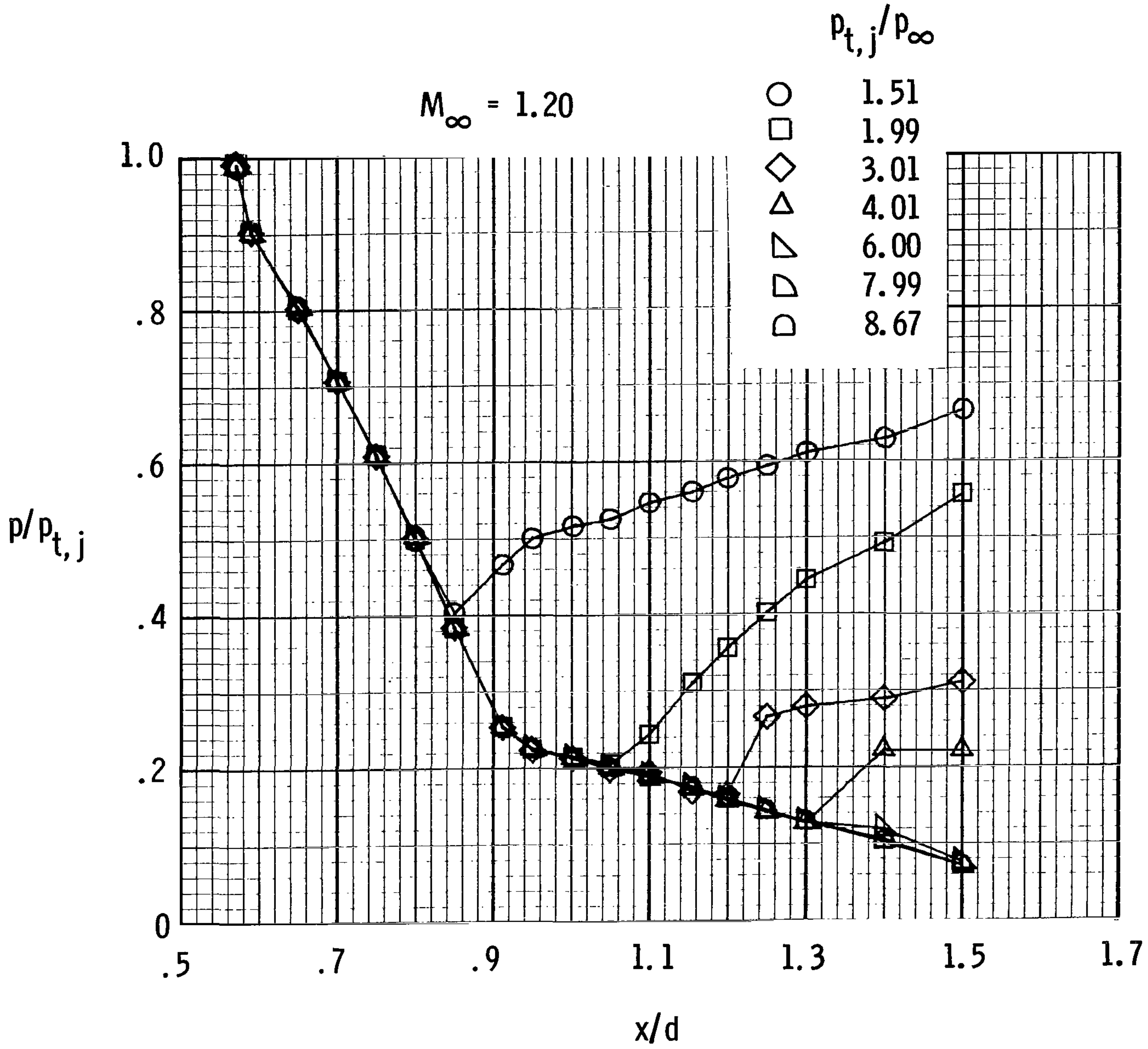

(d) M_∞ = 1.20.

Figure 18.- Concluded.

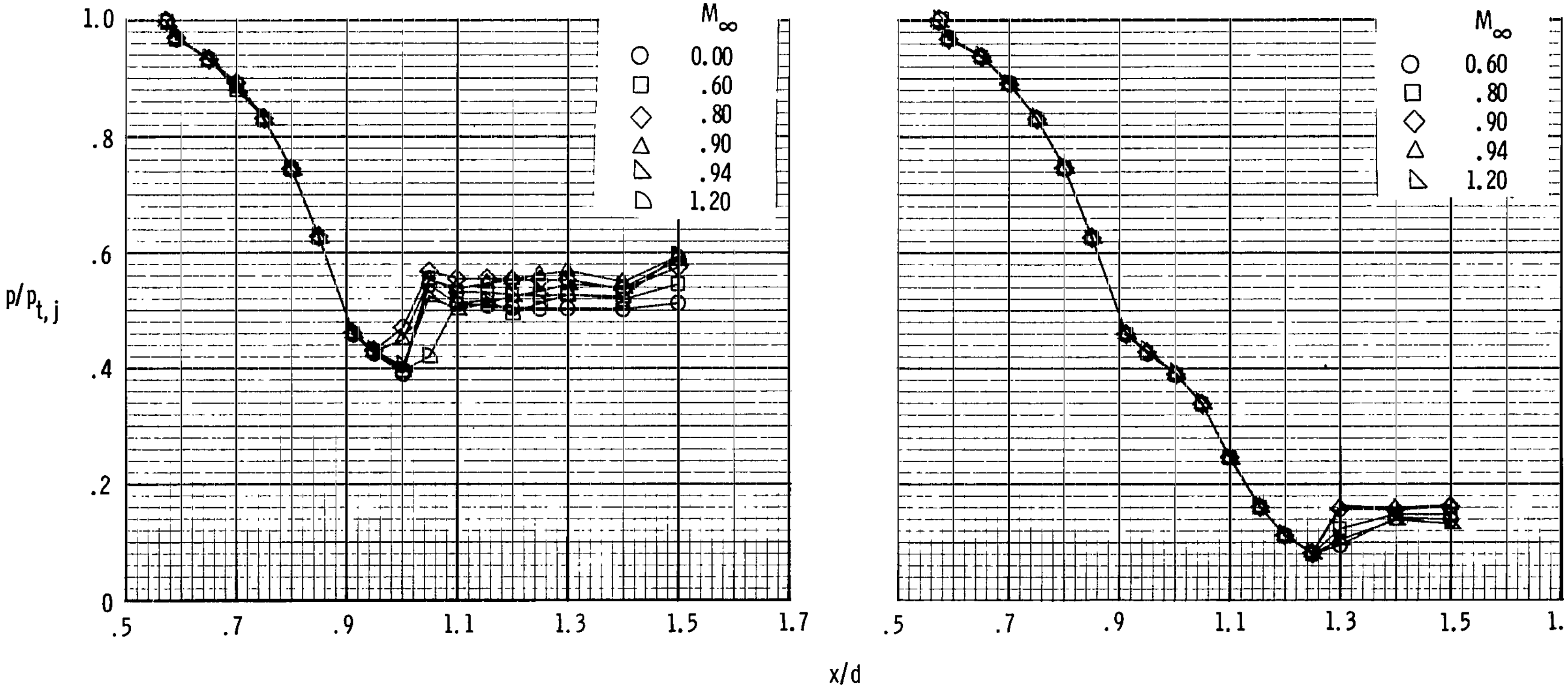

(a) $p_{t,j}/p_\infty = 2.00$.

(b) $p_{t,j}/p_\infty = 6.00$.

Figure 19.- Effect of Mach number on wedge center-line static-pressure profiles at selected test conditions for low-expansion-ratio nozzle.

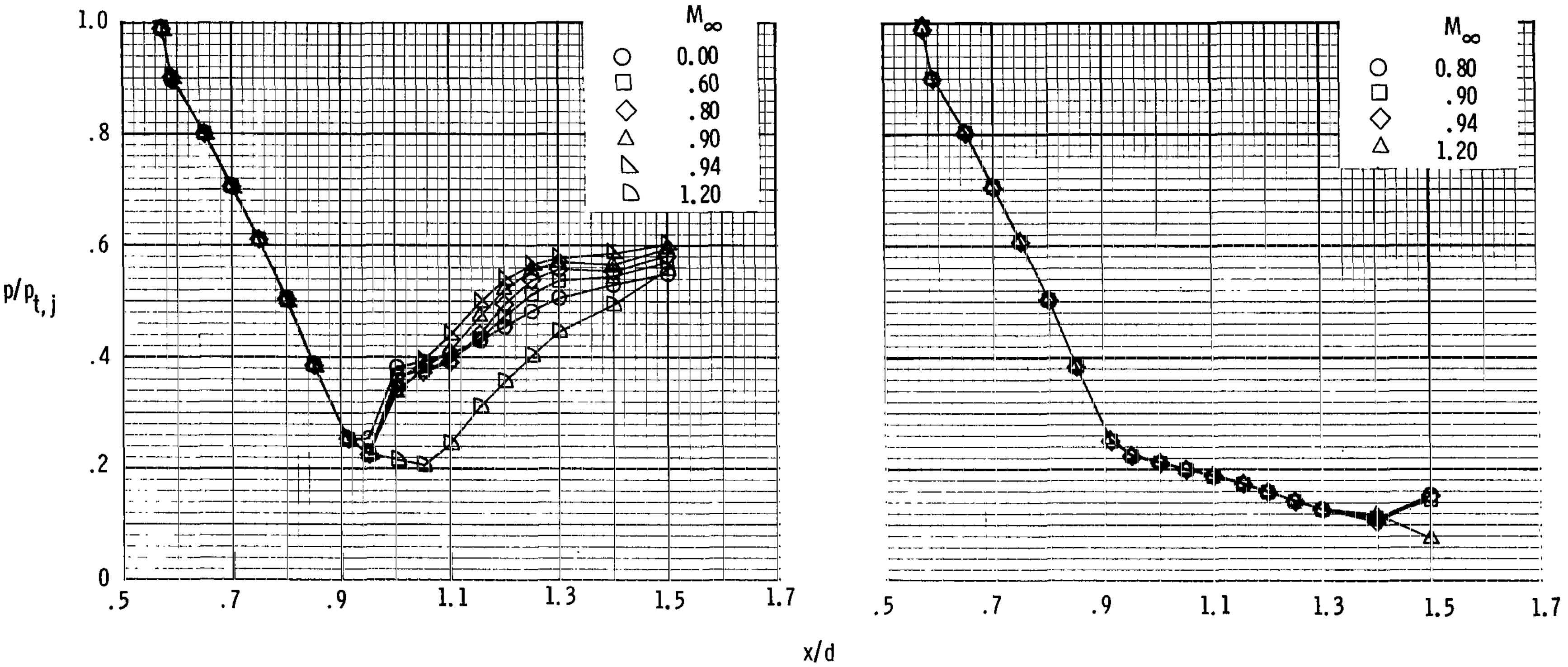

(a) $p_{t,j}/p_\infty = 2.00$.

(b) $p_{t,j}/p_\infty = 6.00$.

Figure 20.- Effect of Mach number on wedge center-line static-pressure profiles at selected test conditions for high-expansion-ratio nozzle.

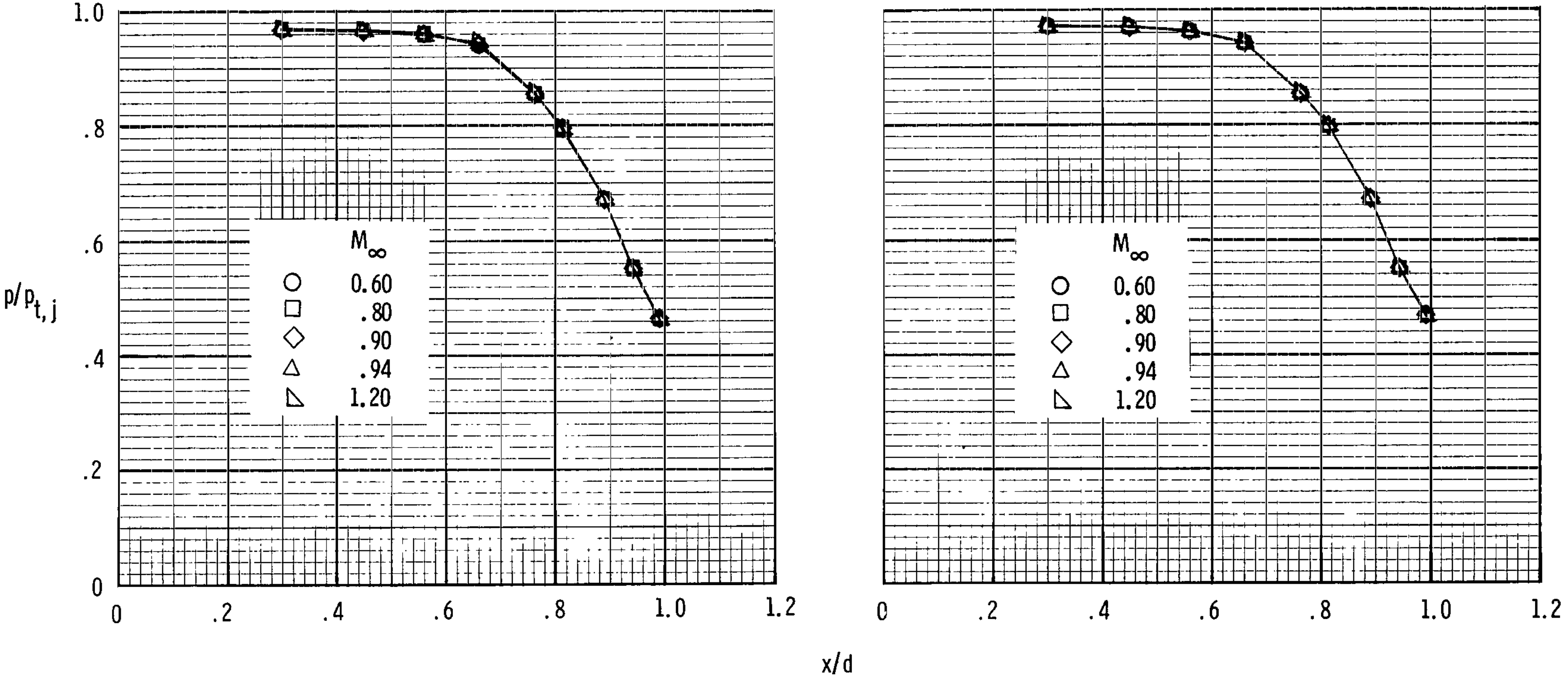

(a) $p_{t,j}/p_\infty = 2.00$.

(b) $p_{t,j}/p_\infty = 6.00$.

Figure 21.- Effect of Mach number on internal flap center-line static-pressure distributions at selected test conditions for low-expansion-ratio nozzle.

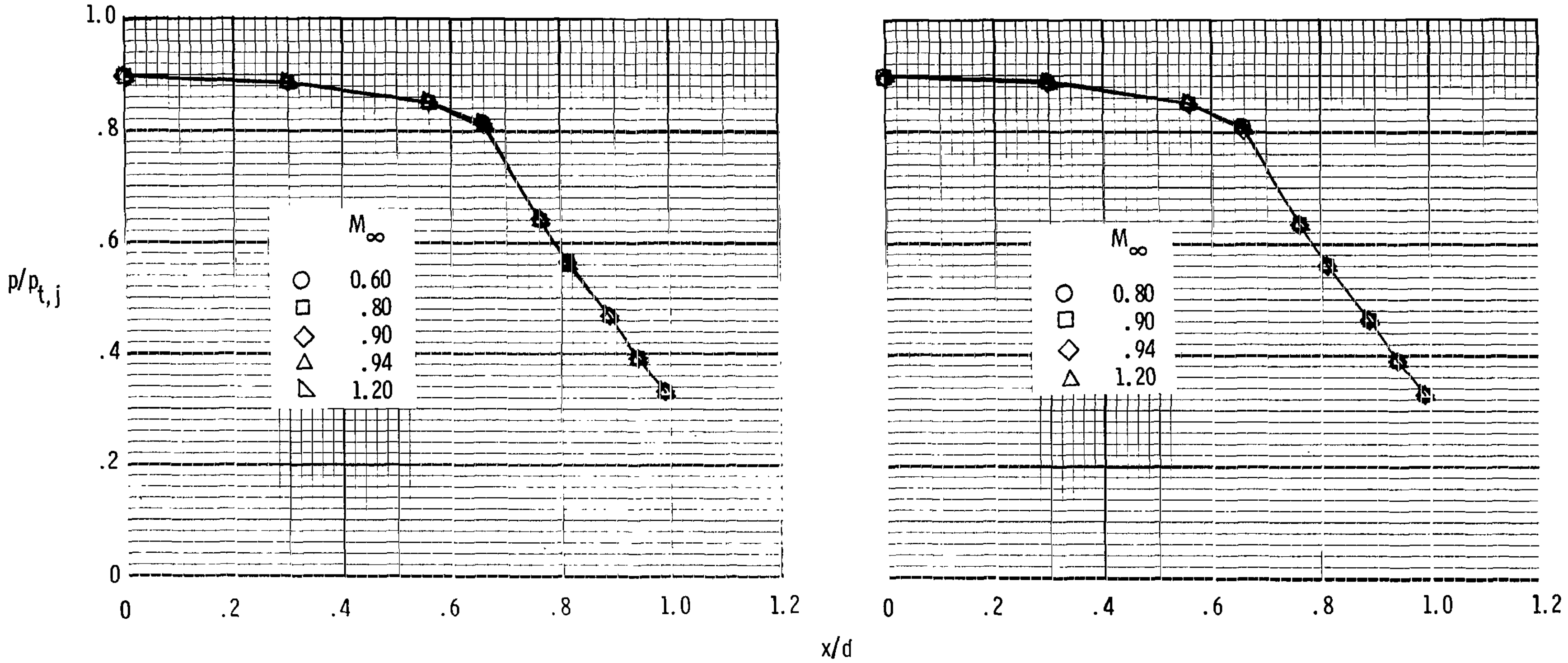

(a) $p_{t,j}/p_\infty = 2.00$.

(b) $p_{t,j}/p_\infty = 6.00$.

Figure 22.- Effect of Mach number on internal flap center-line static-pressure profiles at selected test conditions for high-expansion-ratio nozzle.

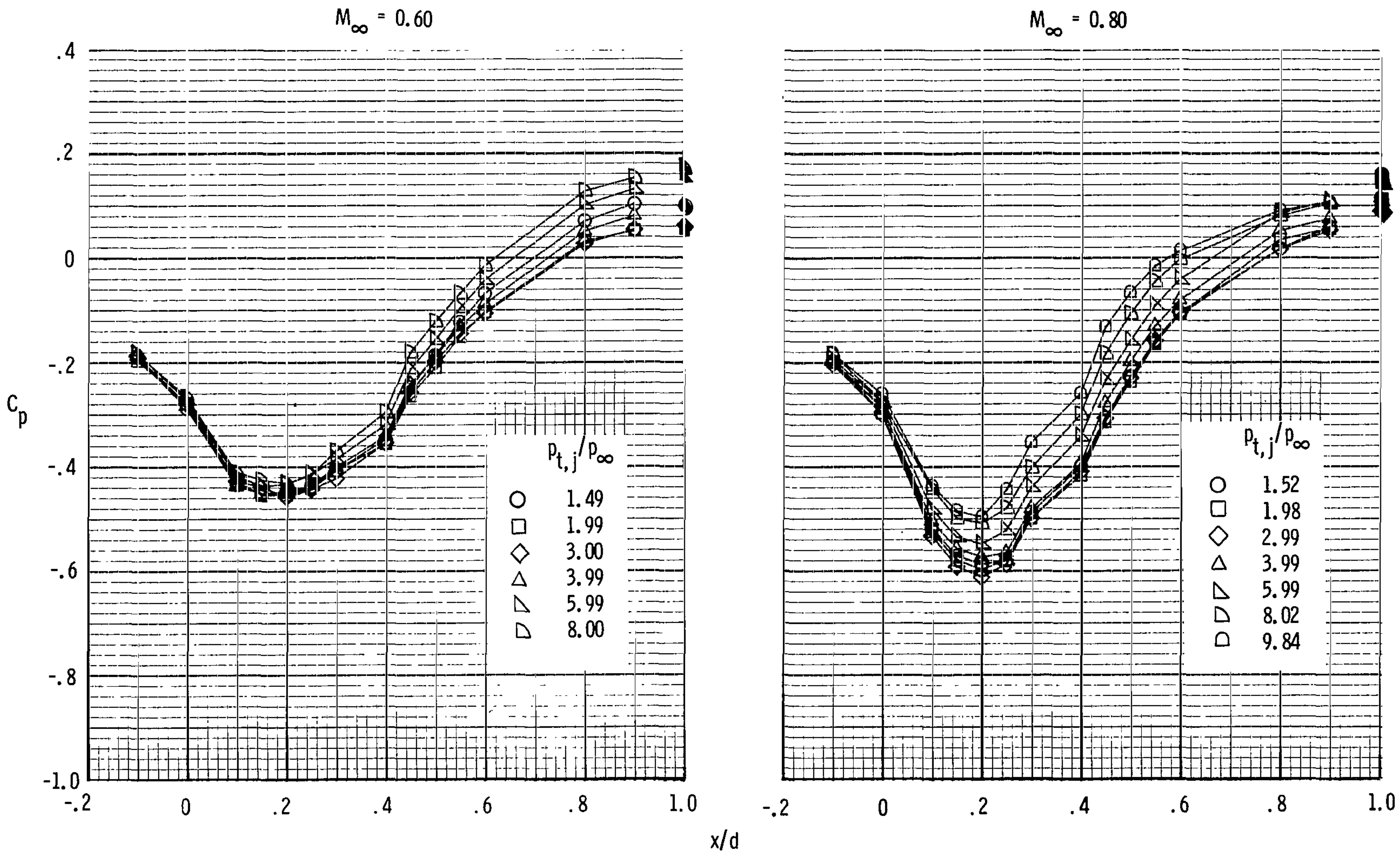

(a) M_∞ = 0.60 and 0.80.

Figure 23.- Effect of nozzle pressure ratio on flap center-line external pressure profiles for low-expansion-ratio nozzle. Base pressure is indicated by solid symbol.

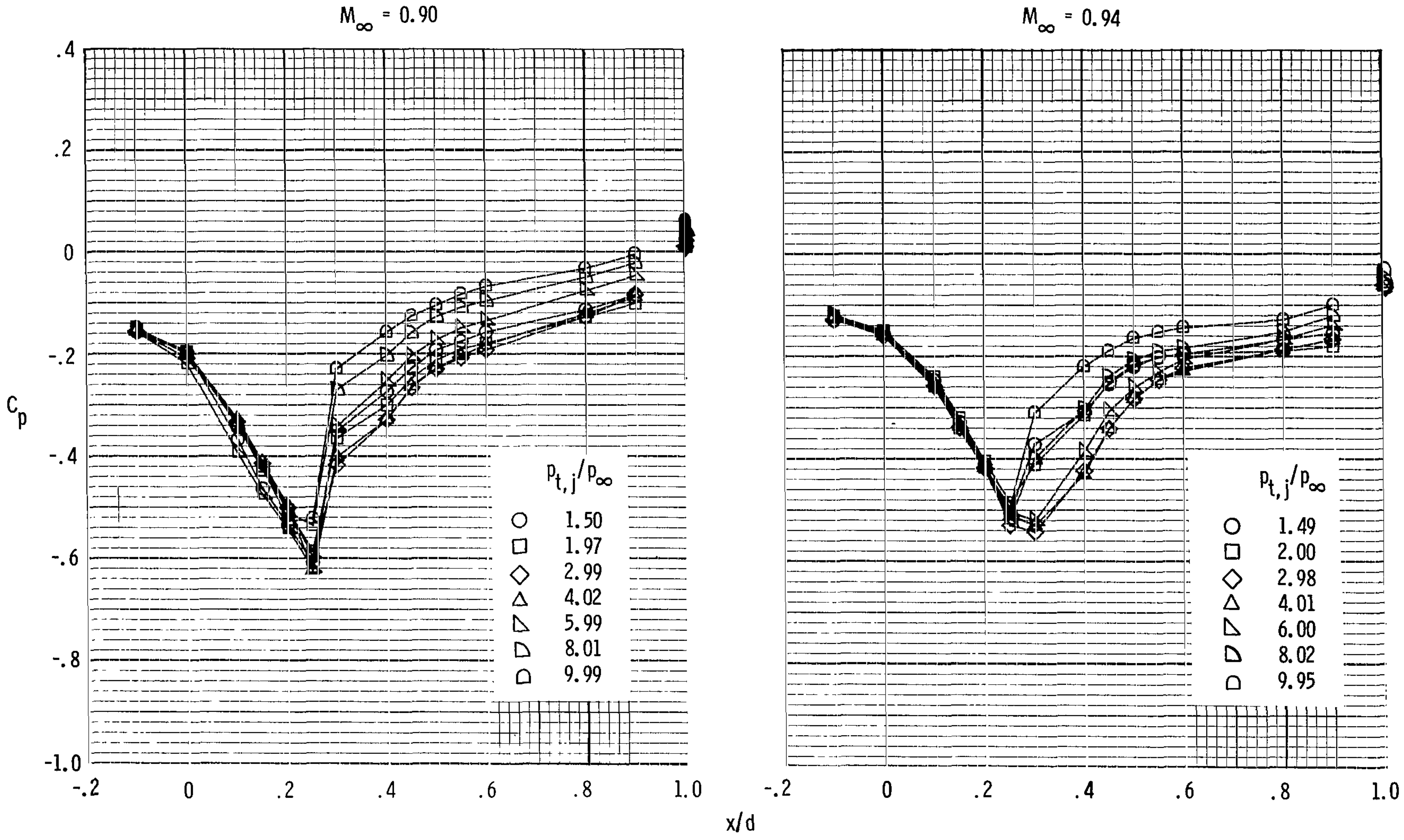

(b) M_∞ = 0.90 and 0.94.

Figure 23.- Continued.

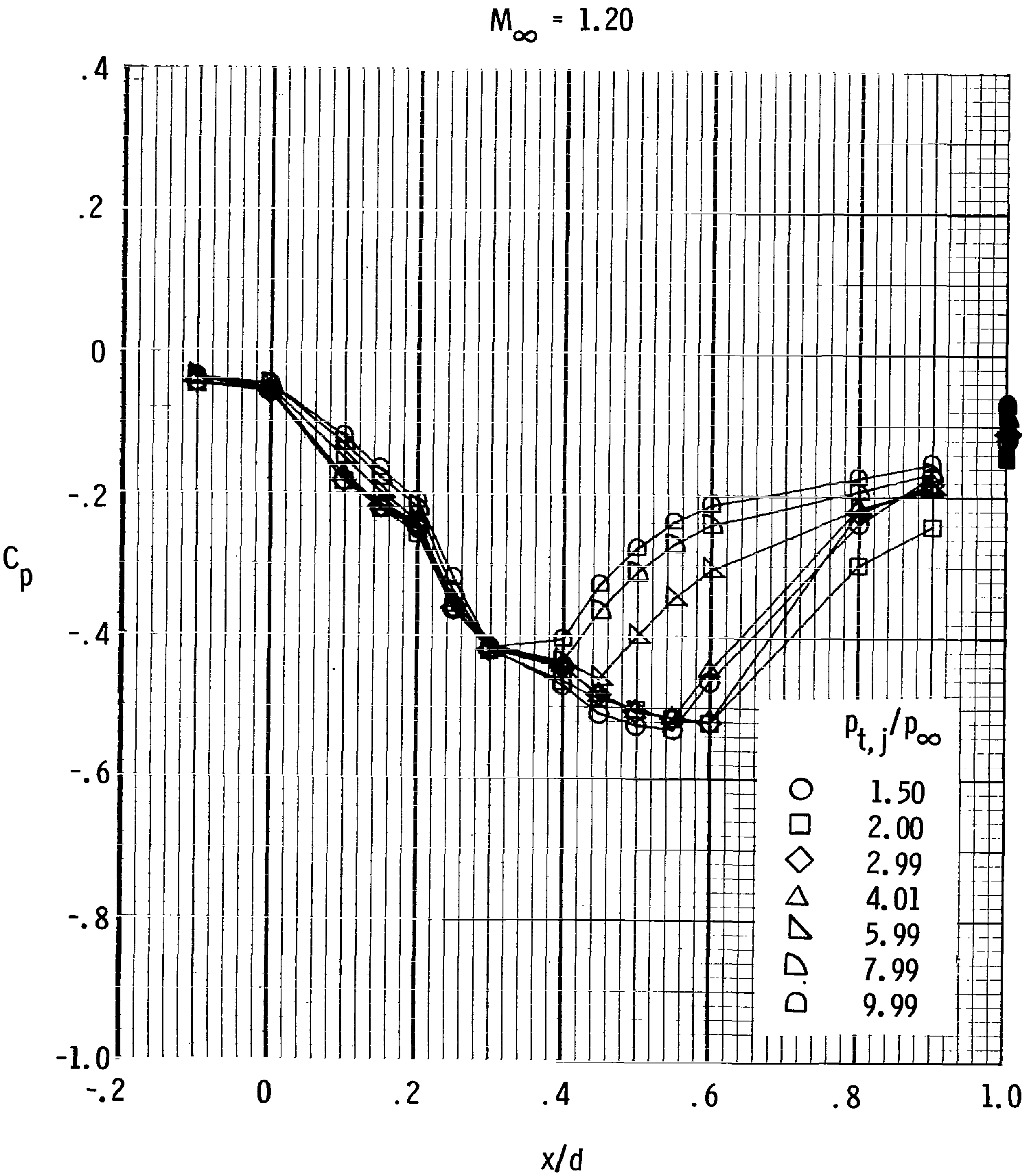

(c) M_∞ = 1.20.

Figure 23.- Concluded.

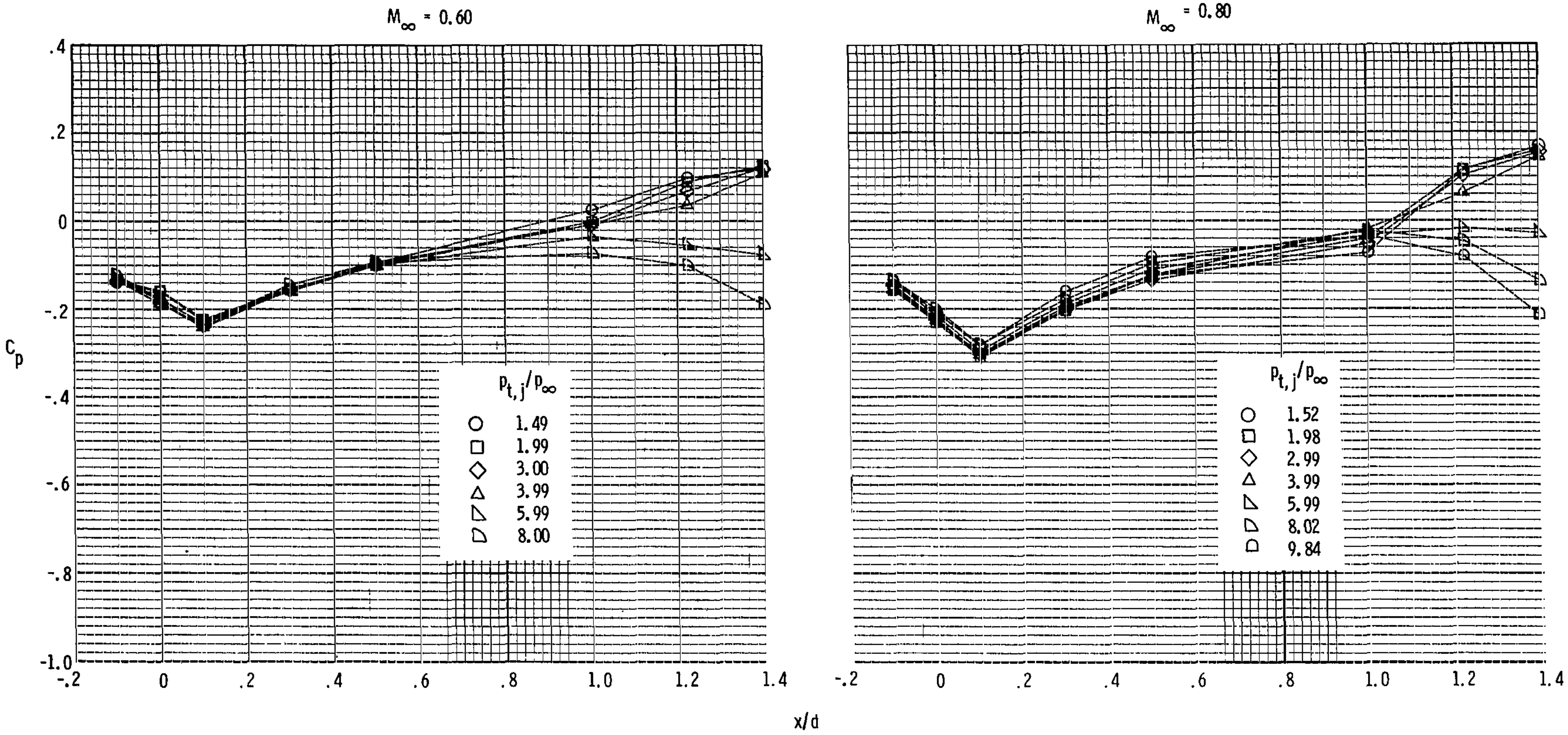

(a) M_∞ = 0.60 and 0.80.

Figure 24.- Effect of nozzle pressure ratio on sidewall center-line external pressure profiles for low-expansion-ratio nozzle.

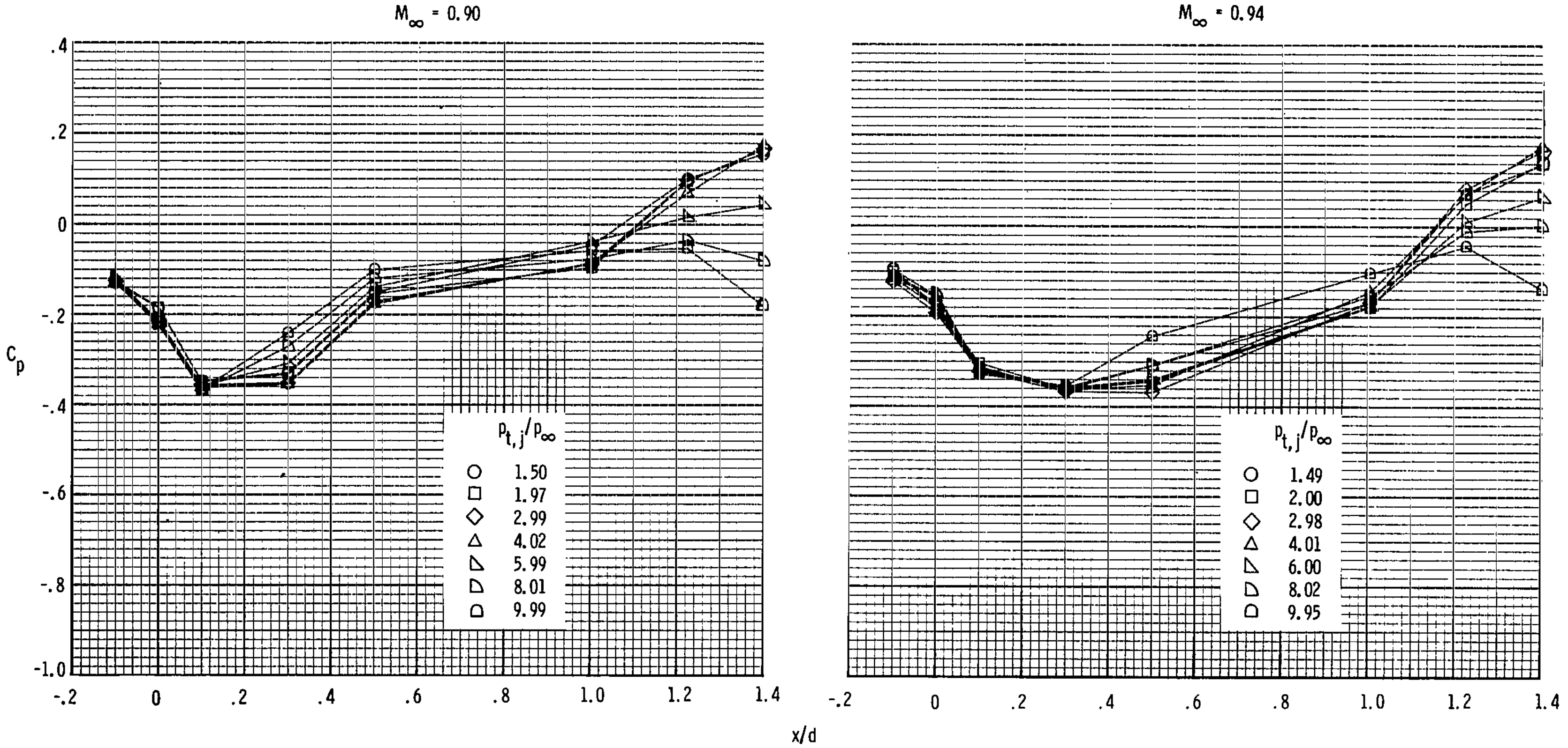

(b) M_∞ = 0.90 and 0.94.

Figure 24.- Continued.

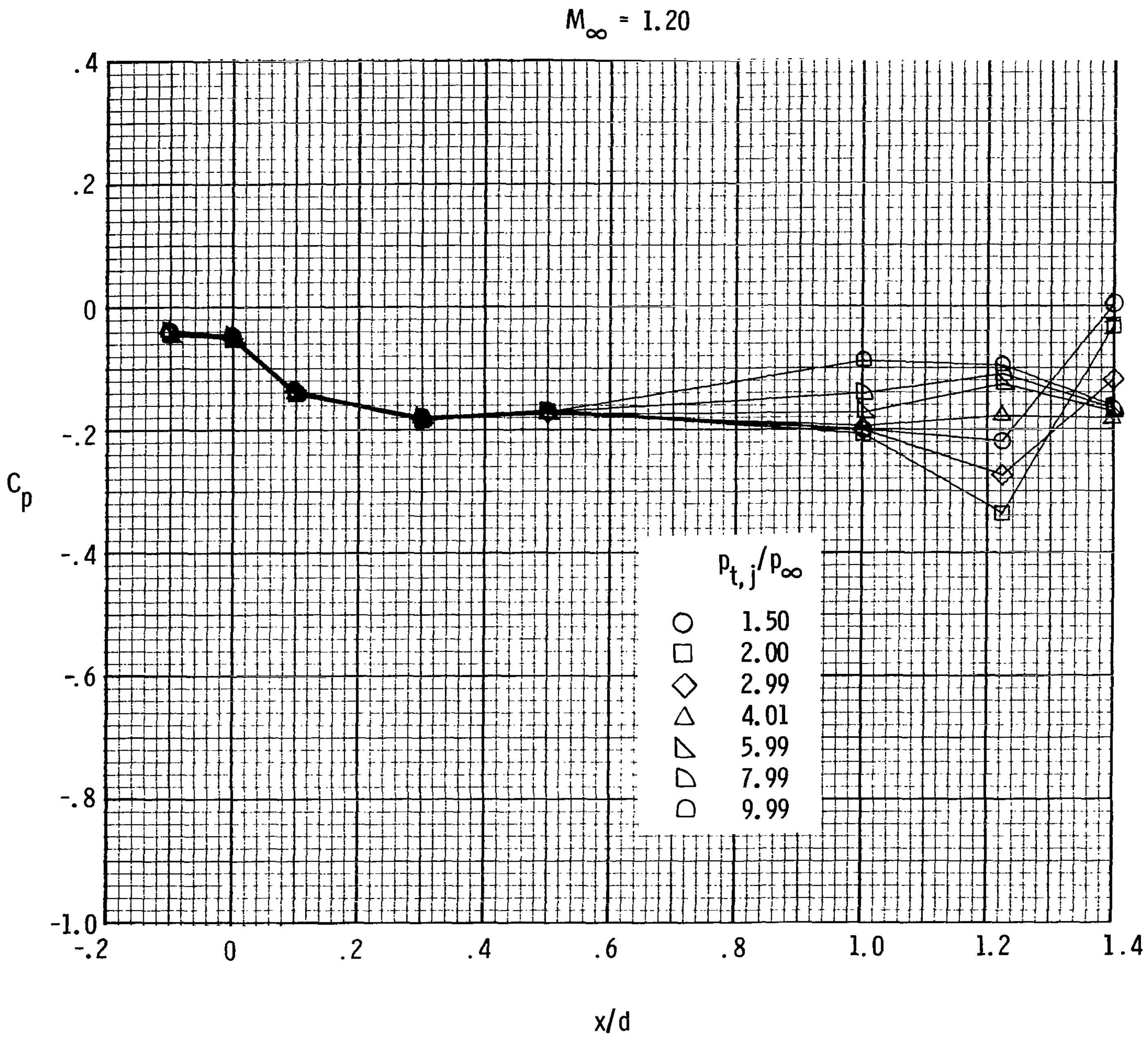

(c) M_∞ = 1.20.

Figure 24.- Concluded.

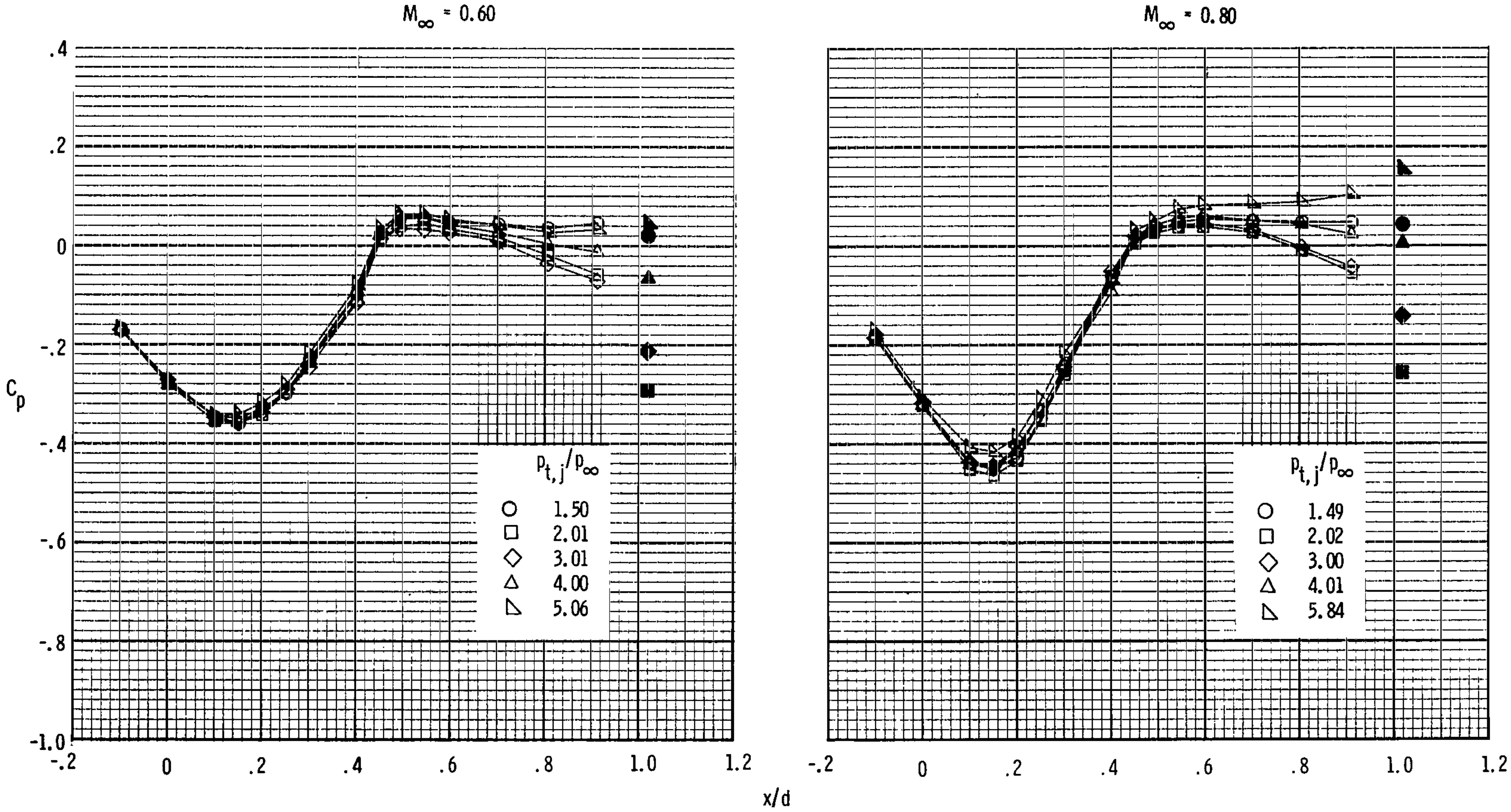

(a) M_∞ = 0.60 and 0.80.

Figure 25.- Effect of nozzle pressure ratio on flap center-line external pressure profiles for high-expansion-ratio nozzle. Base pressure is indicated by solid symbol.

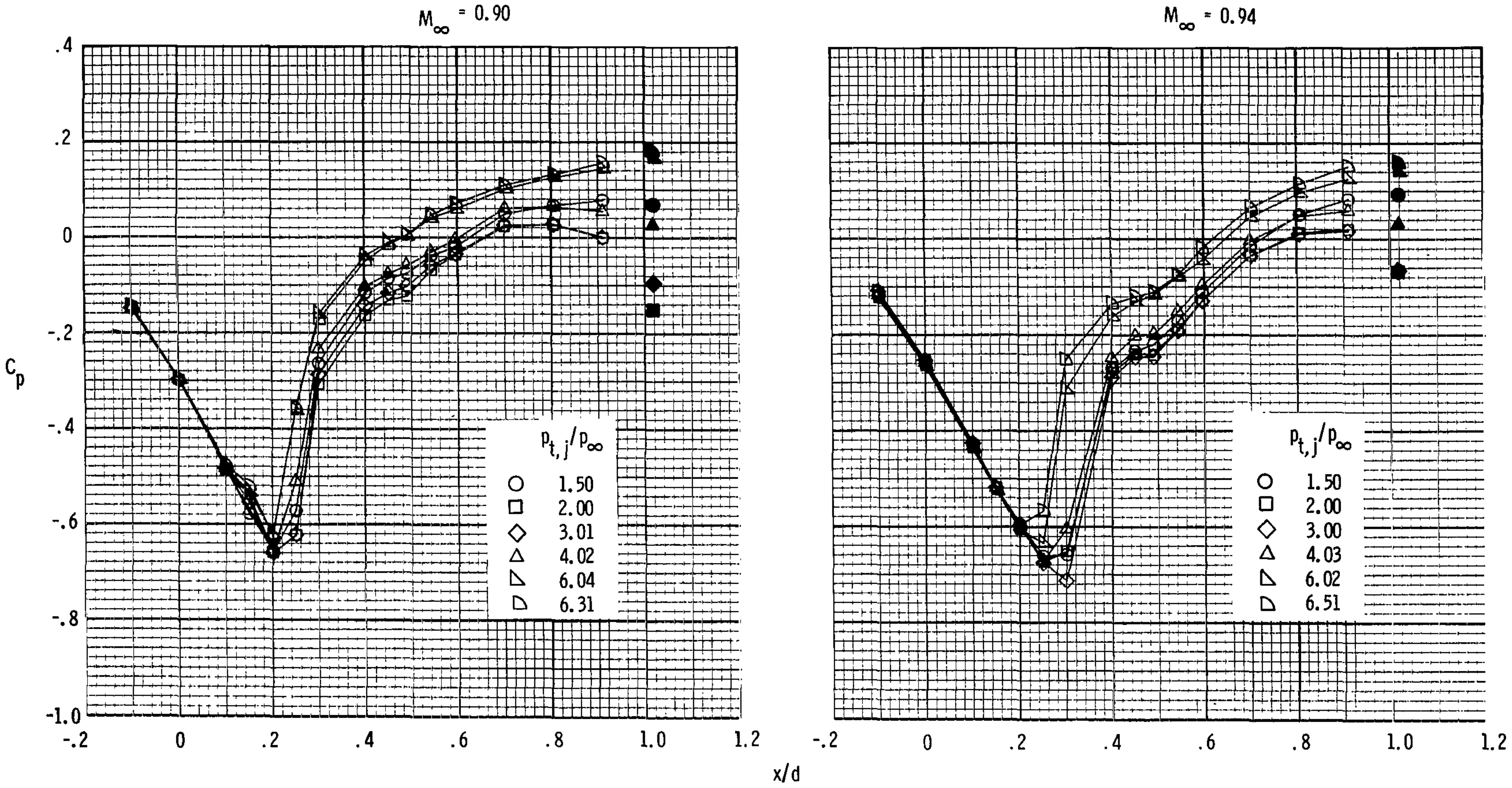

(b) M_∞ = 0.90 and 0.94.

Figure 25.- Continued.

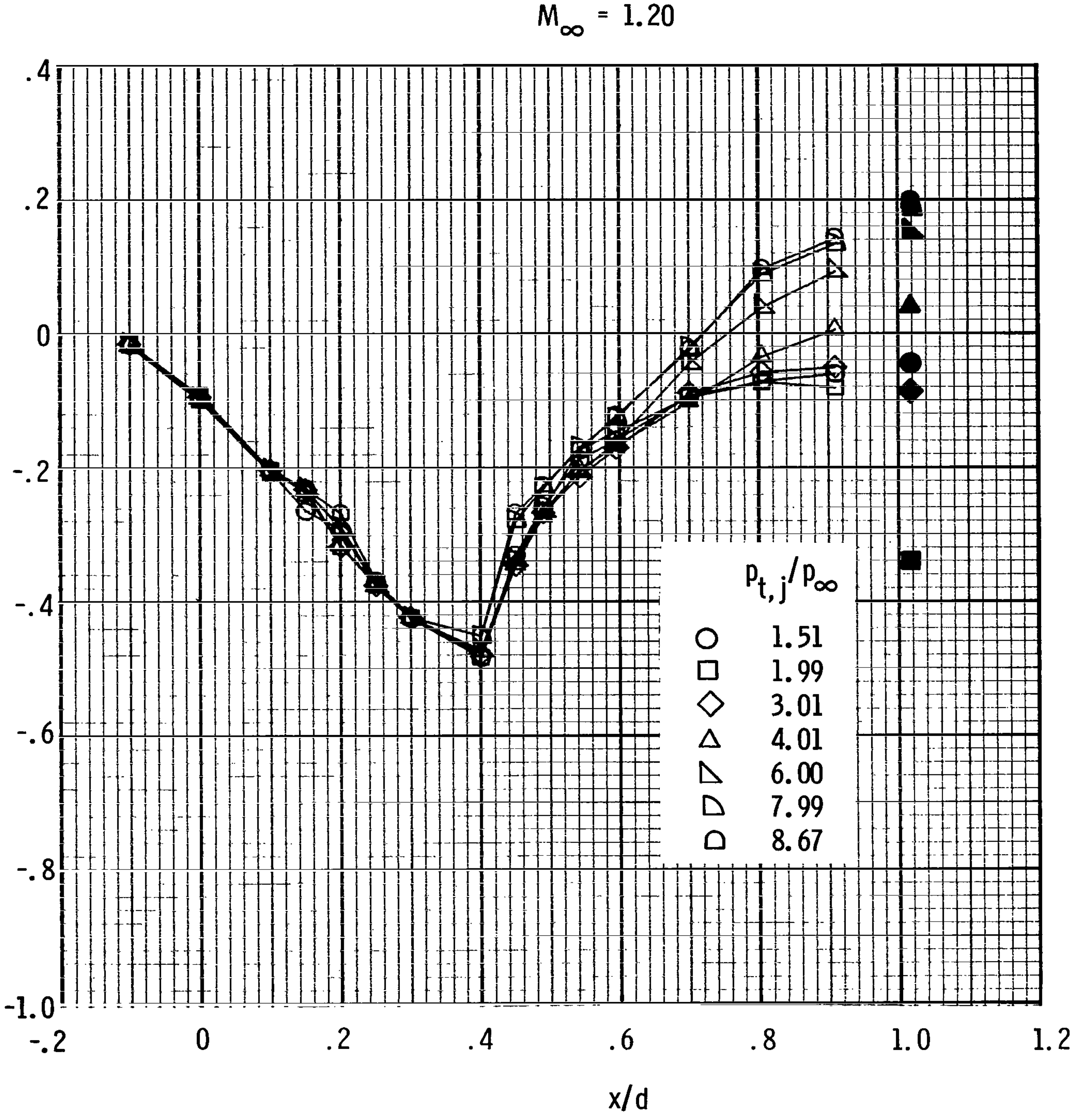

(c) M_∞ = 1.20.

Figure 25.- Concluded.

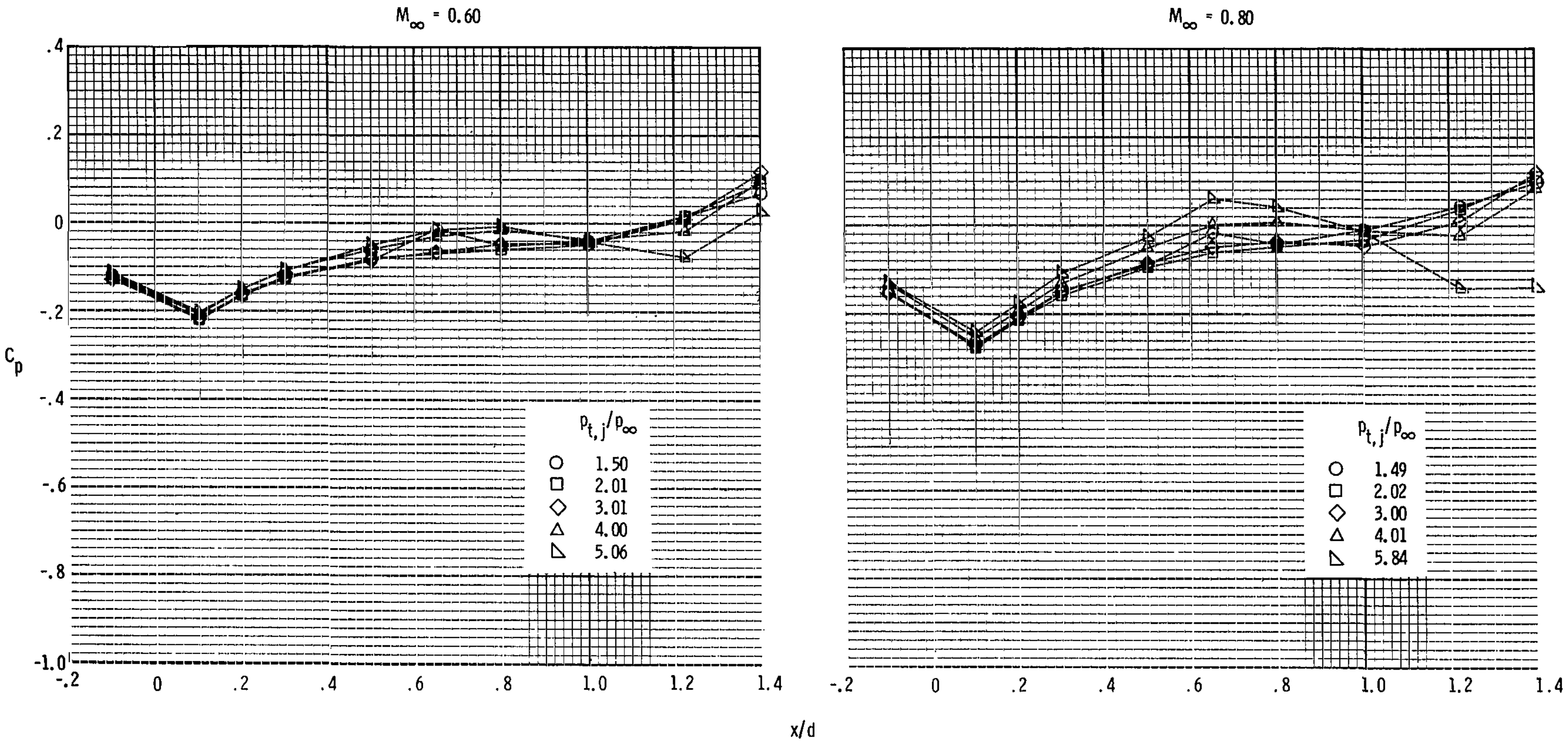

(a) M_∞ = 0.60 and 0.80.

Figure 26.- Effect of nozzle pressure ratio on sidewall center-line external pressure profiles for high-expansion-ratio nozzle.

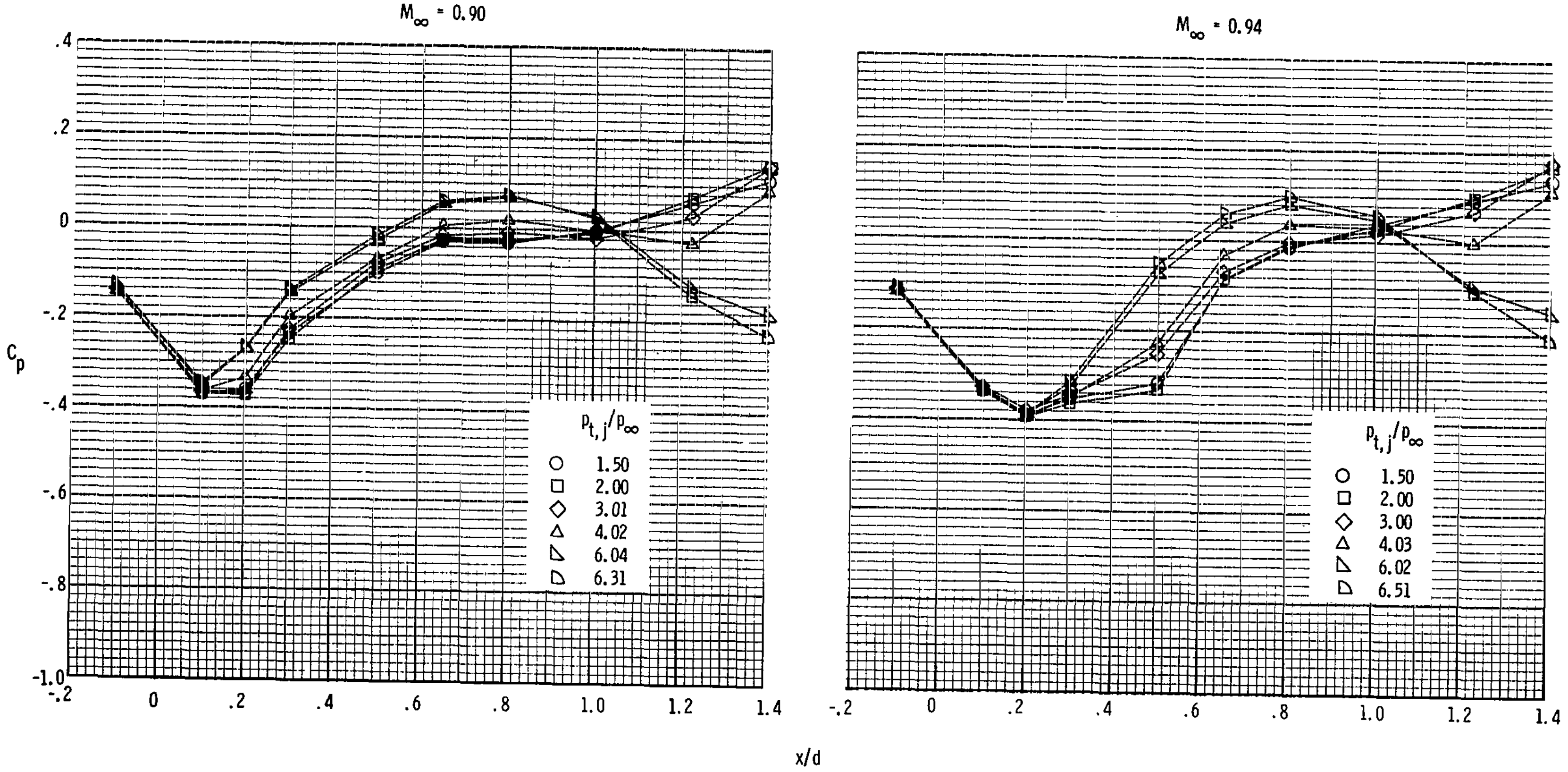

(b) $M_\infty = 0.90$ and 0.94.

Figure 26.- Continued.

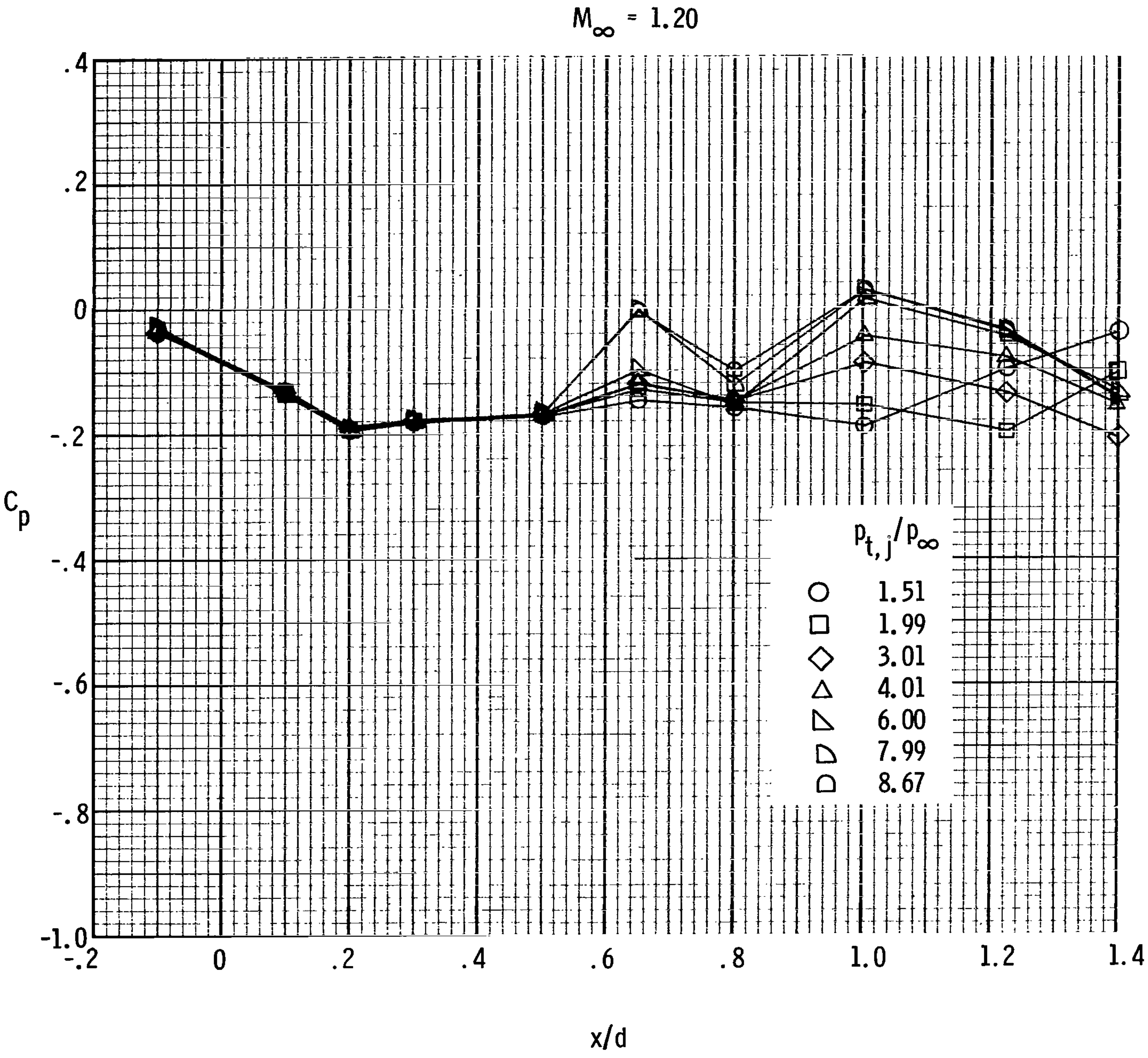

(c) M_∞ = 1.20.

Figure 26.- Concluded.

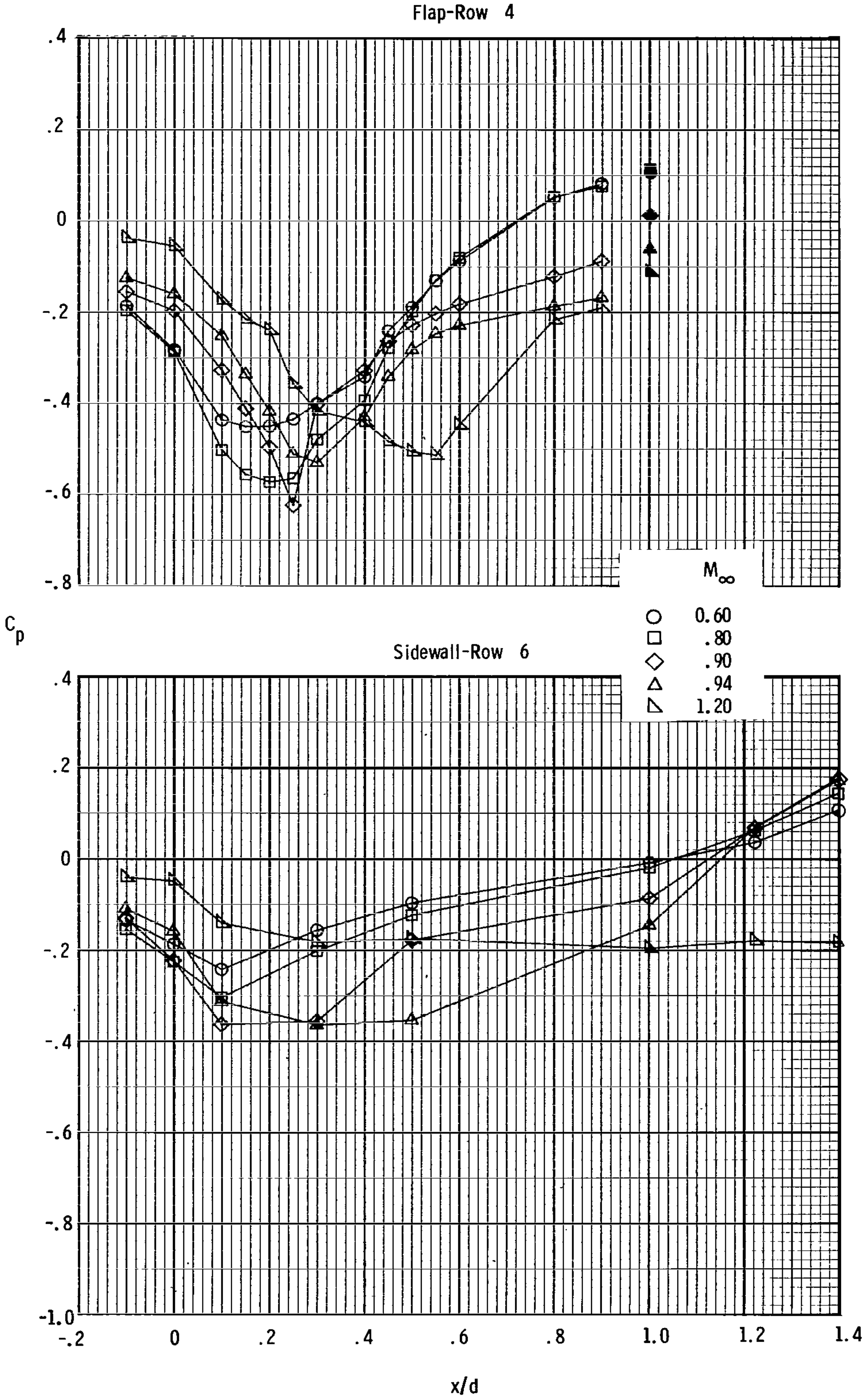

Figure 27.- Effect of Mach number on external center-line pressure profiles at $p_{t,j}/p_\infty = 4.00$ for low-expansion-ratio nozzle. Base pressure is indicated by solid symbol.

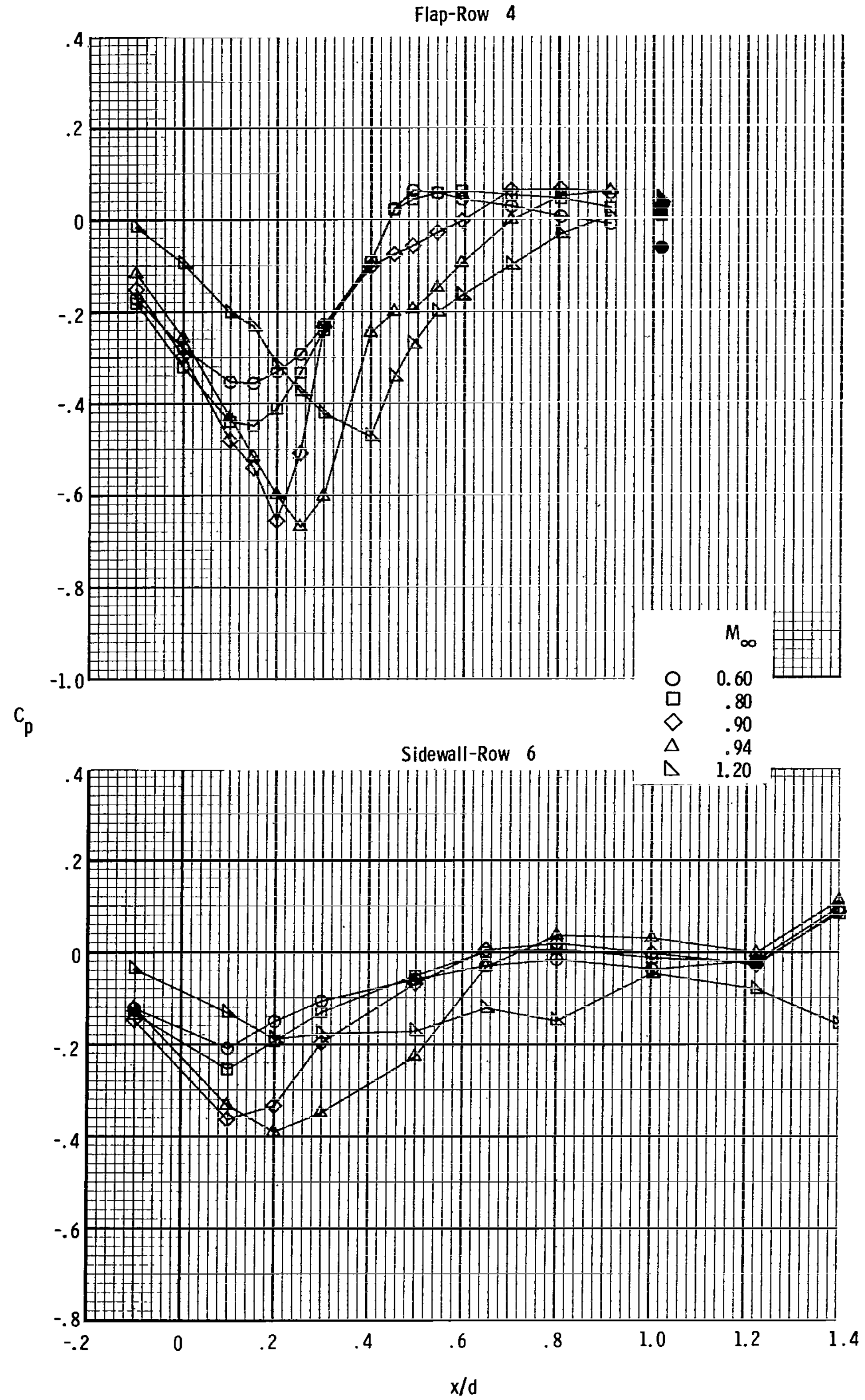

Figure 28.- Effect of Mach number on external center-line pressure profiles at $p_{t,j}/p_\infty = 4.00$ for high-expansion-ratio nozzle. Base pressure is indicated by solid symbol

1. Report No.
NASA TP-2054

2. Government Accession No.

3. Recipient's Catalog No.

4. Title and Subtitle
EXPERIMENTAL INVESTIGATION OF TWO NONAXISYMMETRIC WEDGE NOZZLES AT FREE-STREAM MACH NUMBERS UP TO 1.20

5. Report Date
September 1982

6. Performing Organization Code
505-32-13-01

7. Author(s)
Mary L. Mason and William K. Abeyounis

8. Performing Organization Report No.
L-15276

9. Performing Organization Name and Address
NASA Langley Research Center
Hampton, VA 23665

10. Work Unit No.

11. Contract or Grant No.

12. Sponsoring Agency Name and Address
National Aeronautics and Space Administration
Washington, DC 20546

13. Type of Report and Period Covered
Technical Paper

14. Sponsoring Agency Code

15. Supplementary Notes

16. Abstract

An experimental investigation has been conducted in the Langley 16-Foot Transonic Tunnel to measure forces and pressures on two nonaxisymmetric wedge nozzles. Tests were conducted at static conditions and at free-stream Mach numbers of 0.60, 0.80, 0.90, 0.94, and 1.20. The range of nozzle pressure ratios varied with configuration and Mach number. The internal and external geometry of the nozzles and the test model are defined in detail. Nozzle performance data are presented as discharge coefficients, internal thrust ratios, thrust-minus-nozzle drag ratios, and ideal thrust coefficients. Extensive internal and external pressure measurements are presented in figures and tables.

17. Key Words (Suggested by Author(s))
Propulsion nozzles
Nonaxisymmetric nozzles
Wedge nozzles
Internal performance

18. Distribution Statement
Unclassified - Unlimited

Subject Category 02

19. Security Classif. (of this report)
Unclassified

20. Security Classif. (of this page)
Unclassified

21. No. of Pages
115

22. Price
A06

For sale by the National Technical Information Service, Springfield, Virginia 22161

NASA-Langley, 1982

National Aeronautics and
Space Administration

Washington, D.C.
20546

Official Business
Penalty for Private Use, $300

THIRD-CLASS BULK RATE

Postage and Fees Paid
National Aeronautics and
Space Administration
NASA-451

U.S.MAIL

6 1 1U,A, 820901 S00903DS
DEPT OF THE AIR FORCE
AF WEAPONS LABORATORY
ATTN: TECHNICAL LIBRARY (SUL)
KIRTLAND AFB NM 87117

S

NASA

POSTMASTER: **If Undeliverable (Section 158 Postal Manual) Do Not Return**